5-2012

Design and Synthesis of Solid State Materials Constructed from Polyoxomolybdate Clusters

Stephanie Jones
Syracuse University

Abstract

This work encompasses detailed investigations of the synthesis and structures of polyoxomolybdate materials. The design and synthesis of hybrid organic-inorganic materials constructed from various anionic polyoxomolybdate units and cationic secondary metal-ligand units, and the synthesis and ligand-exchange capacity of the giant polyoxomolybdate cluster Mo-132 are described. These studies aim to increase our understanding of the formation and physiochemical properties of these materials, and thereby aid in the ability to control and predict their structural chemistry.

The analysis of a number of structural determinants in the oxomolybdenum-organodiphosphonate system aims to expand the current knowledge of this family of materials. We have focused on variables such as: the organic tether length of alkyldiphosphonate ligands; the size, flexibility, and number of nitrogen donor groups of secondary organoimine ligands; the oxidation state of the cationic transition metal center; and the incorporation of fluoride into the molybdodiphosphonate substructure.

In order to explore the range of possible anionic charges that the polyoxomolybdate Mo-132 cluster may posses, ligand-exchange reactions were conducted. This has been accomplished through the incorporation of various ratios of ligands contributing different degrees of anionic charge into the molybdate framework. Assorted structural characterization techniques reveal a range of ligand exchange based on the pH of the reaction solution.

Design and Synthesis of Solid State Materials Constructed from Polyoxomolybdate Clusters

By

Stephanie Jones

B.A. Wells College, 2006

DISSERTATION

Submitted in partial fulfillment of the requirements for the

degree of Doctor of Philosophy in Chemistry

in the Graduate School of Syracuse University

May 2012

Acknowledgement

The successful completion of this work would not have been possible without the help of many individuals.

I would like to express my sincere gratitude to Professor Jon Zubieta for his support and guidance over the past six years.

Several members of the Zubieta group from 2006 to 2012 have proved invaluable, particularly Amanda Aldous and Katherine Schmidtke who contributed directly to the projects presented here.

I am very grateful to Professor Achim Müller for his mentorship and collaboration, as well as Dr. Alice Merca and Dr. Ana Maria Todea for their advice.

My family has provided a constant source of motivation throughout my education. They have always believed in me, and I could not have accomplished so much without them.

I owe a special thank you to Brock Labadie for his patience and support, and to the Labadie family for their encouragement.

I am thankful for everyone who has supported me along this journey.

Table of Contents

List of Abbreviations

4-Hpt	5-(4'-Pyridyl)tetrazole
AuNP	Gold nanoparticle
AuTMA	N,N,N-trimethyl(11-mercaptoundecyl)ammonium-functionalized gold nanoparticles
Bpy	2,2'-Bipyridine
Bisterpy	2,2':4',4":2",2'"-Quarterpyridyl-6',6"-di-2-pyridine
DFT	Density functional theory
DLS	Dynamic light scattering
HOMO	Highest energy occupied molecular orbital
IR	Infrared
LUMO	Lowest energy unoccupied molecular orbital
Mo-132	$(NH_4)_{42}[Mo^{VI}_{72}Mo^{V}_{60}O_{372}(C_2H_3O_2)_{30}(H_2O)_{72}]$
MOF	Metal-organic framework
NMR	Nuclear magnetic resonance spectroscopy
Phen	1,10-Phenanthroline
Phenbisterpy	1,4-Bis(2,2':6',2"-terpyridin-4'-yl-benzene
POM	Polyoxometalate
TIP	Temperature-independent paramagnetism
Tpyprz	Tetrapyridylpyrazine
Trz	1,2,4-Triazole
UV-vis	Ultraviolet-visible

List of Figures

List of Tables

Chapter 1

Introduction

1.1 Introduction

Inorganic oxides find use in a range of chemistry and materials science applications stemming from a wide array of properties as a result of diverse chemical compositions and structure types.[1-15] Modifications may be made to covalency, geometry, and oxidation states, and a diverse crystal chemistry offers a variety of pore structures and dimensions, coordination sites, and juxtapositions of functional groups. Inorganic oxides are prevalent across the geosphere and biosphere;[16-22] many silicates, ores, gems, rocks, and soils are examples of naturally-occurring oxides of simple and highly symmetrical composition with small unit cells. Properties of such simple oxides include piezoelectricity, ferromagnetism, sorptive properties, and catalytic and optical activity.[23-33]

In addition to these simple oxide materials, many exist with more complex structures and compositions that exhibit higher functionality. One example seen in nature of this structure-function relationship is provided by the abalone shell, which is known for its exceptional strength.[34] The shell is composed of microscopic calcium carbonate tiles stacked one on top of the other, with masses of folded proteins located between the tiles (**Figure 1.1**). When the shell is struck, the proteins stretch to allow the tiles to slide to absorb the force of the blow without shattering.[35-38] Emulating nature's use of organic components to modify inorganic oxide microstructures provides the potential to design novel functional materials through exploitation of the correlation between increased structural complexity and increased functionality.

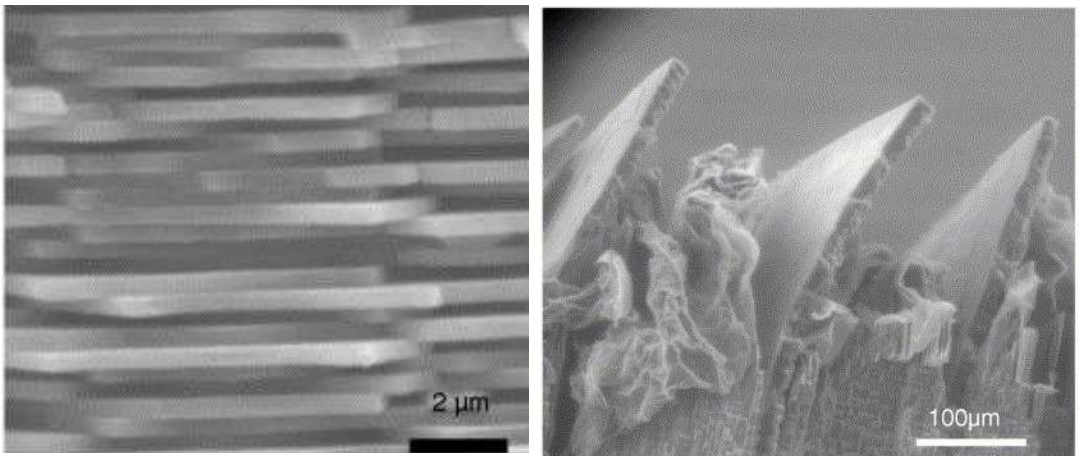

(a) **(b)**

Figure 1.1. Electron micrograph images of **(a)** the calcium carbonate tiles and **(b)** the folded protein mass between tiles of the abalone shell.[34]

1.2 Hybrid Organic-Inorganic Materials

One approach to the design of new oxide solids exploits the use of organic components as templates or structure-directing agents to imprint or transmit structural information.[39-42] The inorganic subunits coexist with the organic molecules in a synergistic fashion to allow higher order organization of hierarchical structures.[43-45] These hybrid organic-inorganic materials combine multiple components that each exhibit a range of properties, facilitating the construction of novel multifunctional materials. The inorganic component may provide magnetic, dielectric, or optical properties, mechanical hardness, and thermal stability while the organic compounds offer processability, chelation between metal centers, structural diversity, polarizability, and luminescent properties.[46-47] The hybrid material may then possess either composite or unique properties. For example, a microporous hybrid material may be designed with the

appropriate pore topology, environment, and molecular juxtaposition for reactivity ideal for applications in catalysis, separation, and gas storage.[48-61] The inorganic substructure offers chemical and thermal stability, and the metal sites provide nodes for ligand coordination with directional preferences. The incorporation of transition metal cations also results in a structure combining the reactivity of these metal centers with the size and shape selectivity of zeolites.[62-65] The organic component allows the construction of cavities and channels functionalized with the organic groups to allow the modification of the cavity shape, size, and function.

The incorporation of metal sites within hybrid materials provides structural versatility based on their variable coordination polyhedra and differences in size, ligand preferences, and crystal field energies. The most common type of hybrid materials, known as metal-organic frameworks (MOFs), consists of metal atoms or clusters bridged by polyfunctional organic molecules into extended arrays (**Scheme 1.1**).[48-61] An

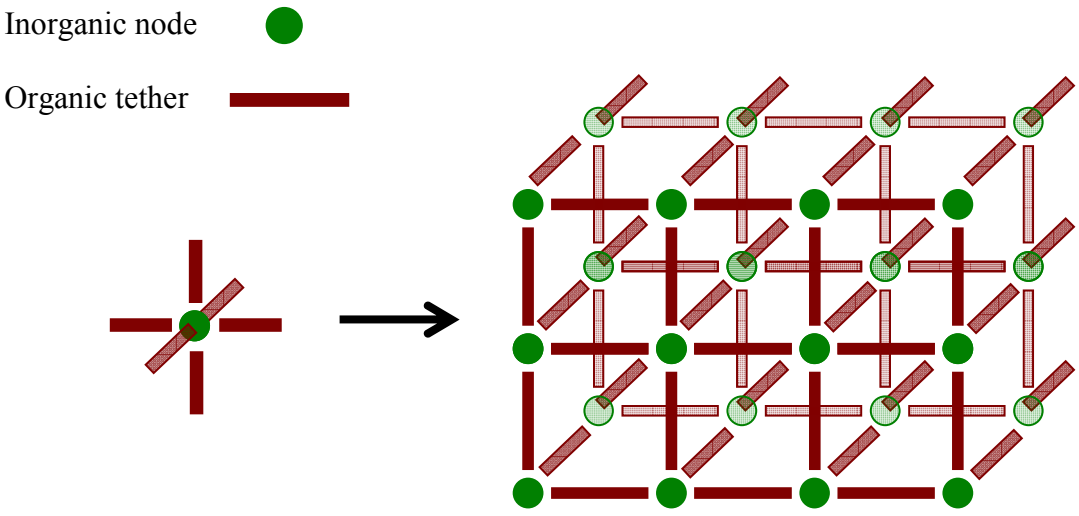

Scheme 1.1.

important subset of metal-organic frameworks is hybrid metal oxides, characterized by metal-oxygen-metal (M – O – M) arrays embedded within the overall architecture. [66-67] In these materials, the inorganic oxide contributes to the structural complexity as one unit in a multi-component material. Our strategy for the construction of new metal oxides links molecular oxide building blocks through appropriate organic molecules or secondary metal-ligand units, resulting in either the linking of oxide clusters through the secondary metal-ligand unit or encapsulation of the oxide within a metal-ligand framework (**Scheme 1.2**).[67-88] Polyoxometalates (POMs) form robust clusters demonstrating a variety of sizes, topologies, and oxidation states, and may be utilized in the construction of solid oxides with more or less predictable connectivity.[89-95]

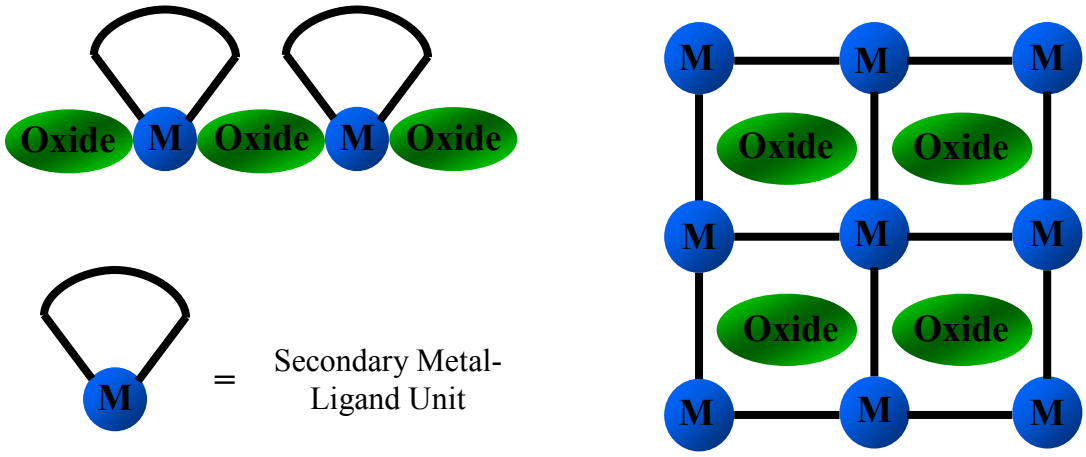

Scheme 1.2.

1.3 Polyoxomolybdates

The polyoxomolybdate family exhibits a diverse structural chemistry providing chemically robust building units around which metal-organic compounds can be constructed..[96-106] Due to interesting properties resulting from the broad range of structural motifs, these materials find application in areas such as catalysis and photochemistry.[103,107-110] The array of polyoxomolybdate dimensionalities includes isolated tetrahedral and octahedral moieties, several different polyanions including giant nanoscopic clusters, two-dimensional layers, and three-dimensional frameworks.

Of particular interest in the construction of hybrid organic-inorganic materials are the lower-dimensionality polyanions that can be linked through organic tethers or provide charge balance to cationic transition metal-ligand components. Of the class of materials constructed from polyoxomolybdate clusters, octamolybdate $\{Mo_8O_{26}\}^{4-}$ anions are quite common.[111] Eight isomeric forms of octamolybdates have been observed, α through θ, composed of a combination of tetrahedral MoO_4, square pyramidal MoO_5, and octahedral MoO_6 polyhedra linked through corner- and edge-sharing interactions.[112-121] The structures of the α, β, and γ isomers are shown in **Figure 1.2**.

Another highly stable polyoxomolybdate cluster is the Keggin type polyanion, composed of a central heteroatom surrounded by twelve corner- and edge-sharing MoO_6 octahedra arranged in four Mo_3O_{13} units.[123-127] Five isomers exist, in which different rotational orientations of the Mo_3O_{13} units produce clusters of varying degrees of symmetry.[128] **Figure 1.3** shows the structure of the common α-Keggin anion. These clusters crystallize from an acidic molybdate solution in the presence of a heteroatom

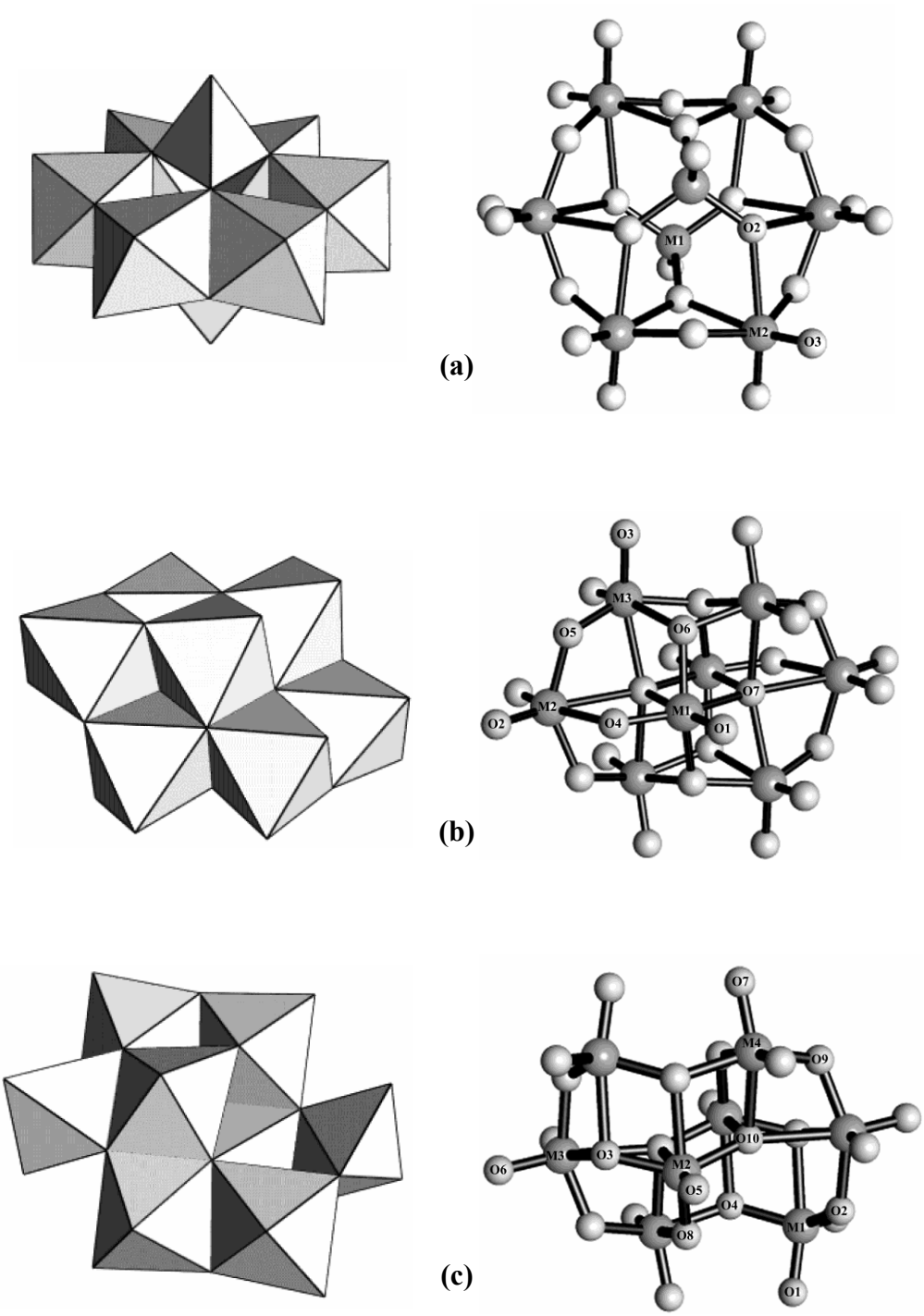

Figure 1.2. Polyhedral and ball-and-stick representations of three octamolybdate isomers; **(a)** $\{\alpha\text{-}Mo_8O_{26}\}^{4-}$ formed from a ring of six edge-sharing MoO_6 octahedra bicapped by two MoO_4 tetrahedra; **(b)** $\{\beta\text{-}Mo_8O_{26}\}^{4-}$ formed from a compact arrangement of eight edge-sharing MoO_6 octahedra; and **(c)** $\{\gamma\text{-}Mo_8O_{26}\}^{4-}$ formed from an edge-sharing arrangement of six MoO_6 octahedra and two MoO_5 square pyramids.[122]

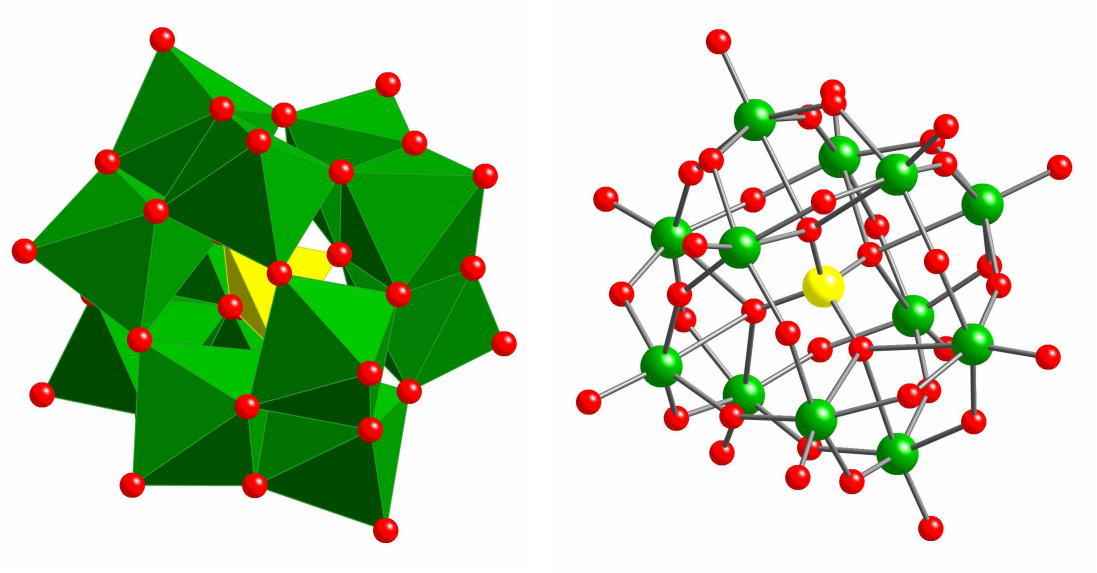

Figure 1.3. Polyhedral and ball-and-stick representations of the α-keggin cluster $\{PMo_{12}O_{40}\}^{3-}$.

such as phosphorus or arsenic, and reduction of one or more metal centers often leads to the formation of a mixed-valence cluster.

More recently, a new class of giant polyoxomolybdate clusters with nanoscopic dimensions has been studied with significance to nanochemistry and nanomaterials science.[129] Such clusters are formed via self-assembly following reduction of an acidic molybdate solution, and structures containing up to 368 molybdenum centers have been isolated.[130] Of particular interest are the $\{Mo_{11}\}_n$ class of polyoxomolybdates, of which the spherical-ball (n = 12) and the wheel-shaped (n = 14) anions such as $(NH_4)_{42}[Mo^{VI}_{72}Mo^{V}_{60}O_{372}(C_2H_3O_2)_{30}(H_2O)_{72}]$ and $Na_{21}[Mo^{VI}_{126}Mo^{V}_{28}O_{462}H_{14}(H_2O)_{54}(H_2PO_4)_7]$, respectively, are representative (**Figure 1.4**).[131] These types of giant clusters have applications in analytical chemistry, catalysis, electrochemistry, electrooptics, medicine, and corrosion protection pigments.[133-134]

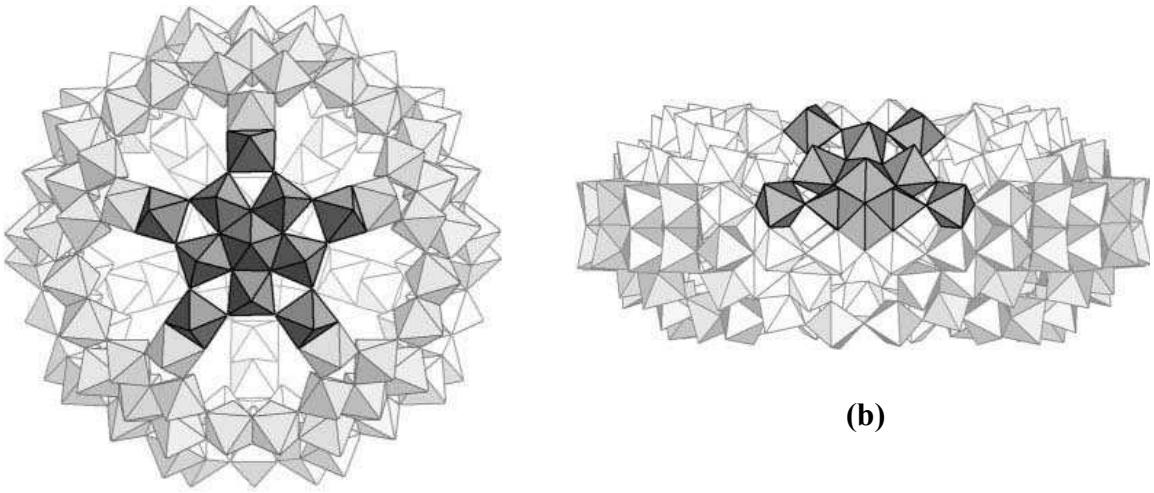

(a) **(b)**

Figure 1.4. Polyhedral representations of the giant polyoxomolybdate anions **(a)** $[Mo^{VI}_{72}Mo^{V}_{60}O_{372}(C_2H_3O_2)_{30}(H_2O)_{72}]^{42-}$ and **(b)** $[Mo^{VI}_{126}Mo^{V}_{28}O_{462}H_{14}(H_2O)_{54}(H_2PO_4)_7]^{21-}$ with the $\{Mo_{11}\}$ unit shown in dark gray.[132]

1.4 The Oxomolybdenum Diphosphonate System

Polyoxomolybdate clusters have been exploited as building blocks in the construction of metal oxides incorporating organic components as ligands, structure-directing agents, and charge-compensating units.[67,135-137] However, bonding between the clusters and the secondary metal-ligand components that link the clusters into one-, two-, or three-dimensional assemblies has proven unpredictable. Through incorporation of a diphosphonic acid ligand, highly versatile $\{Mo_5O_{15}(O_3PR)_2\}^{4-}$ pentanuclear molybdodiphosphonate clusters form persistently[138] and are bridged by the organic tether of the diphosphonate group. These molybdenum-diphosphonate materials can be tailored through modification of the tether type and length of the diphosphonate ligand as well as the introduction of added functionality.

Tethering of molybdodiphosphonate clusters through organodiphosphonates of the type $\{O_3P(CH_2)_nPO_3\}^{4-}$ produces anionic one-dimensional chains as described in **Scheme 1.3**. The prototypical structure of $[Co(bpy)_3][Mo_5O_{14}(OH)\{HO_3P(CH_2)_3PO_3\}]$

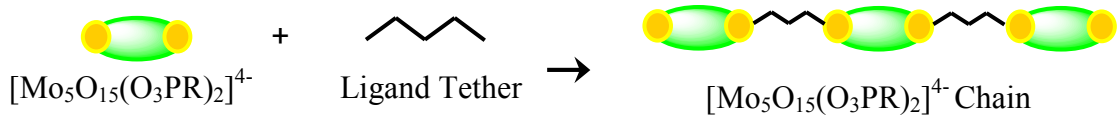

Scheme 1.3.

(**Figure 1.5 (a)**) demonstrates the phosphomolybdate chain substructure in the presence of $\{Co(bpy)_3\}^{2+}$ charge-compensating units.[139] A more readily isolated motif within this chemistry is the molybdodiphosphonate chain decorated by secondary metal-ligand units as in $[\{Cu_2(phen)_3(H_2O)_2\}Mo_5O_{15}\{O_3P(CH_2)_3PO_3\}]$ (**Figure 1.5(b)**), preventing polymerization while providing more effective charge compensation.[140] Variation in the tether length of the diphosphonate ligand can be exploited to produce structures in which the clusters are spaced further apart.

1.4.1 Introduction of a Binucleating Secondary Ligand

A noteworthy feature of the chemistry of one-dimensional structures composed of $\{Mo_5O_{15}(O_3PR)_2\}^{4-}$ clusters linked through the organic tether of the diphosphonate ligand is the facile incorporation of secondary metal-ligand components as intimate structural subunits bonded through oxo groups to the molybdate clusters. Introduction of a binucleating secondary ligand offers the potential for bridging the molybdodiphosphonate chains into two and three dimensions, as illustrated by **Scheme 1.4**. In such structures,

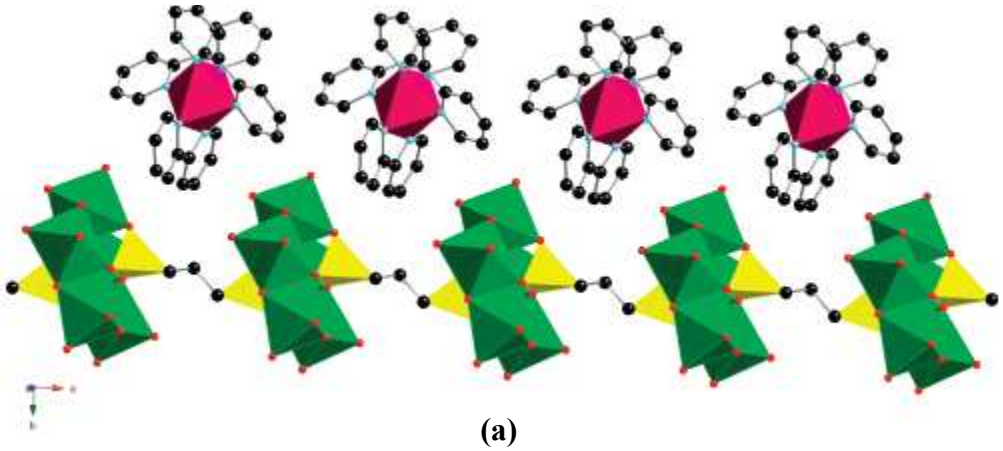

(a)

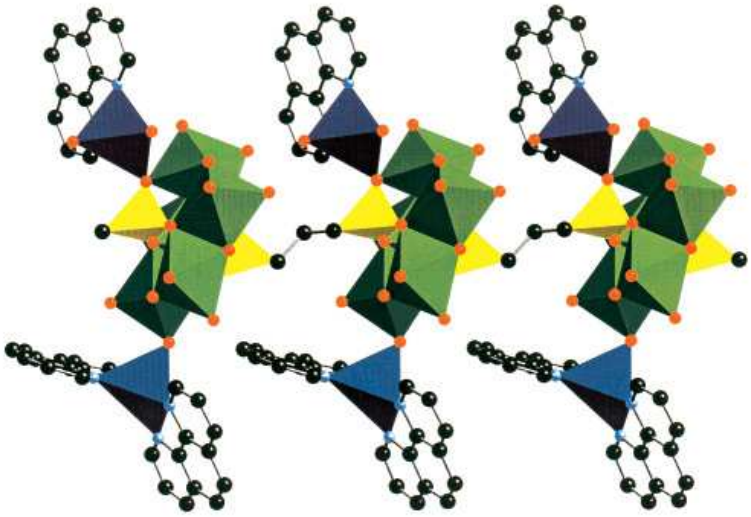

(b)

Figure 1.5. Polyhedral representations of the one-dimensional structures of **(a)** $[Co(bpy)_3][Mo_5O_{14}(OH)\{HO_3P(CH_2)_3PO_3\}]$[139] and **(b)** $[\{Cu_2(phen)_3(H_2O)_2\}Mo_5O_{15}\{O_3P(CH_2)_3PO_3\}]$.[140]

the molybdate cluster acts as a node from which ligand and metal cation coordination provide structural expansion. The overall dimensionality of the resultant material is dependent on the number of accessible binding sites on the surface of each cluster.

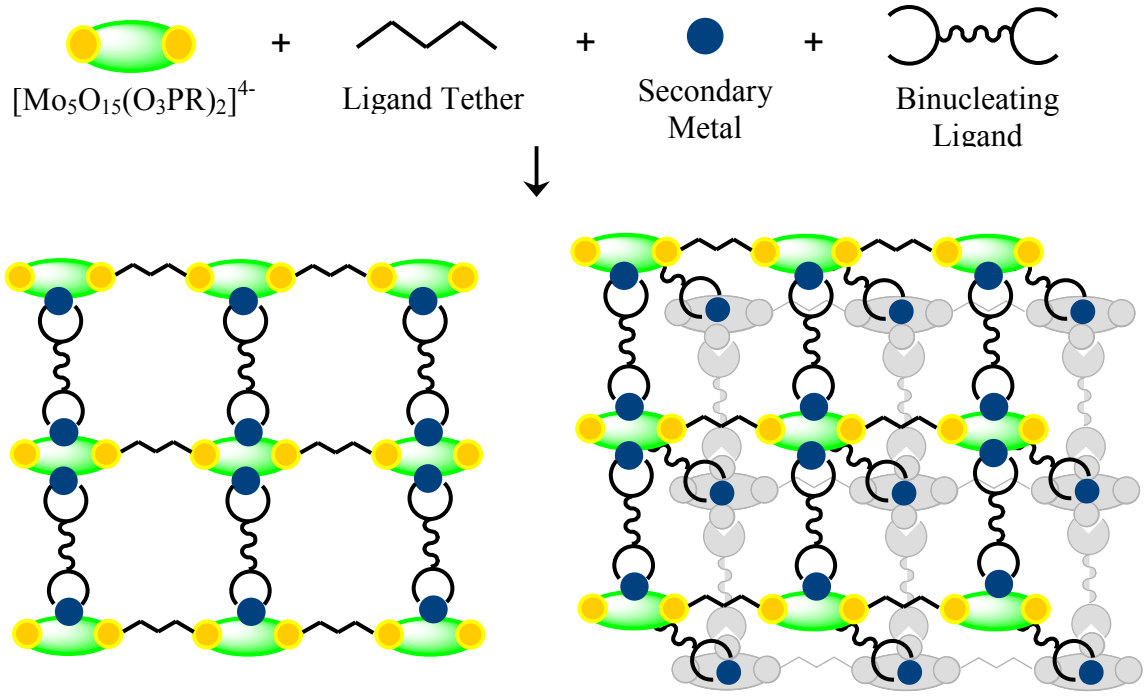

Scheme 1.4.

As expected, compounds of the Cu(II)-tetrapyridylpyrazine/ molybdodiphosphonate family form two- and three-dimensional structures through the linking of molybdodiphosphonate chains by the binucleating tetrapyridylpyrazine (tpyprz) ligand. Typical examples of these higher dimensionality materials are provided by the two-dimensional $[\{Cu_2(tpyprz)(H_2O)_2\}Mo_5O_{15}(O_3P(CH_2CH_2)PO_3)]$ and the three-dimensional $[\{Cu_2(tpyprz)(H_2O)_2\}Mo_5O_{15}(O_3P(CH_2)_3PO_3)]$ (**Figure 1.6**).[139,141] In both structures, the copper-tpyprz unit acts as a rigid rod to increase the space between chains. This observation encouraged the investigation of the structural consequences of further modifying the dimensions of the binucleating ligand (**Scheme 1.5**). Use of phenyl

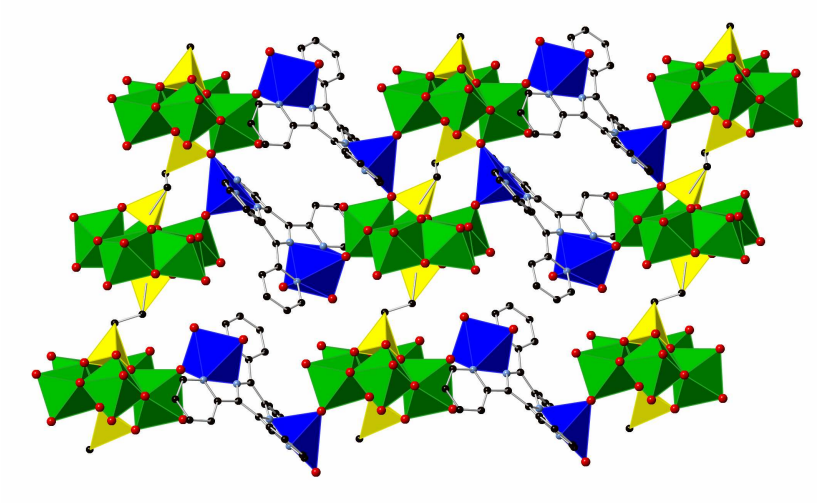

(a)

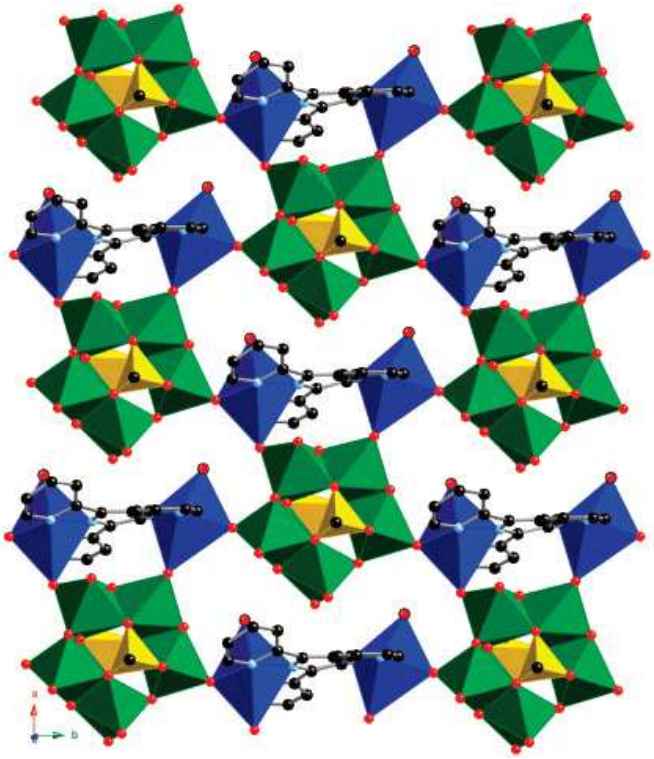

(b)

Figure 1.6. Polyhedral representations of **(a)** the two-dimensional structure of $[\{Cu_2(tpyprz)(H_2O)_2\}Mo_5O_{15}(O_3P(CH_2CH_2PO_3)]$[141] and **(b)** the three-dimensional structure of $[\{Cu_2(tpyprz)(H_2O)_2\}Mo_5O_{15}(O_3P(CH_2)_3PO_3)]$.[139]

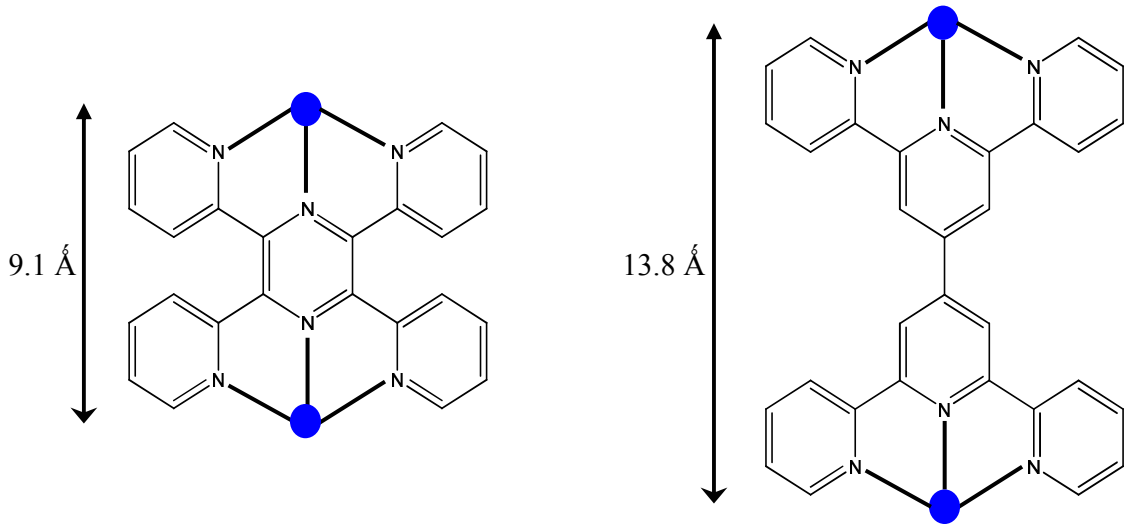

Scheme 1.5.

bridged ligands such as 2,2':4',4":2",2"'-quarterpyridyl-6',6"-di-2-pyridine (bisterpy) could lead to the formation of expanded structures.

1.4.2 Introduction of a Multinucleating Secondary Ligand

Introduction of a secondary metal-ligand unit incorporating a multinucleating ligand can increase the complexity of the overall structure through coordination to more than two metal centers. Polyazaheteroaromatic ligands combine the ability to coordinate to multiple metal centers through three or more nitrogen donors with a superexchange capacity reflected in the interesting magnetic properties of their compounds.[142-149] Specifically, triazole (trz) has shown widespread use as a bridging ligand in the construction of metal-organic materials. Similar to other members of the five-membered azole class of unsubstituted, monocyclic polyazaheteroaromatic ligands, triazole may also exist as an anionic ligand through deprotonation of the acidic N-H group present in the

free ligand.[150] The anionic 1,2,4-triazolate provides structural expansion from one to three dimensions through coordination to all three nitrogen donors; the linking of metal centers through N1 and N2 positions can provide one-dimensional units that can then be linked through the N4 positions to increase the dimensionality of the structure. Examples of N1,N2,N4 coordination modes are provided by the two-dimensional structure of [Cu(trz)] and the three-dimensional structure of $[Cu_3(trz)_3(OH)_3(H_2O)_4]$ (**Figure 1.7**).[151-152]

Another advantage of the use of polyazaheteroaromatic ligands such as triazole as ligands in metal-organic complexes is its facile derivatization to provide bridging ligands with additional functionality.[153-164] Though addition of a tethering group onto 1,2,4-triazole results in the loss of analogous directionality to the parent ligand, the derivatization of tetrazole with a pyridyl ring produces 4-pyridyltetrazole (4-pt) which in the N2,N3 bridging mode can be considered an expanded analogue of 1,2,4-triazolate (**Scheme 1.6**). Materials containing 4-pt ligands exhibit increased void volumes and interesting magnetic properties, and the incorporation of various anionic units into 4-pt frameworks results in the formation of highly complex structures.[165] This structural chemistry can be further exploited through incorporation of additional anion types such as polyoxomolybdate clusters.

1.5 Fluoride Incorporation

Crystallization of zeolite and other open-framework materials is facilitated through the use of fluoride as a mineralizing agent, and it has been determined that fluoride is required for the high quality crystallization of vanadium-organodiphosphonate

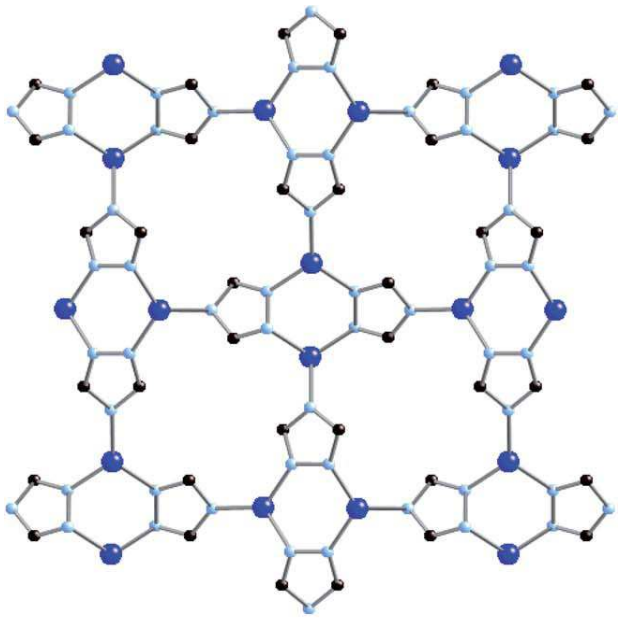

(a)

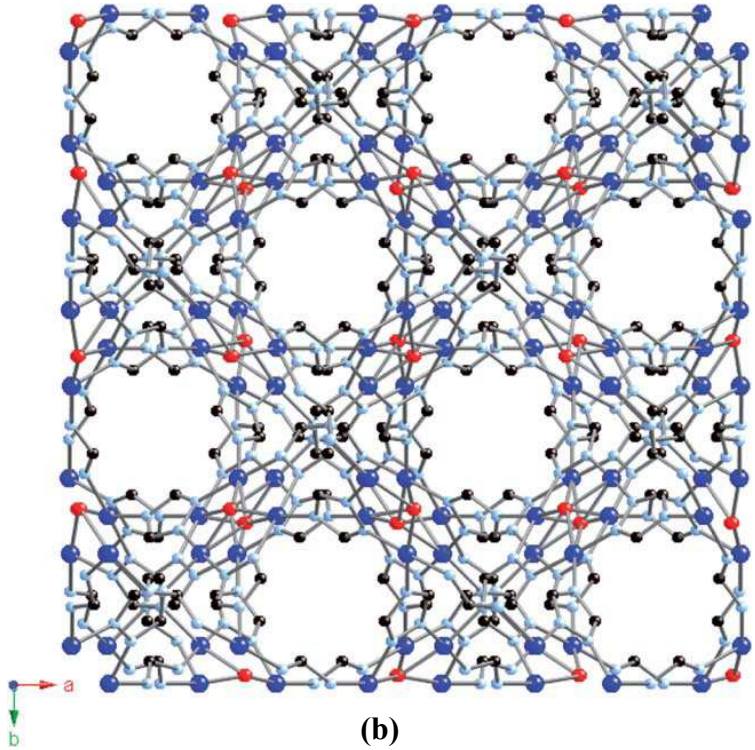

(b)

Figure 1.7. Ball-and-stick representations of **(a)** the two-dimensional structure of [Cu(trz)][151] and **(b)** the three-dimensional structure of $[Cu_3(trz)_3(OH)_3(H_2O)_4]$.[152]

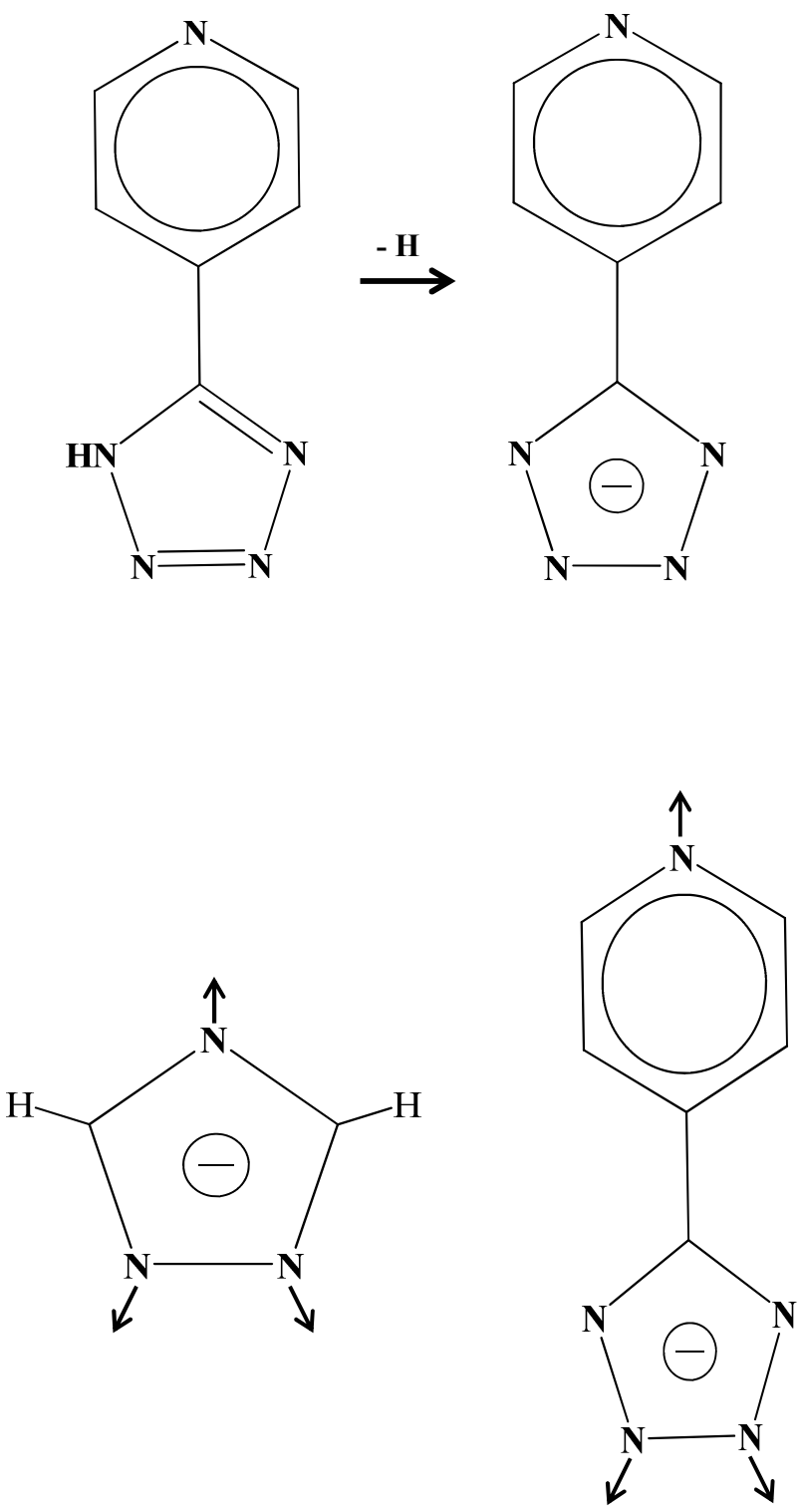

Scheme 1.6.

materials.[166] Upon incorporation into the metal oxide framework, fluoride replaces oxo groups within the coordination sphere of the metal center resulting in changes in the charge and structure of the metal-oxyfluoride subunit. Investigations of both molybdenum and vanadium oxyfluoride materials have uncovered a vast structural chemistry.[167] Specifically, uptake of fluoride into the oxovanadium and oxomolybdenum organophosphonates has been shown to result in unusual structural complexity due to the altered anionic charge of the metal-diphosphonate unit, as well as enhanced thermal stability of the fluorinated products.[71,81,168-181]

1.6 Hydrothermal Synthesis

Hydrothermal synthesis provides a useful technique for the preparation of hybrid organic-inorganic materials,[182-187] exploiting the self-assembly of soluble precursors in the formation of the product. Hydrothermal reactions are carried out between 100 ^{o}C and 200 ^{o}C under autogenous pressure greater than 1 atm, under which conditions the reduced viscosity of water favors crystal growth from solution. The increased temperature and pressure aids in the solubilizing of starting materials, allowing the introduction of a variety of organic and inorganic structure-directing or charge-balancing components regardless of differences in solubilities. However, the conditions are relatively mild to support retention of the structural elements of all reactants in the final product phases. Several reaction parameters are easily varied including temperature, crystallization time, solution pH, identity and ratios of starting materials, and additives.

1.7 General Research Considerations

This work encompasses a detailed investigation of the synthesis and structures of polyoxomolybdate materials including the design and synthesis of hybrid organic-inorganic materials constructed from various polyoxomolybdate anionic units and secondary metal-ligand units incorporating binucleating and multinucleating secondary ligands. In addition to the structural chemistry, thermal behavior and magnetic properties were also examined. A number of structural determinants were revealed, including the tether length of the organic component within diphosphonate ligands, the orientation and number of nitrogen donors of the secondary ligand, the effect of fluoride incorporation and the oxidation state of the secondary metal cation. Additionally, the variation of hydrothermal reaction conditions such as temperature, pH, stoichiometries, crystal growth time, and the use of mineralizing agents may influence the identity of the product. The exploration of synthetic conditions required for the preparation of hybrid organic-inorganic materials is essential to our understanding of how these compounds form. The ability to control structural aspects of the product will lead to the ability to predict the outcome of these syntheses, and will finally result in the deliberate exploitation of properties for specific applications.

The ability of the giant polyoxomolybdate cluster Mo-132 to exchange ligands coordinated to the molybdate framework is dependent upon the presence of a secondary ligand anion and the pH of the reaction solution. Through careful control of the solution pH, a range of clusters incorporating various ratios of ligands can be crystallized to expand the scope of anionic charges these clusters may exhibit. Concerning their potential applications to different aspects of chemistry and materials science, the

preparation of clusters of similar dimensions with assorted overall charges will aid in the study of electrostatic effects in solutions containing such ordered nanoscopic spherical clusters with metal nanoparticles.

1.8 References

[1] M. Jansen, *Nachrichten Chem.* **2007**, *55*, 622.

[2] L. A. D. Carlos, R. A. S. Ferreira, V. de Zea Bermudey, Hybrid Materials for Optical Applications in *Hybrid Materials*, G. Kickelbick, ed., Wiley-VCH Verlag GmbH & Co. KGaA, Weinheim, Germany, **2007**, 337.

[3] P. Rabu, M. Drillon, *Adv. Eng. Mater.* **2003**, *5*, 189.

[4] S. G. Mackay, O. S. Wengner, K. W. Kramer, H. U., Gudel, *Curr. Opin. Solid State & Mater. Sci.* **2003**, *6*, 487.

[5] C. T. Kresge, S. S. Dhingra, Molecular Sieves, *Kirk-Othmer Separation Technology*, 2nd Ed., **2008**, *2*, 732.

[6] S. M. Auerbach, K. A. Carrado, P. K. Dutta, *Handbook of Zeolite Science and Technology*, Marcel Dekker, Inc., New York, **2003**.

[7] *Metal Oxides: Chemistry and Applications*, J. L. G. Fierro, ed., CRC Press, Boca Raton, FL, **2005**.

[8] *Inorganic Materials*, D. W. Bruce, D. O'Hare, eds., Wiley, Chichester, **1992**.

[9] A. K. Cheetham, *Science* **1994**, *264*, 794.

[10] W. Büchner, R. Schliebs, G. Winter, K. H. Büchel, *Industrial Inorganic Chemistry*, VCH, New York, **1989**.

[11] W. H. McCarroll, Oxides: Solid State Chemistry in *Encyclopedia of Inorganic Chemistry*, R. B. King, ed., Joh Wiley and Sons, New York, **1994**, *6*, 2903.

[12] G. H. Haertling, Piezoelectric and Electrooptic Ceramics in *Ceramic Materials for Electronics*, 2nd Ed., R. C. Buchanan, ed., Marcel Dekker, New York, **1991**, 129.

[13] H. W. Leverenz, *Luminescence of Solids*, Wiley, New York, **1980**.

[14] A. Clearfield, *Chem. Rev.* **1988**, *88*, 125.

[15] J. M. Newsam, *Zeolites, Solid State Chemistry: Compounds*, A. K. Cheetham, P. Day, eds., Clarendon Press, Oxford, **1992**, 234.

[16] A. F. Wells, *Structural Inorganic Chemistry*, 6th Ed., Oxford University Press, New York, **1987**.

[17] N. N. Greenwood, A. Earnshaw, *Chemistry of the Elements*, 2nd Ed., Butterworht-Heinemann, Oxford, England, **1997**.

[18] J. R. Smyth, S. D. Jacobson, R. M. Hazen, *Rev. Mineral. Geochem.* **2001**, *41*, 157.

[19] B. Mason, *Principles of Geochemistry*, 3rd Ed., Wiley, New York, **1966**.

[20] G. Sen, *Earth's Materials: Minerals and Rocks*, Prentice Hall, Upper Saddle River, NJ, **2001**.

[21] L. L. Hench, *Materials Chemistry, an Emerging Discipline*, L. V. Interrante, L. A. Casper, A. B. Ellis, eds., ACS Series 245, **1995**, 523.

[22] *Handbook of Biomineralization: Biomimetic and Bioinspired Chemistry*, S. Mann, ed., Wiley-VCH Verlag GmbH & Co. KGaA, Weinheim, Germany, **2007**.

[23] H. L. Ngo, A. G. Hu, W. B. Lin, *J. Col. Catal. A* **2004**, *215*, 177.

[24] O. R. Evans, H. L. Ngo, W. B. Lin, *J. Am. Chem. Soc*. **2001**, *123*, 10395.

[25] A. Vioux, J. le Bideau, P. H. Mutin, D. Leclercq, *New Aspects in Phosphorus Chemistry IV* **2004**, *232*, 145.

[26] C. Sanchez, B. Lebeau, F. Chaput, J. P. Boilet, *Adv. Mater*. **2003**, *15*, 1969.

[27] O. R. Evans, W. B. Lin, *Chem. Mater*. **2001**, *13*, 3009.

[28] P. Jannasch, *Curr. Opin. Coll. Inter. Sci*. **2003**, *8*, 96.

[29] A. Javaid, M. P. Hughey, V. Varutbangkul, D. M. Ford, *J. Membrane Sci*. **2001**, *187*, 141.

[30] I. Honma, S. Nomura, H. Nakajima, *J. Membrane Sci*. **2001**, *185*, 83.

[31] A. C. Sudik, A. R. Millward, N. W. Ockwig, A. P. Côté, J. Kim, O. M. Yaghi, *J. Am. Chem. Soc*. **2005**, *127*, 7110.

[32] J. L. C. Rowsell, A. R. Millward, K. S. Park, O. M. Yaghi, *J. Am. Chem. Soc*. **2005**, *126*, 5666.

[33] R. Kitaura, S. Kitagawa, Y. Kubota, T. C. Kobayashi, K. Kindo, Y. Mita, A. Matsuo, M. Kobayashi, H. C. Chang, T. C. Ozawa, M. Suzuki, M. Sakata, M. Takata, *Science* **2002**, *298*, 2358.

[34] A. Lin, M. A. Meyers, *Mater. Sci. and Eng*. **2005**, *A390*, 27.

[35] J. F. V. Vincent, P. Owers, *J. Zool. (A)* **1986**.

[36] G. Mayer, M. Sarikaya, *Exp. Mech*. **2002**, *42*, 395.

[37] L. F. Kuhn-Spearing, H. Kessler, E. Chateau, R. Ballarin, A. H. Heuer, *J. Mater. Sci*. **1996**, *31*, 6583.

[38] S. I. Stupp, P. V. Braun, *Science* **1997**, *277*, 1242.

[39] H. Maekawa, *Materia* **2006**, *45*, 359.

[40] S. L. Suib, *Ann. Rev. Mater. Sci*. **1996**, *26*, 135.

[41] M. E. Davis, *CATTECH* **1997**, *1*, 19.

[42] R. F. Lobo, S. I. Zones, M. E. Davis, *J. Inclusion Phenom. Mol. Recog. Chem*. **1995**, *21*, 47.

[43] H. Imai, *Topics Curr. Chem*. **2007**, *270* (Biomineralization I), 43.

[44] H. Cölfen, S. Mann, *Angew. Chem., Int. Ed. Engl*. **2003**, *42*, 2350.

[45] G. J. de A. A. Soler-Illia, C. Sanchez, B. Lebeau, J. Patarin, *Chem. Rev*. **2002**, *102*, 4093.

[46] C. Janiak, *Dalton Trans*. **2003**, 2781 and references therein.

[47] D. B. Mitzi, *Dalton Trans*. **2001**, 1.

[48] B. Wang, A. P. Côté , H. Furukawa, M. O'Keeffe, O. M. Yaghi, *Nature* **2008**, *453*, 207.

[49] R. Banerjee, A. Phan, B. Wang, C. Knobler, H. Furukawa, M. O'Keeffe, O. M. Yaghi, *Science* **2008**, *319*, 939.

[50] G. Férey, *Stud. Surf. Sci. Catal*. **2007**, *170A*, 66 and references therein.

[51] G. Férey, *Stud. Surf. Sci. Catal*. **2007**, *168*, 327.

[52] G. Férey, *Chem. Soc. Rev*. **2008**, *37*, 191.

[53] Y. Kubota, M. Takata, T. C. Kobayashi, S. Kitagawa, *Coord. Chem. Rev*. **2007**, *251*, 2510.

[54] B. Moulton, M. J. Zaworotko, *Curr. Opinion Solid State & Mater. Sci*. **2002**, *6*, 117.

[55] M. J. Zaworotko, *Crystal Engineering: The Design and Application of Functional Solids*, K. R. Seddon, M. Zaworotko, eds., NATO Series C, **1999**, *539*, 383.

[56] L. Ma, J. Y. Lee, J. Li, W. Lin, *Inorg. Chem*. **2008**, *47*, 3955.

[57] W. J. Rieter, K. M. L. Taylor, W. Lin, *J. Am. Chem. Soc*. **2007**, *129*, 9852.

[58] H. J. Choi, M. Dinca, J. R. Long, *J. Am. Chem. Soc*. **2008**, *130*, 7848.

[59] M. Dinca, A. Dailly, C. Tsay, J. R. Long, *Inorg. Chem*. **2008**, *47*, 11.

[60] M. Eddaoudi, J. F. Eubank, *Org. Nanostruct*. **2008**, 251.

[61] D. F. Sava, V. Ch. Kravtsov, F. Nouar, L. Wojtas, J. F. Eubank, M. Eddaoudi, *J. Am. Chem. Soc*. **2008**, *130*, 3768.

[62] D. W. Beck, *Zeolite Molecular Sieves*, John Wiley, New York, **1974**.

[63] *Verified Syntheses of Zeolitic Materials*, H. Robson, ed., 2nd revised edition, Elsevier, New York, **2001**.

[64] H. S. Sherry, *Handbook of Zeolite Science and Technology*, S. M. Auerbach, K. A. Carrado, P. K. Dutta, M. Dekker, eds., New York, 1007.

[65] International Symposium on Zeolite Microporous Crystals 2006, *Micropor. Mesopor. Mater*., **2007**, *101*, 1442.

[66] P. M. Forster, A. K. Cheetham, *Top, Catal*. **2003**, *24*, 79.

[67] P. J. Hagrman, D. Hagrman, J. Zubieta, *Angew. Chem. Int. Ed*. **1999**, *38*, 2638.

[68] D. Hagrman and J. Zubieta, *ACA Transactions* **1999**, *33*, 105.

[69] D. J. Chesnut, D. Hagrman, P. J. Zapf, R. P. Hammond, R. LaDuca, Jr., R. C. Haushalter, J. Zubieta, *Coord. Chem. Rev*. **1999**, *190–192*, 737.

[70] D. Hagrman, P. J. Hagrman, J. Zubieta, *Inorg. Chem. Comm*. **1999**, *21*, 225.

[71] E. Burkholder, J. Zubieta, *Inorg. Chim. Acta* **2004**, *357*, 279.

[72] E. Burkholder, J. Zubieta, *Inorg. Chim. Acta* **2004**, *357*, 301.

[73] E. Burkholder, V. Golub, C. J. O'Connor, J. Zubieta, *Inorg. Chem*. **2003**, *42*, 6729.

[74] D. G. Allis, R. S. Rarig, E. Burkholder, J. Zubieta, *J. Mol. Struct*. **2004**, *688*, 11.

[75] E. Burkholder, S. Wright, V. Golub, C. J. O'Connor, J. Zubieta, *Inorg. Chem*. **2003**, *42*, 7460.

[76] E. Burkholder, J. Zubieta, *Inorg. Chim. Acta*. **2004**, *357*, 1229.

[77] E. Burkholder, V. Golub, C. J. O'Connor, J. Zubieta, *Inorg. Chem. Comm*. **2004**, *7*, 363.

[78] T. Soumahoro, E. Burkholder, W. Ouellette, J. Zubieta, *Inorg. Chim. Acta* **2005**, *358*, 606.

[79] E. Burkholder, J. Zubieta, *Solid State Sci*. **2004**, *6*, 1421.

[80] E. Burkholder, J. Zubieta, *Inorg. Chim. Acta* **2005**, *358*, 116.

[81] E. Burkholder, V. Golub, C. J. O'Connor, J. Zubieta, *Inorg. Chem*. **2004**, *43*, 7014.

[82] N. G. Armatas, E. Burkholder, J. Zubieta, *J. Solid State Chem*. **2005**, *178*, 2430.

[83] R. S. Rarig, Jr., J. Zubieta, *J. Solid State Chem*. **2002**, *167*, 370.

[84] R. S. Rarig, J. Zubieta, *Polyhedron* **2003**, *22*, 177.

[85] R. S. Rarig Jr, L. Bewley, V. Golub, C. J. O'Connor, J. Zubieta, *Inorg. Chem. Comm*. **2003**, *6*, 539.

[86] R. C. Finn, E. Burkholder, J. Zubieta, *Persp. Supramol. Chem*. **2003**, *7*, 241

[87] R. S. Rarig, L. Bewley, E. Burkholder, J. Zubieta, *Ind. J. Chem*. **2003**, *42A*, 2235.

[88] D. G. Allis, E. Burkholder, J. Zubieta, *Polyhedron* **2004**, *23*, 1145.

[89] A. X. Tian, J. Ying, J. Peng, J. Q. Sha, Z. G. Han, J. F. Ma, Z. M. Su, N. H. Hu, H. Q. Jia, *Inorg. Chem*. **2008**, *47*, 3274.

[90] B. Botar, P. Köegerler, C. L. Hill, *Inorg. Chem*. **2007**, *46*, 5398.

[91] C. Sun, E. Wang, D. Xiao, H. An, L. Xu, *J. Mol. Struct*. **2005**, *741*, 149.

[92] Y. Q. Lan, S. L. Li, K. Z. Shao, X. L. Wang, Z. M. Su, *Dalton Trans*. **2008**, 3824.

[93] X. Zhao, D. Liang, S. Liu, C. Sun, R. Cao, C. Gao, Y. Ren, Z. Su, *Inorg. Chem*.

2008, *47*, 7133.

[94] V. Shivaiah, S. K. Das, *Inorg. Chem*. **2005**, *44*, 8846.

[95] S. Bareyt, S. Piligkos, B. Hasenknopf, P. Gouzerh, E. Lacote, S. Thorimbert, M. Malacria, *Angew. Chem., Int. Ed. Engl*. **2003**, *42*, 3404.

[96] Y. Xu, *Curr. Opin. Solid State Mater. Sci*. **1999**, *4*, 133.

[97] A. Clearfield, *Prog. Cryst. Growth Charact. Mater*. **1991**, *21*, 1.

[98] *Perspectives in the Solid State Coordination Chemistry of the Molybdenum Oxides*, M. T. Pope, A. Müller, eds., Kluwer Academic Publishers, Dordrecht, The Netherlands, **2001**.

[99] R. S. Rarig, P. Hagrman, J. Zubieta, *Solid State Sci*. **2002**, *4*, 77.

[100] M. T. Pope, *Heteropoly and Isopoly Oxometalates,* Springer, New York, **1983**.

[101] Special thematic issue on polyoxometalates: C. L. Hill, ed., *Chem. Rev*., **1998**, *98*, 1.

[102] *Polyoxometalate Chemistry: From Topology Via Self-Assembly to Applications*, M. T. Pope, A. Müller, eds., Kluwer Academic, Dordrecht, The Netherlands, **2001**.

[103] *Polyoxometalates: From Platonic Solids to Anti-Retroviral Activity*, M.T. Pope, A. Müller, eds., Kluwer Academic, Dordrecht, The Netherlands, **1994**.

[104] J. P. Jolivet, *Metal Oxide Chemistry and Synthesis: From Solution to Solid State*, John Wiley, New York, **2000**.

[105] D. E. Katsoulis, *Chem. Rev*. **1998**, *98*, 359.

[106] K. Pavani, S. E. Lofland, K. V. Ramanujachary, A. Ramanan, *Eur. J. Inorg. Chem.* **2007**, 568.

[107] A. Baiker, P. Dollenmeier, A. J. Reller, *Catal*. **1987**, *103*, 394.

[108] T. Ressler, J. Wienold, R. E. J. Jentoft, *Catal*. **2002**, *210*, 67.

[109] T. Yamase, J. Chem. Soc., *Dalton Trans*. **1985**, 2585.

[110] T. Yamase, M. T. Pope, *Polyoxometalate Chemistry for Nanocomposites Design*, Kluwer Academic Publishers, Dordrecht, The Netherlands, **2002**.

[111] D. G. Allis, R. S. Rarig, E. Burkholder, J. Zubieta, *J. Mol. Structure* **2004**, *688*, 11.

[112] α-molybdate: (a) V. W. Day, M. F. Fredrich, W. G. Klemperer, W. Shum, *J. Am. Chem. Soc*. **1977**, *99*, 952; (b) W. Yang, C. Lu, H. Zhuang, *J. Chem. Soc., Dalton Trans.* **2002**, 2879.

[113] β-molybdate: (a) X. M. Lu, W. J. Li, X. A. Mao, *Jiegou Huaxe* **2000**, *19*, 163; (b) R. Z. Wang, J. Q. Xu; G. Y. Yang, W. M. Bu, Y. H. Xing, D. M. Li, S. Q. Liu, L. Ye, Y. G. Fan, *Polish J. Of Chem*. **1999**, *73*, 1909; (c) X. M. Lu, S. C. Liu, Y. Liu, X. H. Bu, S. L. Hong, *Huaxue Xuebao* **1997**, *55*, 1009; (d) A. Kitamura, T. Ozeki, A. Yagasaki, *Inorg. Chem*. **1997**, *36*, 4275; (e) C. J. Gomez-Garcia, E. Coronado, S. Triki, L. Ouahab, P. Delhar, *Adv. Mater*. **1993**, *5*, 283; (f) D. Attanasio, M. Bonamico, V. Fores, L. Suber, *J. Chem. Soc., Dalton Trans*. **1992**, 2523; (g) X. Wang, X. Xu, Q. Wang, Y. Zhai, *Polyhedron* **1992**, *11*, 1423; (h) J. Fuchs, I. Bruedgam, *Z. Naturforsch. B* **1977**, *32B*, 853; (i) W. G. Klemperer, W. Shum, *J. Am. Chem. Soc.* **1976**, *98*, 8291; (j) J. Fuchs, H. Hartl, *Angew. Chem.* **1976**, *88*, 385.

[114] γ-molybdate: (a) M. C. Niven, J. J. Cruywagen, J. B. B. Heyns, *J. Chem. Soc., Dalton Trans*. **1991**, 2007; (b) M. Inoue, T. Yamase, *Bull. Chem. Soc. Japan* **1995**, *68*, 3055.

[115] δ-molybdate: R. Xi, B. Wang, K. Isobe, T. Nishioka, K. Toriumi, Y. Ozawa, *Inorg. Chem.* **1994**, *33*, 833.

[116] R. N. Devi, J. Zubieta, *Inorg. Chim. Acta* **2002**, *332*, 72.

[117] R. S. Rarig, J. Zubieta, *J. Solid State Chem*. **2002**, *167*, 370.

[118] C. Z. Lui, C. D. Wu, H. H. Zhuang, J. S. Huang, *Chem. Mater.* **2002**, *14*, 2649.

[119] R. S. Rarig, L. Bewley, E. Burkholder, J. Zubieta, *Ind. J. Chem*. **2003**, *42A*, 2235.

[120] J. Q. Xu, R. Z. Wang, G. Y. Yang, Y. H. Xing, D. M. Li, W. M. Bu, L. Ye, Y. G. Fan, G. D. Yang, Y. Xing, Y. H. Lin, H. Q. Jia, *Chem. Commun.* **1999**, 983.

[121] D. G. Allis, E. Burkholder, J. Zubieta, *Polyhedron* **2004**, *23*, 1145.

[122] A. J. Bridgeman, *J. Phys. Chem. A* **2002**, *106*, 12151.

[123] Y. Xu, J. Q. Xu, K. L. Zhang, Y. Zhang, X. Z. You, *Chem. Commun*. **2000**, 153.

[124] N. Nyman, F. Bonhomme, T. M. Alam, A. M. Rodriguez, B. R. Cherry, J. L. Krumhansl, T. M. Nenoff, A. M. Sattler, *Science* **2002**, *297*, 996.

[125] C. Ritchie, E. Burkholder, P. Kögerler, L. Cronin, *Dalton Trans*. **2006**, 1712.

[126] R. N. Devi, E. Burkholder, J. Zubieta, *Inorg. Chim. Acta* **2003**, *348*, 150.

[127] P. Q. Zheng, Y. P. Ren, L. S. Long, R. B. Huang, L. S. Zheng, *Inorg. Chem*. **2005**, *44*, 1190.

[128] L. C. W. Baker, J. S. Figgis, *J. Am. Chem. Soc*. **1970**, *92*, 3794.

[129] M. Che, C. O. Bennett, *Adv. Catal.* **1989**, *36*, 55.

[130] A. Müller, E. Beckmann, H. Bögge, M. Schmidtmann, A. Dress, *Angew. Chem. Int. Ed.* **2002**, *41*, 1162.

[131] A. Müller, S. Roy, *The Chemistry of Nanomaterials*: *Syntheses, Properties and Applications*, C. N. R. Rao, A. Müller, A. K. Cheetham, eds., Wiley-NCH Verlag GmbH & Co. K Ga A, Weinheim, **2004**, 452.

[132] A. Müller, P. Kögerler, H. Bögge, *Structure and Bonding* **2000**, *96*, 203.

[133] D. G. Kurth, S. Liu, D. Volkmer, *Polyoxometalate Molecular Science*, J. J. Borras-Almenar, E. Coronado, A. Müller, M. T. Pope, eds., NATO Science Series II, Vol. 98, Kluwer Academic Publishers, **2003**, 441.

[134] D. L. Long, L. Cronin, *Chem. Eur. J.* **2006**, *14*, 2698 and references therein.

[135] D. Hagrman, C. Zubieta, D. J. Rose, J. Zubieta, *Angew. Chem., Int. Ed. Engl*. **1997**, *36*, 873.

[136] J. Niu, D. Guo, J. Zhao, J. Wang, *New J. Chem*. **2004**, *28*, 980, and references therein.

[137] S. Jones, H. Liu, W. Ouellette, K. Schmidtke, C. J. O'Connor, J. Zubieta, *Inorg. Chem. Comm*. **2010**, *13*, 491.

[138] W. Kwak, M. T. Pope, T. F. Scully, *J. Am. Chem. Soc*. **1975**, *97*, 5735.

[139] N. G. Armatas, D. G. Allis, A. Prosvirin, G. Carnutu, C. J. O'Connor, K. Dunbar, J. Zubieta, *Inorg. Chem.* **2008**, *47*, 832.

[140] R. C. Finn, J. Zubieta, *Inorg. Chem.* **2001**, *40*, 2466.

[141] R. C. Finn, E. Burkholder, J. Zubieta, *Chem. Commun.* **2001**, 1852.

[142] K. T. Potts, *Chem. Rev*. **1961**, *61*, 87.

[143] L. N. Dawe, L. K. Thompson, *Dalton Trans*. **2008**, 3610.

[144] J. P. Zhang, Y. Y. Lin, X. C. Huang, X. M. Chen, *J. Am. Chem. Soc*. **2005**, *127*, 5495.

[145] J. P. Zhang, S. L. Zheng, X. C. Huang, X. M. Chen, *Angew. Chem., Int. Ed*. **2004**, *43*, 206.

[146] S. Ferrer, F. Lloret, I. Bertomeu, G. Alzuet, J. Borras, S. Garcia-Granda, M. Liu-González, J. G. Haasnoot, *Inorg. Chem*. **2002**, *41*, 5821.

[147] J. H. Zhou, R. M. Cheng, Y. Song, Y. Z. Li, Z. Yu, X. T. Chen, Z. L. Xue, X. Z. You, *Inorg. Chem*. **2005**, *44*, 8011 and references therein.

[148] M. Du, X. J. Jiang, X. J. Zhao, *Chem. Commun*. **2005**, 5521.

[149] J. P. Zhang, Y. Y. Lin, W. X. Zhang, X. M. Chen, *J. Am. Chem. Soc*. **2005**, *127*, 14162.

[150] P. J. Steel, *Coord. Chem. Rev*. **1990**, *106*, 227.

[151] J. P. Zhang, Y. Y. Lin, X. C. Huang, X. M. Chen, *J. Am. Chem. Soc*. **2005**, *17*, 5495.

[152] W. Ouellette, A. V. Prosvirin, J. Valeich, K. R. Dunbar, J. Zubieta, *Inorg. Chem*. **2007**, *46*, 9067.

[153] J. P. Zhang, Y. Y. Lin, X. C. Huang, X. M. Chen, *Cryst. Growth Des*. **2006**, *6*, 519.

[154] M. F. Wu, F. K. Zheng, G. Xu, A. Q. Wu, Y. Li, H. F. Chen, S. P. Guo, F. Chen, Z. F. Liu, G. C. Guo, J. S. Huang, *Inorg. Chem. Comm*. **2010**, *13*, 250.

[155] A. Demessence, D. M. D'Alessandro, M. L. Foo, J. R. Long, *J. Am. Chem. Soc*. **2009**, *131*, 8784.

[156] J. P. Zhang, X. M. Chen, *J. Am. Chem. Soc*. **2008**, *130*, 6010.

[157] Q. X. Jia, Y. Q. Wang, Q. L. Wang, E. Q. Gao, *Chem. Commun*. **2008**, 4894.

[158] A. Rodriguez, R. Kivekaes, E. Colacio, *Chem. Commun*. **2005**, 5228.

[159] H. Zhao, Z. R. Qu, H. Y. Ye, R. G. Xiong, *Chem. Soc. Rev*. **2008**, *37*, 84.

[160] M. Dinc¸ a, J. R. Long, *Angew. Chem. Int. Ed*. **2008**, *47*, 6766.

[161] M. Dinc¸ a, A. Dailly, J. R. Long, *Chem. Eur. J*. **2008**, *14*, 10280.

[162] S. Horike, M. Dincá, K. Tamaki, J. R. Long, *J. Am. Chem. Soc*. **2008**, *130*, 5854.

[163] L. J. Murray, M. Dincá, J. R. Long, *Chem. Soc. Rev*. **2009**, *38*, 1294.

[164] Y. Li, G. Xu, W. Q. Zou, M. S. Wang, F. K. Zheng, M. F. Wu, H. Y. Zeng, G. C. Guo, J. S. Huang, *Inorg. Chem*. **2008**, *47*, 7945.

[165] W. Ouellette, S. Jones, J. Zubieta, *Cryst. Eng. Com.* **2011**,*13*, 4457.

[166] W. Ouellette, M. H. Yu, C. J. O'Connor, J. Zubieta, *Inorg. Chem.* **2006**, *45*, 7628.

[167] G. A. Senchyk, A. B. Lysenko, H. Krautschied, K. V. Domasevitch, *Inorg. Chem. Comm.* **2011**, *14*, 1365.

[168] D. Riou, G. Férey, *J. Solid State Chem*. **1994**, *111*, 422.

[169] D. Riou, F. Taulelle, G. Férey, *Inorg. Chem*. **1996**, *35*, 6392.

[170] G. Bonavia, R. C. Haushalter, J. Zubieta, *J. Solid State Chem*. **1996**, *126*, 292.

[171] W. Ouellette, V. Golub, C. J. O'Connor, J. Zubieta, *Dalton Trans*. **2005**, 291.

[172] W. Ouellette, V. Golub, C. J. O'Connor, J. Zubieta, *J. Solid State Chem*. **2007**, *180*, 2500.

[173] W. Ouellette, M. H. Yu, C. J. O'Connor, J. Zubieta, *Inorg. Chem*. **2006**, *45*, 7628.

[174] T. Mahenthirarajah, Y. Li, P. Lightfoot, *Inorg. Chem*. **2008**, *47*, 9097.

[175] F. H. Aidoudi, P. J. Byrne, P. K. Allan, S. J. Teat, P. Lightfoot, R. E. Morris, E. Russell, *Dalton Trans*. **2011**, *40*, 4324.

[176] F. A. Himeur, P. K. Allan, S. J. Teat, R. J. Goff, R. E. Morris, P. Lightfoot, *Dalton Trans*. **2010**, *39*, 6018.

[177] K. Adil, M. Leblanc, V. Maisonneuve, P. Lightfoot, *Dalton Trans*. **2010**, *39*, 5983.

[178] D. W. Aldous, A. M. Z. Slawin, P. Lightfoot, *J. Solid State Chem*. **2008**, *181*, 3033.

[179] D. W. Aldous, N. F. Stephens, P. Lightfoot, *Dalton Trans*. **2007**, 4207.

[180] D. W. Aldous, N. F. Stephens, P. Lightfoot, *Dalton Trans*. **2007**, 2271.

[181] N. F. Stephens, M. Buck, P. Lightfoot, *J. Mater. Chem*. **2005**, *15*, 4298.

[182] S. Feng, R. Xu, *Acc. Chem. Res.* **2001**, *34*, 239.

[183] J. Zubieta, Solid State Methods, Hydrothermal in *Comprehensive Coordination Chemistry II*, **2003**, *1*, p. 697.

[184] J. Gopalakrishnan, N. S. P. Bhuvanesh, K. K. Rangan, *Curr. Opin. Solid State Mater. Sci.* **1996**, *1*, 285.

[185] J. Gopalakrishnan, *Chem. Mater*. **1995**, *7*, 1265.

[186] A. Rabenau, *Angew. Chem., Int. Ed. Engl.* **1985**, *24*, 1026.

[187] A. Stein, S. W. Keller, T. E. Mallouk, *Science* **1993**, *259*, 1558.

Chapter 2

Solid State Coordination Chemistry: Structural Influence of Diphosphonate Tether Length on Bimetallic Copper-Molybdodiphosphonates

2.1 Introduction

The significant interest in the synthesis of inorganic oxides is attributed to their structural diversity and potential applications in materials science and chemistry.[1,2] One approach to the synthesis of novel inorganic oxide materials exploits organic components as structure-directing agents of the inorganic substructure. The organic molecule acts as a bridge between metal clusters or metal cations, thereby increasing the complexity of the structure, which results in increased functionality of the material.[3,4] These hybrid organic-inorganic materials may possess unique properties generated from the combination of inorganic and organic components.[5-7]

One strategy for the synthesis of such materials employs the building block approach of linking molecular oxide clusters through organic tethers or secondary metal-ligand subunits.[8-15] Transition metal organophosphonates have been studied for their ability to form one-, two-, and three-dimensional frameworks by achieving incorporation of an organic moiety through direct derivatization of the tetrahedral phosphate component.[16] The oxomolybdenum-organophosphonate family of structures is characterized by polyoxomolybdophosphonate clusters that can be tethered through the organic chains of diphosphonate groups.[17-21] Such metal-diphosphonate materials may be tailored by the modification of tether type and length of the diphosphonate ligand, as well as the introduction of additional functionality.[22-27]

One-dimensional anionic structures are formed by the tethering of the persistent $\{Mo_5O_{15}(O_3PR)_2\}^{4-}$ clusters[19] through a variety of organic chains (**Scheme 2.1(a)**). Inclusion of a cationic secondary metal-ligand component provides both charge compensation and additional intimate structural subunits that coordinate to surface oxo

groups of the oxomolybdate cluster through available oxophilic metal sites. Increased dimensionality may be achieved through the incorporation of a binucleating secondary ligand, through which the secondary metal-ligand units can bridge oxomolybdate-organodiphosphonate chains (**Scheme 2.1(b)**).

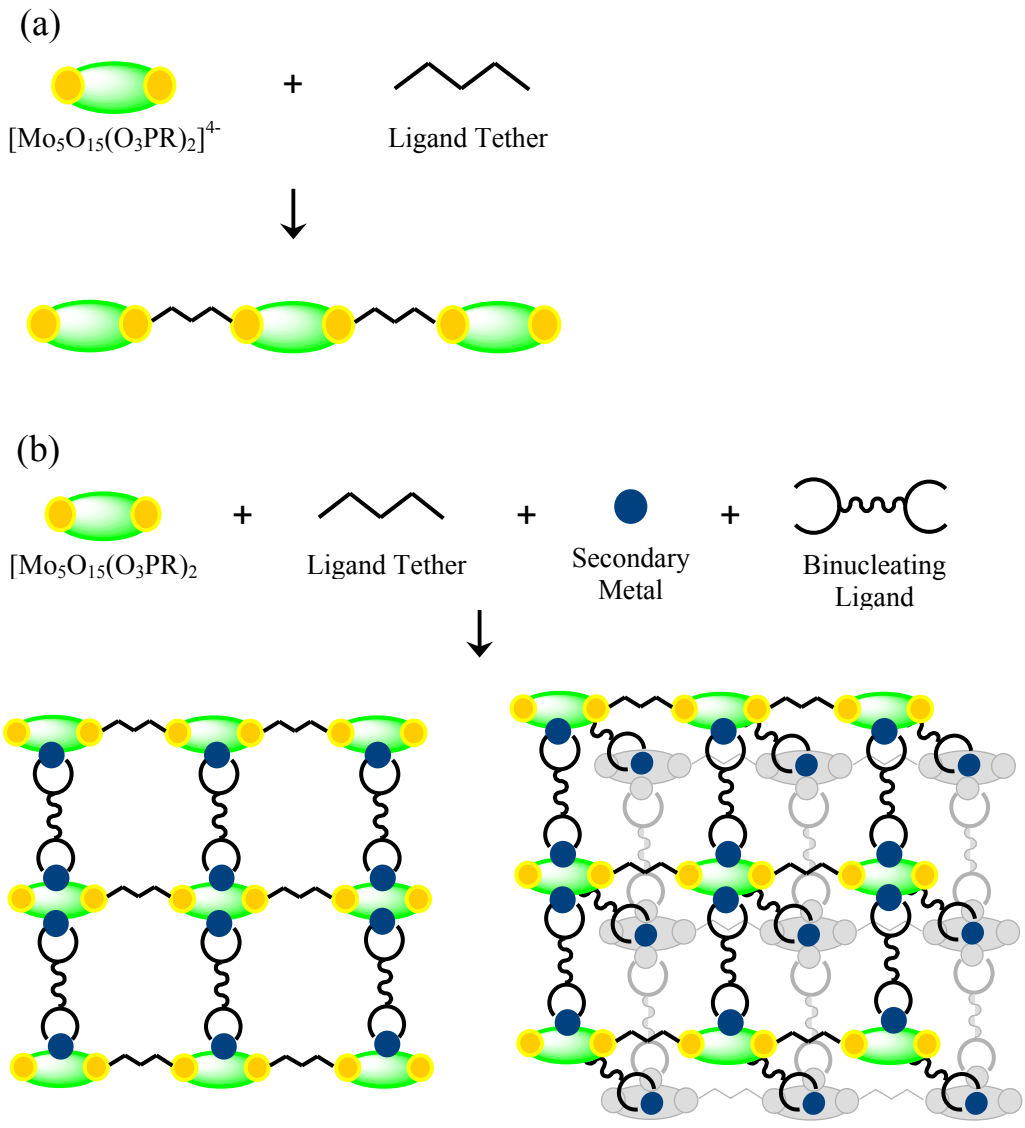

Scheme 2.1.

Several factors influence the structure of the framework produced, including the carbon chain length of the diphosphonate ligand, and the identity of both the ligand and the metal in the secondary metal-ligand component. Much work has focused on copper(II) as the secondary metal as a result of its versatility evidenced by the ability to adopt Jahn-Teller distorted "4+1" and "4+2" geometries. Specifically, copper-organoimine units are particularly effective charge compensating components with the capacity to coordinate to oxo groups of the molybdophosphonate clusters. Previous investigations have shown that the $\{Mo_5O_{15}(O_3PR)_2\}^{4-}$ motif is maintained within materials incorporating copper-bipyrimidine[28] (bpy) and copper-tetrapyridylpyrazine[18,29] (tpyprz) secondary units.

The complex structures of the Cu(II)-tpyprz/polyoxomolybdodiphosphonate family generally derive from the linking of $\{Mo_5O_{15}(O_3PR)_2\}_n^{4n-}$ chains through $\{Cu_2(tpyprz)\}^{4+}$ rods, an observation that encouraging us to investigate the structural consequences of further modifying the dimensions of the binucleating organoimine ligand (**Scheme 2.2**). The distance between the donor groups of the ligand can be expanded through the use of phenyl-bridged ligands such as 2,2':4',4":2",2"'-quarterpyridyl-6',6"-di-2-pyridine (bisterpy) to form expanded structures with layers of polyoxomolybdodiphosphonate chains linked via the rod-like Cu(II)-bisterpy units in a fashion reminiscent of the "pillared" layer prototypes.

Hydrothermal synthesis provided the novel Cu(II)-bisterpy/polyoxomolybdodiphosphonate materials $[\{Cu_2(bisterpy)(H_2O)\}Mo_5O_{15}\{O_3P(CH_2)_4PO_3\}]\bullet 4.5H_2O$ (**1**•$4.5H_2O$) and $[\{Cu_2(bisterpy)(H_2O)_2\}Mo_5O_{15}\{O_3P(CH_2)_5PO_3\}]$ (**2**).

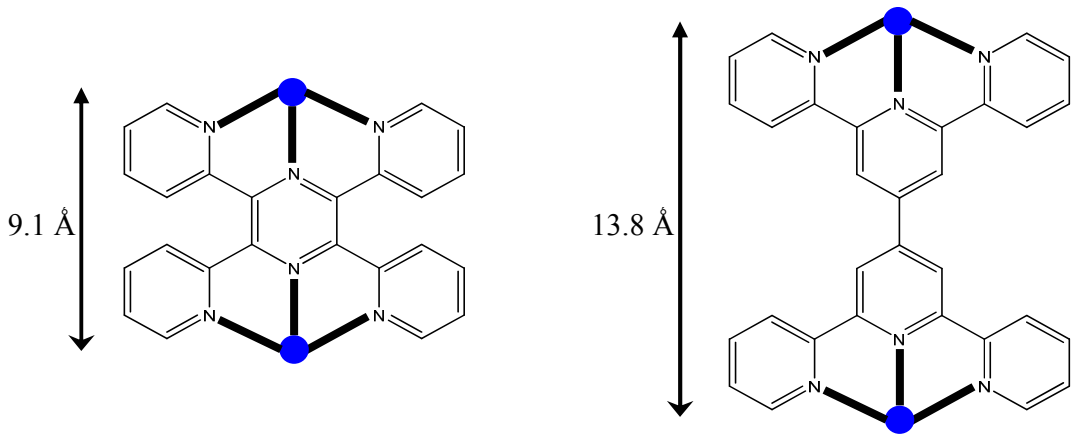

Scheme 2.2.

2.2 Experimental Section

All chemicals were used as obtained without further purification. Molybdenum(VI) Oxide (99.5%) was purchased from Alfa Aesar. Cupric Acetate was purchased from Baker. The diphosphonate ligands 1,4-butylenediphosphonic acid and 1,5-pentylenediphosphonic acid were synthesized according to methods reported in the literature,[30] as was the 2,2':4',4":2",2"'-quarterpyridyl-6',6"-di-2-pyridine (bisterpy) ligand.[31] All syntheses were carried out in 23mL poly(tetrafluroethylene) lined stainless steel containers under autogenous pressure. The pH of the solutions were measured both prior to and following heating using *color pHast*® pH sticks. Water was distilled above 3.0MΩ in-house using a Barnstead Model 525 Biopure Distilled Water Center.

2.2.1 Synthesis of $[\{Cu_2(bisterpy)(H_2O)\}Mo_5O_{15}\{O_3P(CH_2)_4PO_3\}]\bullet 4.5H_2O$ ($1\bullet 4.5H_2O$)

A solution of cupric acetate (0.045g, 0.2263mmol), molybdenum(VI) oxide (0.087g, 0.6034mmol), bisterpy (0.050g, 0.1078mmol), 1,4-butylenediphosphonic acid

(0.059g, 0.2694mmol), H_2O (10.00g, 556mmol), and HF (0.300mL, 17.24mmol) with the mole ratio 2.10:5.60:1.00:2.50:5157.70:159.93 was stirred briefly before heating to 150°C for 48hrs with initial and final pH values of 1.5 and 1.0, respectively. Blue crystals were isolated in 30% yield that were suitable for X-ray diffraction. IR (KBr pellet, cm^{-1}): 3423(m), 1606(m), 1561(m), 1476(m), 1409(m), 1248(w), 1159(w), 952(m), 912(s), 793(m), 671(w), 580(m).

2.2.2 Synthesis of [{Cu_2(bisterpy)(H_2O)$_2$}Mo_5O_{15}{$O_3P(CH_2)_5PO_3$}] (2)

A solution of cupric acetate (0.045g, 0.2263mmol), molybdenum(VI) oxide (0.087g, 0.6034mmol), bisterpy (0.050g, 0.1078mmol), 1,5-pentylenediphosphonic acid (0.062g, 0.2694mmol), H_2O (10.00g, 556mmol), and HF (0.300mL, 17.24mmol) with the mole ratio 2.10:5.60:1.00:2.50:5157.70:159.93 was stirred briefly before heating to 150°C for 48hrs with initial and final pH values of 1.5. Blue crystals were isolated in 50% yield that were suitable for X-ray diffraction. IR (KBr pellet, cm^{-1}): 3447(s), 3067(w), 2928(w), 1604(m), 1560(m), 1475(m), 1413(m), 1126(w), 1100(s), 1037(m), 973(m), 933(s), 906(s), 887(m), 870(m), 779(w), 671(s), 557(m).

2.2.3 X-ray Crystallography

Crystallographic data of **1** and **2** were collected at low temperature (90K). Data for compound **1** were collected on a Bruker KAPPA APEX DUO diffractometer using Mo-K_α radiation (λ = 0.71073Å) equipped with an APEX II CCD system.[32] Data for compound **2** were collected on a Bruker P4 diffractometer using Mo-K_α radiation (λ = 0.71073Å) equipped with a SMART CCD system.[33] The data were corrected for Lorentz and polarization effects,[34] and adsorption corrections were made using SADABS.[35] The structures were solved by direct methods and refinements were made using the

SHELXTL[36] crystallographic software. After first locating all of the nonhydrogen atoms from the initial solution of each structure, the models were refined against F^2 using first isotropic and then anisotropic thermal displacement parameters until the final value of Δ/σ_{max} was less than 0.001. Hydrogen atoms were introduced in calculated positions and refined isotropically. Neutral atom scattering coefficients and anomalous dispersion corrections were taken from the *International Tables*, Vol. C. Crystallographic details for the structures of **1** and **2** are summarized in **Table 2.1**.

2.2.4 Magnetism

Magnetic data were recorded on polycrystalline samples in the 2-300 K temperature range using a Quantum Design MPMS-5S SQUID spectrometer. Calibrating and operating procedures have been reported previously.[37] The temperature-dependent magnetic data were obtained at a magnetic field of H = 1000 Oe.

2.2.5 Thermal Gravimetric Analysis

Thermogravimetric studies were performed in an Auto TGA Q500 instrument under a 50 mL/min flow of synthetic air. The temperature was ramped from 25 to 800 ^{o}C at a rate of 5 ^{o}C/min for the decomposition.

2.3 Results and Discussion

2.3.1 Synthesis and Infrared Spectroscopy

Hydrothermal synthesis has been extensively studied as a method for the preparation of organic-inorganic hybrid materials through use of milder conditions that allow retention of the structural elements of the reactants in the final product phases.[38-43] The hydrothermal reactions of MoO_3, $Cu(CH_3CO_2)_2 \cdot H_2O$, the appropriate diphosphonic

Table 2.1. Summary of crystallographic data for the structures of [{Cu_2(bisterpy)(H_2O)}Mo_5O_{15}{$O_3P(CH_2)_4PO_3$}]•4.5H_2O (**1**), [{Cu_2(bisterpy)(H_2O)$_2$}Mo_5O_{15}{$O_3P(CH_2)_5PO_3$}] (**2**), [{Cu_2(bisterpy)(OH)}$Mo_2F_3O_4${$O_3P(CH_2)PO_3$}]•11H_2O (**3**•11H_2O), [{Cu_2(bisterpy)(H_2O)$_2$}$Mo_4F_4O_{10}${$O_3P(CH_2)_2PO_3$}] (**4**), [{Cu_2(bisterpy)}$Mo_4F_6O_9${$O_3P(CH_2)_3PO_3$}] (**5**), [{Cu_2(bisterpy)(H_2O)$_2$}$Mo_2F_6O_4${$HO_3P(CH_2)_4PO_3H$}]•2H_2O (**6**•2H_2O), [{Cu_2(bisterpy)}$Mo_2F_4O_4${$HO_3P(CH_2)_5PO_3H$}$_2$]•2H_2O (**7**•2H_2O), [{Cu_2(bisterpy)(H_2O)$_2$}$Mo_4F_8O_8${$O_3P(CH_2)_6PO_3$}]•H_2O (**8**•H_2O) and [{Cu_2(bisterpy)(H_2O)$_2$}$Mo_4F_8O_8${$O_3P(CH_2)_9PO_3$}] (**9**).

	1•4.5H_2O	**2**
Empirical Formula	$C_{34}H_{39}Cu_2Mo_5N_6O_{26.50}P_2$	$C_{35}H_{34}Cu_2Mo_5N_6O_{23}P_2$
FW	1624.43	1575.40
Crystal System	Triclinic	Triclinic
Space Group	$P\bar{1}$	$P\bar{1}$
a, Å	10.4478(16)	10.5271(14)
b, Å	15.021(2)	11.4603(15)
c, Å	15.994(2)	20.941(3)
α, deg	100.314(3)	98.655(3)
β, deg	104.841(3)	95.150(3)
γ, deg	90.885(3)	117.037(2)
V, Å^3	2382.1(6)	2188.5(5)
Z	2	2
D_{calcd}, g cm^{-1}	2.265	2.391
μ, mm^{-1}	2.315	2.510
T, K	90(2)	90(2)
λ, Å	0.71073	0.71073
R1[a]	0.0196	0.0658
wR2[b]	0.0856	0.1580

[a] $R1 = \Sigma||F_o| - |F_c||/\Sigma|F_o|$. [b] $wR2 = \{\Sigma[w(F_o^2 - F_c^2)^2]/\Sigma[w(F_o^2)^2]\}^{1/2}$.

acid ligand, and bisterpy in H_2O in the presence of HF in the temperature range 150-200 ^oC for 48 h produced crystalline samples of **1** and **2** in good yields. The stoichiometry of starting materials was held constant while the reaction temperature and pH was optimized for each compound. Use of hydrofluoric acid as a mineralizing agent achieved the acidic conditions required for the synthesis of these materials.

The infrared spectra of **1** and **2** are characterized by two medium intensity bands in the 900-955 cm^{-1} region associated with ν(Mo=O) and a medium or strong band between 775 and 800 cm^{-1} assigned to ν(Mo-O-Mo). A series of three to four bands in the 1000-1600 cm^{-1} region are attributed to the diphosphonate ligand.

2.3.2 X-ray Structures

The three-dimensional structure of $[\{Cu_2(bisterpy)(H_2O)\}Mo_5O_{15}\{O_3P(CH_2)_4PO_3\}]\bullet 4.5H_2O$ (**1**$\bullet 4.5H_2O$) consists of $[Mo_5O_{15}\{O_3P(CH_2)_4PO_3\}]^{4-}$ clusters linked through $\{Cu_2(bisterpy)(H_2O)\}^{4+}$ binuclear units as seen in **Figure 2.1**. The molybdophosphonate cluster is based on a pentanuclear ring of edge- and corner-sharing $\{MoO_6\}$ octahedra capped above and below by the $\{RPO_3\}^{2-}$ units of the diphosphonate ligand. The terminal phosphate tetrahedra each share three vertices with the central molybdate ring, while the organic tether links these molybdodiphosphonate clusters into chains along the *c* axis.

Two distinct Cu(II) sites exhibit distorted square pyramidal geometry. One site is defined by three nitrogen donors of one terpyridine terminus of the bisterpy ligand and one molybdate oxygen donor in the basal plane, and one aqua ligand in the apical position. The second site binds to three nitrogen donors of the bisterpy ligand and an oxygen donor of a molybdate cluster in the basal plane, and an oxygen donor of a

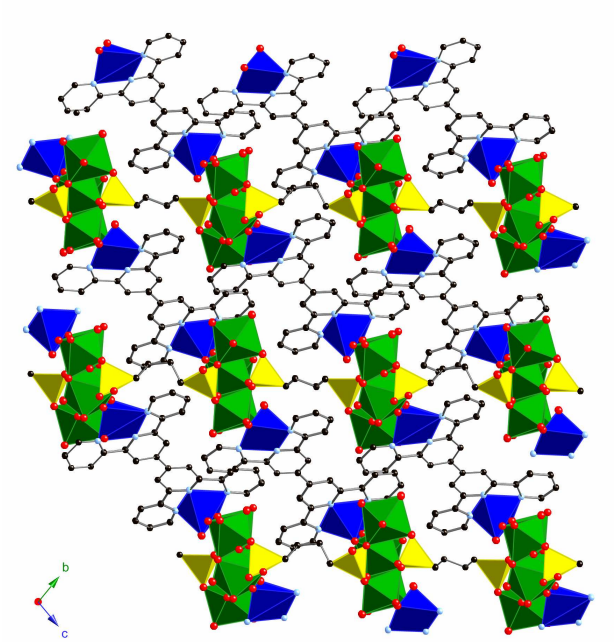

(a)

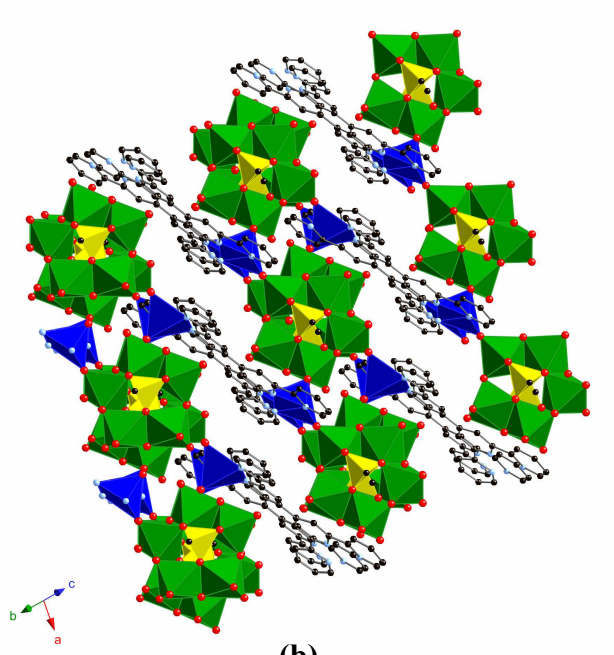

(b)

Figure 2.1. Polyhedral representations of $[\{Cu_2(bisterpy)(H_2O)\}Mo_5O_{15}\{O_3P(CH_2)_4PO_3\}]\bullet 4.5H_2O$ (**1**•$4.5H_2O$) viewed **(a)** normal to the *bc* plane and **(b)** down the molybdodiphosphonate chains. Molybdenum, green polyhedra; copper, blue polyhedra; phosphorus, yellow polyhedra; oxygen, red spheres; carbon, black spheres; nitrogen, light blue spheres; fluorine, light green spheres.

neighboring molybdate cluster in the apical position. Three copper square pyramids coordinate to each molybdodiphosphonate cluster through the bridging oxo groups. The bisterpy ligands link copper atoms on adjoining molybdodiphosphonate clusters, forming the overall three-dimensional structure. The structure can also be described as layers of molybdodiphosphonate clusters linked via the $\{Cu_2(bisterpy)(H_2O)\}^{4+}$ units, which are then pillared by the organic tethers of the diphosphonate ligand (**Figure 2.1(b)**).

Due to the accordion-like arrangement of the copper-bisterpy units in relation to the molydodiphosphonate chains, a higher density structure is formed. Water molecules of crystallization reside in the cavities formed within the structure bordered by the bisterpy ligands and the organic tethers of the diphosphonate ligands.

The one-dimensional structure of $[\{Cu_2(bisterpy)(H_2O)_2\}Mo_5O_{15}\{O_3P(CH_2)_5PO_3\}]$ (**2**) is composed of $[Mo_5O_{15}\{O_3P(CH_2)_5PO_3\}]^{4-}$ chains linked through $\{Cu_2(bisterpy)(H_2O)_2\}^{4+}$ units into a ladder type structure (**Figure 2.2a**). As in the previous structure, the pentanuclear molybdate clusters are capped on two faces by the terminal phosphonate tetrahedra of the diphosphonate ligands. The organic tethers of the diphosphonate ligands propogate the molybdodiphosphonate chains by linking the phosphonate tetrahedra of the clusters. Two chains form the sides of each ladder-type chain, while $\{Cu_2(bisterpy)(H_2O)_2\}^{4+}$ units form "rungs" by coordinating to the molybdate clusters through bridging oxo groups.

Two distinct distorted square pyramidal Cu(II) sites coordinate to three nitrogen donors of the bisterpy ligand, one molybdate oxo group, and one aqua ligand. The aqua ligands are directed to the side between chains as well as between "rungs" within each chain. The bisterpy ligand is found in a canted position caused by rotation along the

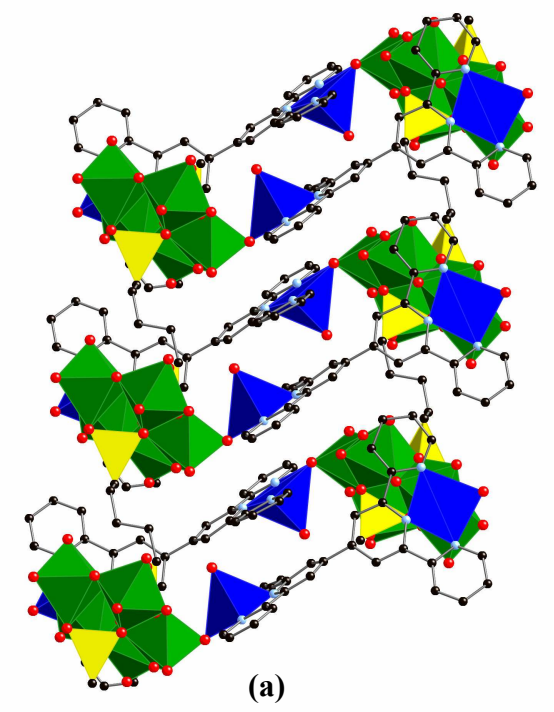

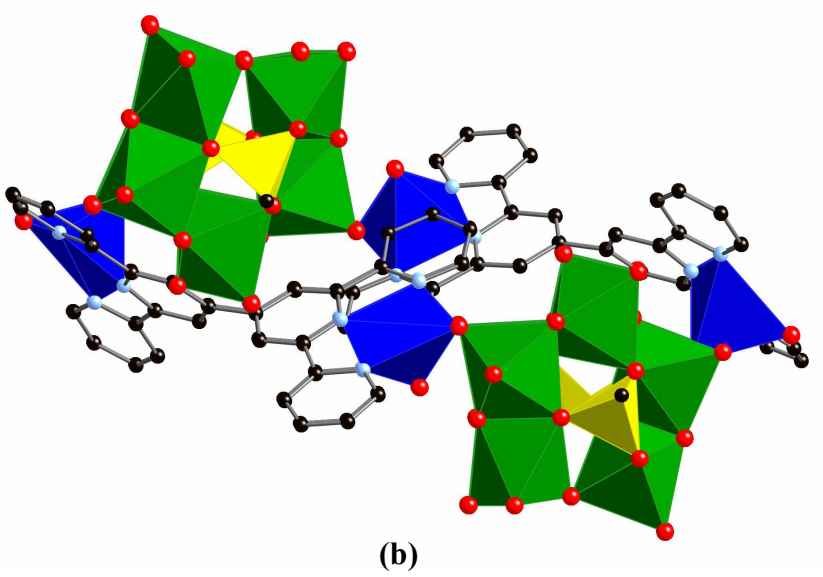

Figure 2.2. A polyhedral representation of **(a)** the one-dimensional structure of [{Cu_2(bisterpy)$(H_2O)_2$}Mo_5O_{15}{$O_3P(CH_2)_5PO_3$}] (**2**); **(b) 2** viewed down the molybdodiphosphonate chain.

central C-C bond, allowing very close proximity of the bisterpy ligands to the molybdodiphosphonate chains (**Figure 2.2b**). Due to the dense packing of chains in the *bc* plane, there is no incorporation of solvent molecules within the structure.

2.3.3 General Structural Observations

Compounds **1**•4.5H_2O and **2** derive from the prototypical $\{Mo_5O_{15}(O_3PR)_2\}^{4-}$ building block that is commonly observed in polyoxomolybdate systems. The organic tether of the diphosphonate ligand links the molybdodiphosphonate clusters to form the expected one-dimensional chains. Contrary to the proposed structural scheme, the unanticipated positioning of the Cu/bisterpy unit has caused the development of densely packed and lower dimensionality structures. While **1** exhibits three copper coordination sites on each molybdate cluster and appropriate orientation of the bisterpy ligand to form a three-dimensional structure, the $\{Cu_2(bisterpy)(H_2O)\}^{4+}$ units link the molybdodiphosphonate chains in an accordian-like manner as opposed to the naively predicted square grid arrangement (**Scheme 2.3**).

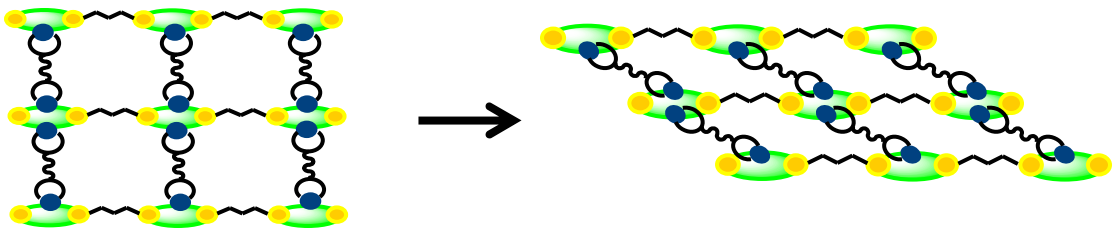

Scheme 2.3.

The ladder-type one-dimensional structure of **2** forms due to both a decreased number of copper coordination sites on each molybdate cluster and a rotation along the central bond within the bisterpy ligand that allows close proximity of this ligand to the clusters. Each cluster coordinates to only two copper centers causing a decrease in the overall dimensionality, and the copper centers of each $\{Cu_2(bisterpy)(H_2O)_2\}^{4+}$ unit link to opposite sides of neighboring molybdate clusters, thereby decreasing the distance between neighboring molybdodiphosphonate chains (**Scheme 2.4**).

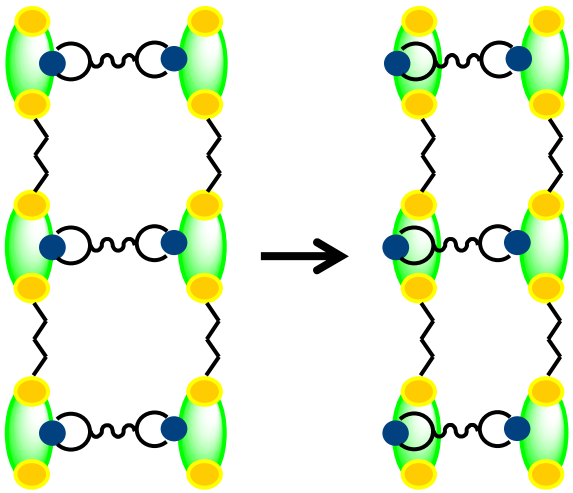

Scheme 2.4.

2.3.4 Magnetic Susceptibility Studies

Magnetic measurements were collected for both compounds. A representative plot of magnetic susceptibility and effective magnetic moment as a function of the temperature is shown in **Figure 2.3**. Both compounds exhibit Curie-Weiss paramagnetism. The high temperature data were fit to the Curie-Weiss law:

$$\chi = \chi_h + TIP = \frac{\mu_{eff}^2}{8[T-\theta]} + TIP$$

$$\mu_{eff}^2 = g^2 S(S+1)$$

For these compounds, the paramagnetism is derived exclusively from the Cu(II)-d^9 sites. The data gave the following fits: **1**•4.5H_2O, θ = -0.17 K, TIP = 0.0006 cm^3/mol, μ_{eff} = 2.91; **2**, θ = -0.31 K, TIP = 0.0005 cm^3/mol, μ_{eff} = 2.67. In each case, the effective magnetic moment is consistent with two Cu(II) sites per formula unit. The data show no evidence of antiferromagnetic ordering even at low temperatures, which is indicative of a lack of communication between electrons on neighboring copper centers through the bisterpy ligand. This observation can be attributed to the size of the ligand for **1**, while the rotation along the central C-C bond of the ligand in **2** likely diminishes any possible communication between the π orbitals of the terpyridine ends.

2.3.5 Thermal Gravimetric Analysis

The thermogravimetric profiles of **1** and **2** display an initial weight loss associated with a simultaneous loss of water molecules of crystallization and aqua ligands, and partial decomposition of the organic groups. Additional weight loss to above 700 ^oC is due to the continued decomposition of the organic ligands (**Figure 2.4**).

2.4 Conclusions

Hydrothermal reaction conditions provide a convenient method for the synthesis of organic-inorganic hybrid materials of the copper-bisterpy/molybdodiphosphonate family. Variations in the diphosphonate chain length provided the three-dimensional [{Cu_2(bisterpy)(H_2O)}Mo_5O_{15}{$O_3P(CH_2)_4PO_3$}]•4.5H_2O (**1**•4.5H_2O) and the one-

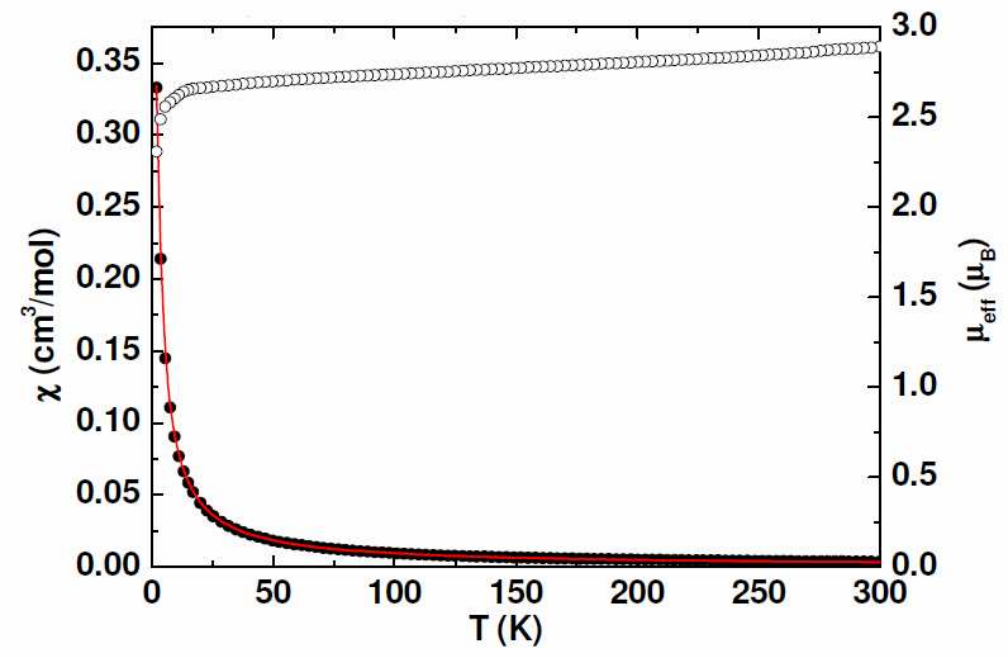

Figure 2.3. The dependence of the magnetic susceptibility χ (●) and effective magnetic moment μ_{eff} (○) of [{Cu_2(bisterpy)(H_2O)$_2$}Mo_5O_{15}{$O_3P(CH_2)_5PO_3$}] (**2**) on temperature T. The line drawn through the data is the fit to the Curie-Weiss law.

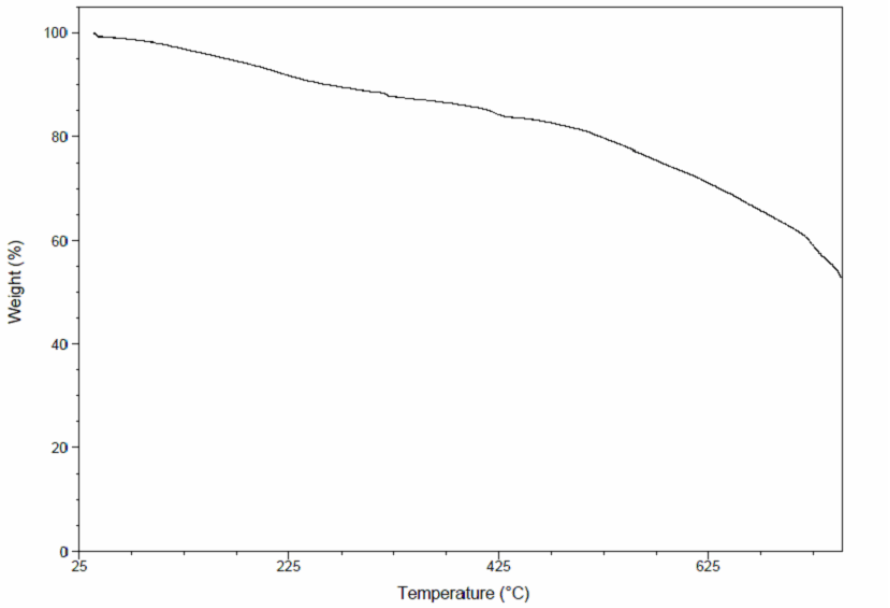

Figure 2.4. Thermogravimetric profile for [{Cu_2(bisterpy)(H_2O)}Mo_5O_{15}{$O_3P(CH_2)_4PO_3$}]•4.5H_2O (**1**·4.5H_2O) in the temperature range 25-750 ^oC.

dimensional [{Cu_2(bisterpy)(H_2O)$_2$}Mo_5O_{15}{$O_3P(CH_2)_5PO_3$}] (**2**), which represent the {$Mo_5O_{15}(O_3PR)_2$}$^{4-}$ chain motif seen as a recurring theme in oxomolybdenum-organodiphosphonate chemistry.

In addition to the tether length of the diphosphonate ligands, it is apparent that the flexibility of both the copper(II) centers and the central C-C bond of the bisterpy ligand ans the irregular number of copper connection sites on each molybdate cluster leads to the construction of unexpected structures of higher density, unpredictable dimensionality, and variable complexity.

2.5 Acknowledgement

This work was supported by a grant from the National Science Foundation, CHE-0242153.

2.6 References

[1] A. K. Cheetham, G. Férey, T. Loiseau, *Angew. Chem. Int. Ed.* **1999**, *38*, 3268.

[2] M. Fernández-García, A. Martínez-Arias, J. C. Hanson, J. A. Rodriguez, *Chem. Rev.* **2004**, *104*, 4063.

[3] P. J. Hagrman, D. Hagrman, J. Zubieta, *Angew. Chem. Int. Ed.* **1999**, *38*, 2638.

[4] A. M. Forster, A. K. Cheetham, *Topics in Catalysis* **2003**, *24*, 79.

[5] D. B. Mitzi, *Dalton Trans.* **2001**, 1.

[6] U. Mueller, M. Schubert, F. Teich, H. Puetter, K. Schierle-Arndt, J. Pastré, *J. Mater. Chem.* **2006**, *16*, 626.

[7] S. Kitagawa, R. Kitaura, S. Noro, *Angew. Chem. Int. Ed.* **2004**, *43*, 2334.

[8] J. R. D. DeBord, R. C. Haushalter, C. M. Meyer, D. J. Rose, P. J. Zapf, J. Zubieta, *J. Inorg. Chim. Acta*, **1997**, *256*, 165.

[9] M. I. Khan, E. Yohannes, R. J. Doedens, *Angew. Chem., Int. Ed. Engl*. **1999**, *38*, 1292.

[10] M. I. Khan, E. Yohannes, R. J. Doedens, *Inorg. Chem*. **2003**, *42*, 3125 and references therein.

[11] J. Chen, S. Lu, R. Yu, Z. Chen, Z. Huang, C. Lu, *Chem. Commun*. **2002**, 2640.

[12] L. Linnard, A. Dolbecq, P. Mialene, J. Marrot, F. Secheresse, *Inorg. Chem. Acta* **2004**, *357*, 845.

[13] S. Farrette, B. Hasenknbopf, J. Vaissermann, P. Gouzerh, C. Roux, *Chem. Commun*. **2003**, 2664.

[14] B. Z. Lin, Y. M. Chen, P. D. Liu, *Dalton Trans*. **2003**, 2474.

[15] R. C. Finn, J. Sims, C. J. O'Connor, J. Zubieta, *J. Chem. Soc, Dalton Trans*. **2002**, 159 and references therein.

[16] A. Clearfield, *Prog. Inorg. Chem.*, **1998**, *47*, 371.

[17] Y. Chunag, J. Zubieta, *Inorg. Chem* **1996**, *245*, 177.

[18] R. C. Finn, E. Burkholder, J. Zubieta, *Chem, Commun.* **2001**, 1852.

[19] W. Kwak, M. T. Pope, T. F. Scully, *J. Am. Chem. Soc.* **1975**, *97*, 5735.

[20] B. Hedman, *Acta Crystallogr.* **1980**, *B36*, 2241.

[21] W. Kwak, L. M. Rajkovic, J. K. Sralick, M. T. Pope, C. O. Quicksall, *Inorg. Chem.* **1976**, *15*, 2778.

[22] A. Vioux, J. LeBideau, P. H. Mutin, D. Leclercq, *Top. Curr. Chem.* **2004**, *232*, 145.

[23] A. Clearfield, *Curr. Opin. Solid State Mater. Sci.* **2002**, *6*, 495.

[24] G. Alberti, in *Comprehensive Supramolecular Chemistry*, J. L. Atwood, J. E. D. Davies, F. Vogel, Eds., Pergamon Press, New York, **1966**, *9*, 152.

[25] A. Clearfield, in *Comprehensive Supramolecular Chemistry*, J. L. Atwood, J. E. D. Davies, F. Vogel, Eds., Pergamon Press, New York, **1966**, *9*, 107.

[26] A. Clearfield, *Chem. Mater.* **1998**, *10*, 2801.

[27] L. A. Vermeulen, *Prog. Inorg. Chem.* **1997**, *44*, 143.

[28] N. G. Armatas, W. Ouellette, K. Whitenack, J. Pelcher, H. Liu, E. Romaine, C. J. O'Connor, J. Zubieta, *Inorg. Chem.* **2009,** *48*, 8897.

[29] E. Burkholder, V. Golub, C. J. O'Connor, J. Zubieta, *Inorg. Chem.* **2003**, *42*, 6729.

[30] D. I. Arnold, X. Ouyang, A. Clearfield, *Chem. Mater.* **2002**, *14*, 2020.

[31] E. C. Constable, A. M. W. Cargill Thompson, *J. Chem. Soc. Dalton Trans.* **1992**, 3467.

[32] APEX2, Data Collection Software, version 2011.8-0, Bruker-AXS Inc., Madison, WI (2011).

[33] SMART, Data Collection Software, version 5.630, Bruker-AXS Inc., Madison, WI (1997-2002).

[34] SAINT plus, Data Reduction Software, version 6.45A, Bruker-AXS Inc., Madison, WI (1997-2002).

[35] G. M. Sheldrick, SADABS, University of Göttingen (1996).

[36] SHELXTL PC, version 6.12, Bruker-AXS Inc., Madison, WI (2002).

[37] O'Connor, C. J., *Prog. Inorg. Chem.* **1979**, *29*, 203.

[38] S. Feng, R. Xu, *Acc. Chem. Res.* **2001**, *34*, 239.

[39] J. Zubieta, Solid State Methods, Hydrothermal in Comprehensive CoordinationChemistry II, 2003, vol. 1, p. 697.

[40] J. Gopalakrishnan, N. S. P. Bhuvanesh, K. K. Rangan, *Curr. Opin. Solid State Mater. Sci.* **1996**, *1*, 285.

[41] J. Gopalakrishnan, *Chem. Mater*. **1995**, *7*, 1265.

[42] A. Rabenau, *Angew. Chem., Int. Ed. Engl.* **1985**, *24*, 1026.

[43] A. Stein, S. W. Keller, T. E. Mallouk, *Science* **1993**, *259*, 1558.

Chapter 3

Structural Consequences of Fluoride Incorporation in the Oxomolybdenum-Copper-Bisterpy-$\{O_3P(CH_2)_nPO_3\}^{4-}$ System, n = 1-6, 9 (bisterpy = 2,2':4',4":2",2"'-quarterpyridyl-6',6"-di-2-pyridine)

3.1 Introduction

Metal oxyfluorides exhibit a variety of useful physical properties including magnetism, catalysis, and optical properties.[1-6] While it is well established that fluoride provides an effective mineralizing agent in the synthesis of various metal oxide based complexes including zeolites and open-framework materials,[7] structural incorporation of fluoride anions may be achieved through careful tuning of reaction conditions leading to variation in the structure morphology.[8] Fluoride replaces oxo groups within the coordination sphere of the metal center, causing the cleavage of M – O – M bridges and resulting in changes in the structure of the metal-oxyfluoride subunit through the breaking of common metal oxide chain or layer motifs into smaller units.[8-11] The difference in bonding nature between M – O and M – F can impact the physical properties of these materials, suggesting the ability to tune those properties based on their composition.[12]

The complex structural chemistry of metal oxyfluorides is exemplified by the vanadium fluorides and oxyfluorides, which exhibit several different oligomeric, chain, and ladder-type building blocks.[4,13-19] Flouride incorporation into molybdenum oxide materials has also led to the discovery of a variety of oxyfluoromolybdate clusters.[9,20-30] Uptake of fluoride into oxovanadium organophosphonate materials has been shown to result in unusual structural complexity aided by the variety of possible geometries and oxidation states of vanadium, while oxyfluoromolybdenum organophosphonates exhibit unexpected molybdate units with structures and charges that vary from expected molybdophosphonate motifs.[27,31-36]

The structures of oxomolybdenum-organodiphosphonate materials are characterized by polyoxomolybdophosphonate clusters generally of the type $\{Mo_5O_{15}(O_3PR)_2\}^{4-}$ tethered through the organic chains of the diphosphonate groups.[37-41] The anionic chains may then be modified through tether type and length of the diphosphonate ligand (**Scheme 3.1(a)**).[42-47] Charge compensation is achieved through incorporation of a cationic secondary metal-ligand unit, while use of a binucleating secondary ligand may also lead to increased dimensionality of the overall structure (**Scheme 3.1(b)**). Few examples exist of fluoride uptake into these materials, in which

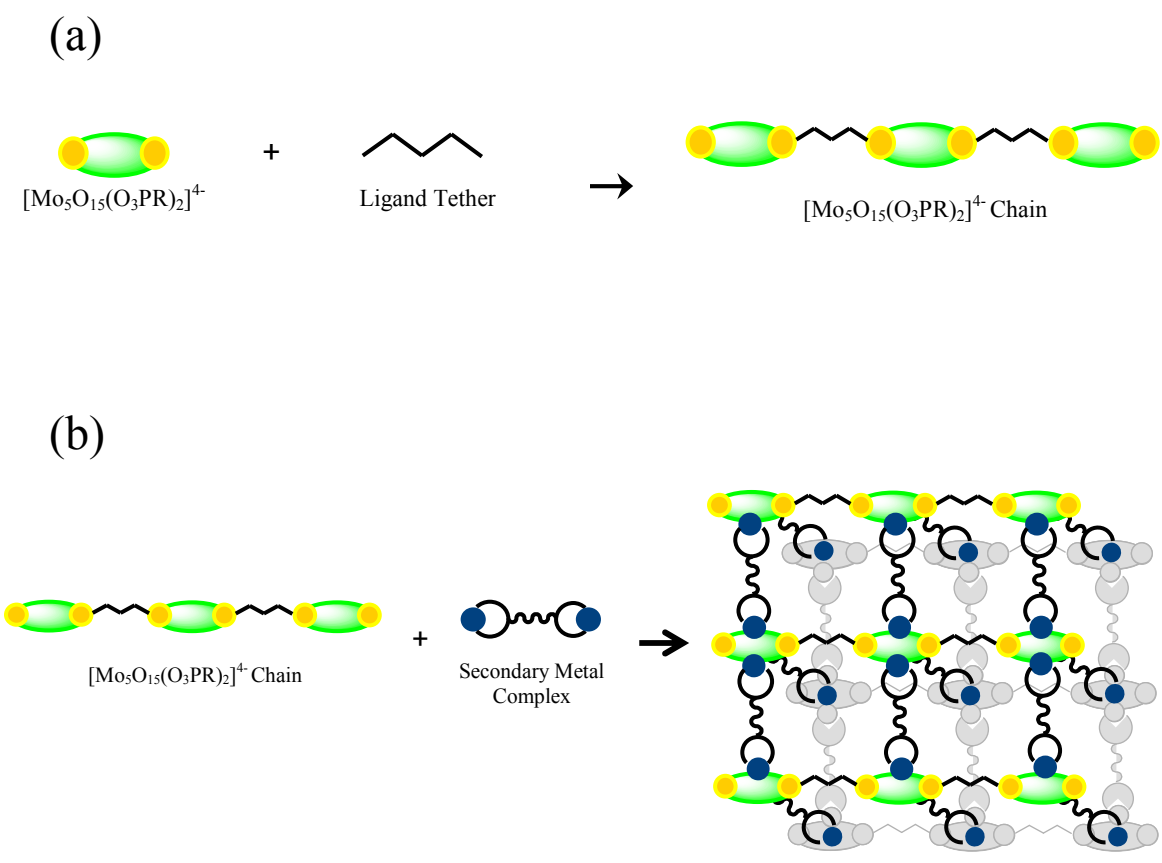

Scheme 3.1.

the pentanuclear $\{Mo_5O_{15}(O_3PR)_2\}^{4-}$ core (**Figure 3.1**) is seen to break down into smaller oxyfluoromolybdate clusters (**Figure 3.2**).[27,30,48]

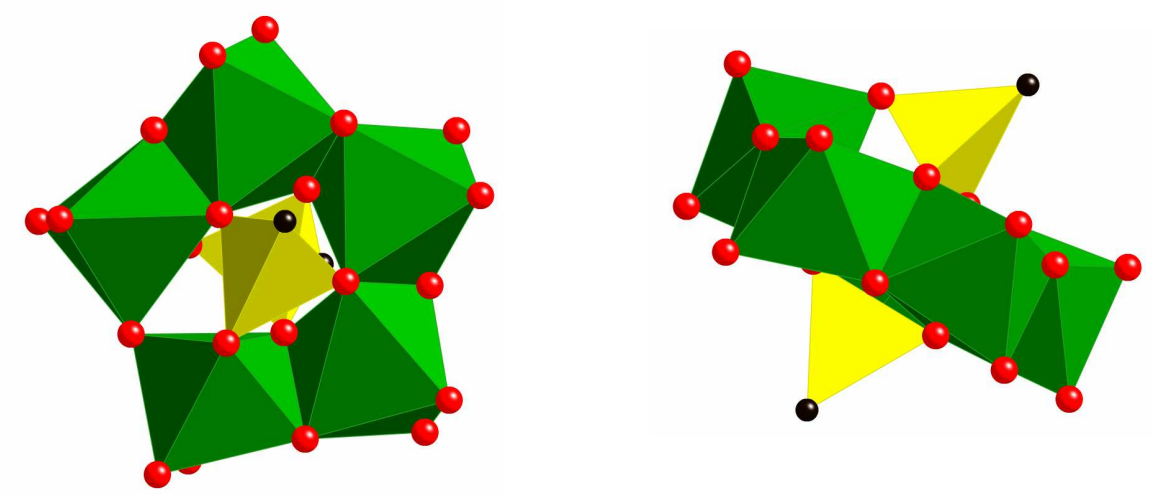

Figure 3.1. Top and side polyhedral views of the $\{Mo_5O_{15}(O_3PR)_2\}^{4-}$ cluster. Molybdenum, green polyhedra; phosphorus, yellow polyhedra; oxygen, red spheres; carbon, black spheres.

Hydrothermal synthesis offers a convenient route for the preparation of metal oxide incorporating organic ligands due to the relatively mild reaction conditions utilized, allowing retention of the organic components.[49-54] The use of fluoride as a mineralizer in hydrothermal reactions is well established, and this technique proves suitable for the synthesis of metal oxyfluorides.[4,55-57] Use of hydrofluoric acid as an additive to the reaction mixtures achieves the neutral or acidic conditions that are often required for the synthesis of hybrid materials based on metal oxide motifs.

Seven new compounds of the Cu(II)-bisterpy/molybdodiphosphonate family exhibiting six novel oxofluoromolybdate clusters were produced using hydrothermal

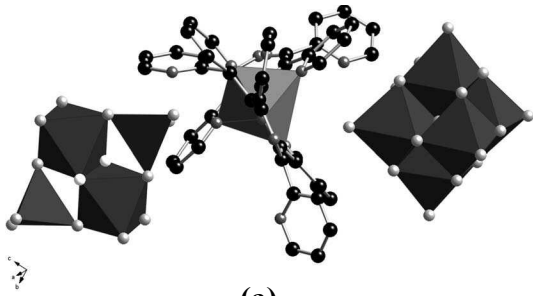

(a)

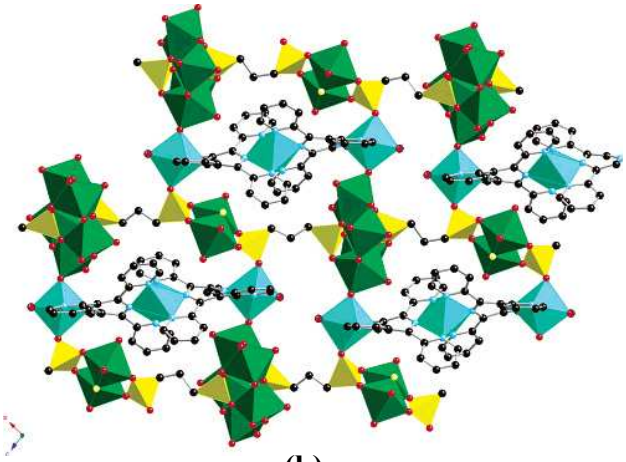

(b)

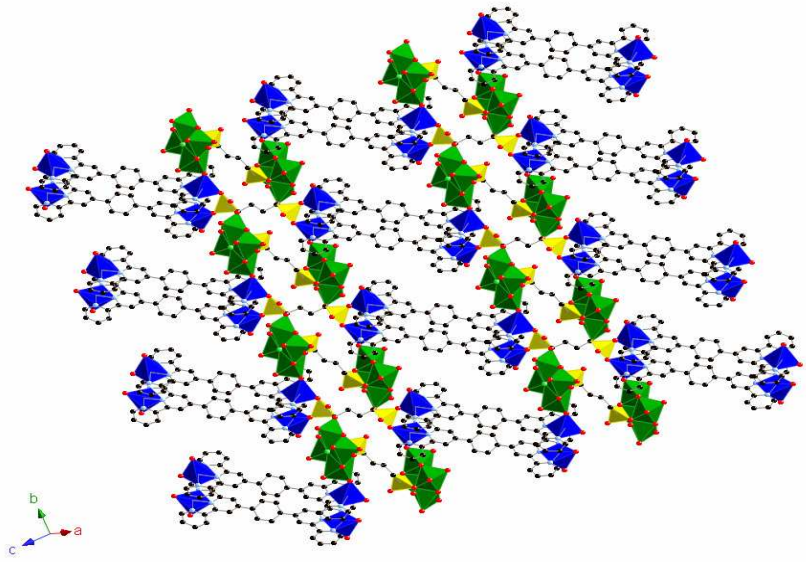

(c)

Figure 3.2. The structures of: **(a)** $Ni(tpyprz)_2]_2[Mo_4O_{12}F_2][Mo_6O_{19}]$ showing the $\{Mo_4O_{12}F_2\}$ clusters on the left; **(b)** $[\{Ni_3(tpyprz)_2(H_2O)_2\}(Mo_5O_{15})(Mo_2O_4F_2)\{O_3P(CH_2)_3PO_3\}_2]$ showing the $\{Mo_2F_2O_4\}$ clusters; **(c)** $[Cu_4(H_2O)_2(Phenbisterpy)_2\{HO_3P(CH_2)_4PO_3H\}][(Mo_4FO_{12})_2\{O_3P(CH_2)_4PO_3\}]\cdot 4H_2O$ showing the $\{Mo_4FO_{12}\}^-$ cluster.[27,30,48]

synthesis techniques: [{Cu_2(bisterpy)(OH)}$Mo_2F_3O_4${$O_3P(CH_2)PO_3$}]•11H_2O (**1**•11H_2O), [{Cu_2(bisterpy)(H_2O)$_2$}$Mo_4F_4O_{10}${$O_3P(CH_2)_2PO_3$}] (**2**), [{Cu_2(bisterpy)}$Mo_4F_6O_9${$O_3P(CH_2)_3PO_3$}] (**3**), [{Cu_2(bisterpy)(H_2O)$_2$}$Mo_2F_6O_4${$HO_3P(CH_2)_4PO_3H$}] (**4**), [{Cu_2(bisterpy)}$Mo_2F_4O_4${$HO_3P(CH_2)_5PO_3H$}$_2$]•2H_2O (**5**•2H_2O), [{Cu_2(bisterpy)(H_2O)$_2$}$Mo_4F_8O_8${$O_3P(CH_2)_6PO_3$}]•2H_2O (**6**•2H_2O) and [{Cu_2(bisterpy)(H_2O)$_2$}$Mo_4F_8O_8${$O_3P(CH_2)_9PO_3$}] (**7**).

3.2 Experimental Section

All chemicals were used as obtained without further purification. Molybdenum(VI) Oxide (99.5%) and methylenediphosphonic acid were purchased from Alfa Aesar. Cupric Acetate was purchased from Baker. The diphosphonate ligands methylenediphosphonic acid, 1,2-ethylenediphosphonic acid, 1,3-propylenediphosphonic acid, 1,4-butylenediphosphonic acid, 1,5-pentylenediphosphonic acid, 1,6-hexylenediphosphonic acid, and 1,9-nonylenediphosphonic acid were synthesized according to methods reported in the literature,[58] as was the 2,2':4',4":2",2"'-quarterpyridyl-6',6"-di-2-pyridine (bisterpy) ligand.[59] All syntheses were carried out in 23mL poly(tetrafluroethylene) lined stainless steel containers under autogenous pressure. The pH of the solutions were measured both prior to and following heating using *color pHast*® pH sticks. Water was distilled above 3.0MΩ in-house using a Barnstead Model 525 Biopure Distilled Water Center.

3.2.1 Synthesis of [{Cu_2(bisterpy)(OH)}$Mo_2F_3O_4${$O_3P(CH_2)PO_3$}]•11H_2O (1•11H_2O)

A solution of cupric acetate (0.045g, 0.2253mmol), molybdenum(VI) oxide (0.087g, 0.6044mmol), bisterpy (0.050g, 0.1077mmol), methylenediphosphonic acid (0.047g, 0.267mmol), H_2O (10.00g, 556mmol), and HF (0.400mL, 22.98mmol) with the mole ratio 2.09:5.61:1.00:2.48:5162.49:213.37 was stirred briefly before heating to 150^{o}C for 48hrs with an initial and final pH value of 1.0. Green crystals were isolated in 90% yield that were suitable for X-ray diffraction. IR (KBr pellet, cm^{-1}): 3421(m), 2924(w), 1606(m), 1560(m), 1476(m), 1410(m), 1245(w), 1154(m), 1089(m), 942(m), 908(m), 798(m), 673(m), 589(m).

3.2.2 Synthesis of [{Cu_2(bisterpy)(H_2O)$_2$}$Mo_4F_4O_{10}${$O_3P(CH_2)_2PO_3$}] (2)

A solution of cupric acetate (0.0450g, 0.2253mmol), molybdenum(VI) oxide (0.0875g, 0.6078mmol), bisterpy (0.0499g, 0.1075mmol), 1,2-ethylenediphosphonic acid (0.0509g, 0.2677mmol), H_2O (10.00g, 556mmol), and HF (0.200mL, 11.49mmol) with the mole ratio 2.10:5.65:1.00:2.49:5172.09:106.88 was stirred briefly before heating to 200^{o}C for 48hrs with initial and final pH value of 2.0 and 1.0, respectively. Green crystals were isolated in 30% yield that were suitable for X-ray diffraction. IR (KBr pellet, cm^{-1}): 3435(m), 1617(m), 1560(m), 1475(m), 1407(m), 1197(w), 1116(w), 1091(w), 939(m), 906(w), 800(m).

3.2.3 Synthesis of [{Cu_2(bisterpy)}$Mo_4F_6O_9${$O_3P(CH_2)_3PO_3$}] (3)

A solution of cupric acetate (0.0451g, 0.2263mmol), molybdenum(VI) oxide (0.0872g, 0.6034mmol), bisterpy (0.0498g, 0.1078mmol), 1,3-propylenediphosphonic acid (0.0548g, 0.2694mmol), H_2O (10.00g, 556mmol), and HF (0.200mL, 11.49mmol)

with the mole ratio 2.10:5.60:1.00:2.50:5157.70:106.59 was stirred briefly before heating to 200°C for 48hrs with initial and final pH values of 1.5 and 1.0, respectively. Green crystals were isolated in 95% yield that were suitable for X-ray diffraction. IR (KBr pellet, cm^{-1}): 3434(m), 1605(m), 1560(m), 1475(m), 1405(m), 1248(w), 1194(w), 1100(m), 1051(m), 951(m), 924(m), 791(m), 714(w), 612(w), 545(w).

3.2.4 Synthesis of [{Cu_2(bisterpy)(H_2O)$_2$}$Mo_2F_6O_4${$HO_3P(CH_2)_4PO_3H$}] (4)

A solution of cupric acetate (0.045g, 0.2263mmol), molybdenum(VI) oxide (0.087g, 0.6034mmol), bisterpy (0.050g, 0.1078mmol), 1,4-butylenediphosphonic acid (0.059g, 0.2694mmol), H_2O (10.00g, 556mmol), and HF (0.300mL, 17.24mmol) with the mole ratio 2.10:5.60:1.00:2.50:5157.70:159.93 was stirred briefly before heating to 150°C for 48hrs with initial and final pH values of 1.5 and 1.0, respectively. Green crystals were isolated in 50% yield that were suitable for X-ray diffraction. IR (KBr pellet, cm^{-1}): 3447(m), 1607(m), 1552(w), 1476(m), 1409(m), 1248(w), 1158(w), 949(m), 912(s), 793(m), 671(w), 580(m).

3.2.5 Synthesis of [{Cu_2(bisterpy)}$Mo_2F_4O_4${$HO_3P(CH_2)_5PO_3H$}$_2$]•$2H_2O$ (5•$2H_2O$)

A solution of cupric acetate (0.045g, 0.2263mmol), molybdenum(VI) oxide (0.087g, 0.6034mmol), bisterpy (0.050g, 0.1078mmol), 1,5-pentylenediphosphonic acid (0.062g, 0.2694mmol), H_2O (10.00g, 556mmol), and HF (0.300mL, 17.24mmol) with the mole ratio 2.10:5.60:1.00:2.50:5157.70:159.93 was stirred briefly before heating to 150°C for 48hrs with initial and final pH values of 1.5. Green crystals were isolated in 50% and 40% yield, respectively, that were suitable for X-ray diffraction. IR (KBr pellet,

cm^{-1}): 3440(m), 1608(m), 1560(w), 1475(m), 1411(m), 1249(w), 1162(w), 1045(w), 936(m), 905(m), 839(w), 796(w), 671(w), 552(w).

3.2.6 Synthesis of [{Cu_2(bisterpy)(H_2O)$_2$}$Mo_4F_8O_8${$O_3P(CH_2)_6PO_3$}]•2H_2O (6•2H_2O)

A solution of cupric acetate (0.045g, 0.2253mmol), molybdenum(VI) oxide (0.087g, 0.6044mmol), bisterpy (0.050g, 0.1077mmol), 1,6-hexylenediphosphonic acid (0.066g, 0.2681mmol), H_2O (10.00g, 556mmol), and HF (0.300mL, 17.24mmol) with the mole ratio 2.09:5.61:1.00:2.49:5162.49:160.07 was stirred briefly before heating to 150^{o}C for 48hrs with initial and final pH values of 1.5 and 1.0, respectively. Green crystals were isolated in 80% yield that were suitable for X-ray diffraction. IR (KBr pellet, cm^{-1}): 3447(s), 2931(w), 1604(s), 1561(m), 1475(s), 1409(s), 1250(m), 1143(s), 1024(s), 948(s), 931(s), 794(m), 673(m), 617(m), 574(m), 543(m).

3.2.7 Synthesis of [{Cu_2(bisterpy)(H_2O)$_2$}$Mo_4F_8O_8${$O_3P(CH_2)_9PO_3$}] (7)

A solution of cupric acetate (0.045g, 0.2253mmol), molybdenum(VI) oxide (0.088g, 0.6113mmol), bisterpy (0.049g, 0.1056mmol), 1,9-nonylenediphosphonic acid (0.079g, 0.2741mmol), H_2O (10.00g, 556mmol), and HF (0.400mL, 22.98mmol) with the mole ratio 2.13:5.79:1.00:2.60:5250.24:217.61 was stirred briefly before heating to 150^{o}C for 48hrs with initial and final pH values of 1.5 and 1.0, respectively. Green crystals were isolated in 80% yield that were suitable for X-ray diffraction. IR (KBr pellet, cm^{-1}): 3504(s), 2929(w), 1616(m), 1561(m), 1474(m), 1410(m), 1256(m), 1132(s), 1021(s), 953(s), 919(s), 799(m), 671(w), 611(s), 568(w).

3.2.8 X-ray Crystallography

Crystallographic data of all compounds were collected at low temperature (90K). Data were collected on a Bruker P4 diffractometer using Mo-K_α radiation (λ = 0.71073Å) equipped with a SMART CCD system.[60] The data were corrected for Lorentz and polarization effects,[61] and adsorption corrections were made using SADABS.[62] The structures were solved by direct methods and refinements were made using the SHELXTL[63] crystallographic software. After first locating all of the nonhydrogen atoms from the initial solution of each structure, the models were refined against F^2 using first isotropic and then anisotropic thermal displacement parameters until the final value of Δ/σ_{max} was less than 0.001. Hydrogen atoms were introduced in calculated positions and refined isotropically. Neutral atom scattering coefficients and anomalous dispersion corrections were taken from the *International Tables*, Vol. C. Crystallographic details for the structures of **1-7** are summarized in **Table 3.1**.

3.2.9 Magnetism

Magnetic data were recorded on polycrystalline samples in the 2-300 K temperature range using a Quantum Design MPMS-5S SQUID spectrometer. Calibrating and operating procedures have been reported previously.[64] The temperature-dependent magnetic data were obtained at a magnetic field of H = 1000 Oe.

3.2.10 Thermal Gravimetric Analysis

Thermogravimetric studies were performed in an Auto TGA Q500 instrument under a 50 mL/min flow of synthetic air. The temperature was ramped from 25 to 800 ^oC at a rate of 5 ^oC/min for the decomposition.

Table 3.1. Summary of crystallographic data for the structures of [{Cu_2(bisterpy)(OH)}$Mo_2F_3O_4${$O_3P(CH_2)PO_3$}]•11H_2O (**1**•11H_2O), [{Cu_2(bisterpy)(H_2O)$_2$}$Mo_4F_4O_{10}${$O_3P(CH_2)_2PO_3$}] (**2**), [{Cu_2(bisterpy)}$Mo_4F_6O_9${$O_3P(CH_2)_3PO_3$}] (**3**), [{Cu_2(bisterpy)(H_2O)$_2$}$Mo_2F_6O_4${$HO_3P(CH_2)_4PO_3H$}]•2H_2O (**4**•2H_2O), [{Cu_2(bisterpy)}$Mo_2F_4O_4${$HO_3P(CH_2)_5PO_3H$}$_2$]•2H_2O (**5**•2H_2O), [{Cu_2(bisterpy)(H_2O)$_2$}$Mo_4F_8O_8${$O_3P(CH_2)_6PO_3$}]•2H_2O (**6**•2H_2O) and [{Cu_2(bisterpy)(H_2O)$_2$}$Mo_4F_8O_8${$O_3P(CH_2)_9PO_3$}] (**7**).

	1•11H_2O	**2**	**3**	**4**	**5**•2H_2O	**6**•2H_2O	**7**
Empirical Formula	$C_{31}H_{45}Cu_2F_3$-$Mo_2N_6O_{22}P_2$	$C_{16}H_{14}CuF_2$-$Mo_2N_3O_9P$	$C_{33}H_{26}Cu_2F_6$-$Mo_4N_6O_{15}P_2$	$C_{17}H_{17}CuF_3$-MoN_3O_6P	$C_{20}H_{24}CuF_2$-$MoN_3O_9P_2$	$C_{18}H_{20}Cu$-F_4 $Mo_2N_3O_9P$	$C_{19.50}H_{21}Cu$-$F_4Mo_2N_3O_8P$
FW	1291.63	716.69	1433.38	606.79	709.84	784.76	787.78
Crystal System	Triclinic	Monoclinic	Triclinic	Triclinic	Triclinic	Triclinic	Monoclinic
Space Group	$P\bar{1}$	*C2/c*	$P\bar{1}$	$P\bar{1}$	$P\bar{1}$	$P\bar{1}$	$P2_1/n$
a, Å	9.4285(10)	14.2755(7)	9.3474(6)	8.4284(6)	9.2086(5)	8.670(3)	9.8943(14)
b, Å	13.1589(13)	15.9451(8)	9.9968(6)	9.8064(7)	9.6673(6)	10.059(3)	16.976(2)
c, Å	15.9484(16)	18.4226(9)	11.2297(7)	13.2542(10)	15.8062(9)	14.185(4)	14.810(2)
α, deg	86.836(2)	90	84.6260(10)	98.2060(10)	92.471(2)	97.739(7)	90
β, deg	78.190(2)	93.6230(10)	70.0640(10)	93.6320(10)	103.8410(10)	92.257(7)	105.290(3)
γ, deg	84.923(2)	90	83.6780(10)	112.9910(10)	115.6630(10)	93.448(7)	90
V, Å^3	1927.8(3)	4185.1(4)	978.70(11)	989.58(12)	1214.05(12)	1222.3(6)	2399.4(6)
Z	2	8	1	2	2	2	4
D_{calcd}, g cm^{-1}	2.225	2.275	2.425	2.036	1.942	2.132	2.181
μ, mm^{-1}	1.925	2.339	2.502	1.860	1.598	2.024	2.059
T, K	90(2)	90(2)	90(2)	90(2)	90(2)	90(2)	90(2)
λ, Å	0.71073	0.71073	0.71073	0.71073	0.71073	0.71073	0.71073
R1[a]	0.0479	0.0425	0.0247	0.0301	0.0512	0.0715	0.0359
wR2[b]	0.1081	0.0871	0.0923	0.0795	0.1182	0.1775	0.0901

[a] $R1 = \Sigma||F_o| - |F_c||/\Sigma|F_o|$. [b] $wR2 = \{\Sigma[w(F_o^2 - F_c^2)^2]/\Sigma[w(F_o^2)^2]\}^{1/2}$.

3.3 Results and Discussion

3.3.1 Synthesis and Infrared Spectroscopy

The hydrothermal reactions of MoO_3, $Cu(CH_3CO_2)_2 \cdot H_2O$, the appropriate diphosphonic acid ligand, and bisterpy in H_2O with HF additive in the temperature range 150-200 ^oC for 48 h produced crystalline samples of **1-7** in good yields. The stoichiometry of starting materials was held constant while the reaction temperature and pH was optimized for each compound.

The infrared spectra of **1-7** are characterized by two medium intensity bands in the 900-955 cm^{-1} region associated with ν(Mo=O) and a medium or strong band between 775 and 800 cm^{-1} assigned to ν(Mo-O-Mo). A series of three to four bands in the 1000-1600 cm^{-1} region are attributed to the diphosphonate ligand.

3.3.2 X-ray Structures

The two-dimensional structure of $[\{Cu_2(bisterpy)(OH)\}Mo_2F_3O_4\{O_3P(CH_2)PO_3\}] \bullet 11H_2O$ (**1**$\bullet 11H_2O$) is shown in **Figure 3.3a** to consist of $[Mo_2F_3O_4\{O_3P(CH_2)PO_3\}]^{3-}$ clusters bridged by $\{Cu_2(bisterpy)(OH)\}^{3+}$ units. The molybdodiphosphonate clusters contain two corner-sharing $\{MoO_4F_2\}$ octahedra linked through a bridging fluoride group. Each $\{PO_3\}$ terminus of the diphosphonate ligand bridges both oxyfluoromolybdate octahedra through oxo groups on two vertices, and the methylene group links the phosphonate tetrahedra (**Figure 3.3b**). It is common for the methylenediphosphonate ligand to chelate one molybdate cluster as opposed to bridging neighboring clusters due to the decreased tether length.[30]

Two distinct Cu(II) sites exhibit distorted square pyramidal geometry; one site coordinates to the three nitrogen donors of one terpyridine terminus of the bisterpy ligand

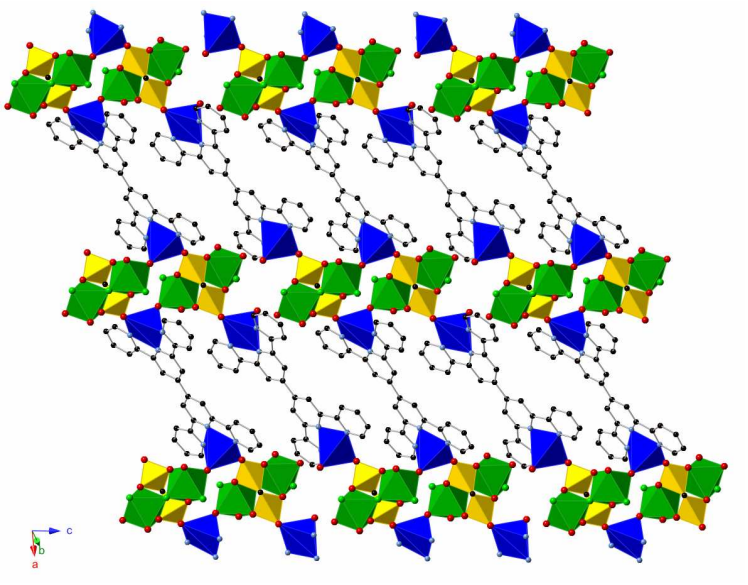

(a)

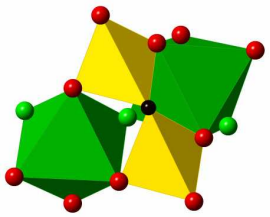

(b)

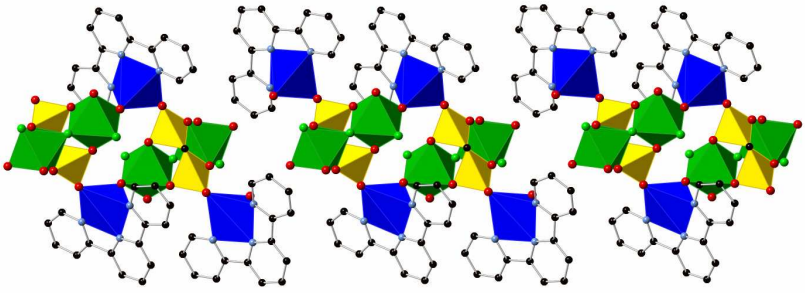

(c)

Figure 3.3. Polyhedral representations of **(a)** the two-dimensional structure of [{Cu_2(bisterpy)(OH)}$Mo_2F_3O_4${$O_3P(CH_2)PO_3$}]•11H_2O (**1**•11H_2O); **(b)** the oxyfluoromolybdate unit; and **(c)** copper coordination to the oxyfluoromolybdate clusters. Molybdenum, green polyhedra; copper, blue polyhedra; phosphorus, yellow polyhedra; oxygen, red spheres; carbon, black spheres; nitrogen, light blue spheres; fluorine, light green spheres.

and one phosphonate oxygen in the basal plane, and one aqua ligand in the apical position. The second site differs from the first in that the apical position connects to a molybdate oxo group (**Figure 3.3c**). The coordinated aqua ligands are directed above and below the layer. The copper sites bridge neighboring molybdodiphosphonate clusters, effectively forming copper-molybdodiphosphonate chains linked into two dimensions through the bisterpy ligand. Free solvent molecules occupy the space between the bisterpy ligands of each layer.

Figure 3.4a shows the two-dimensional structure of $[\{Cu_2(bisterpy)(H_2O)_2\}Mo_4F_4O_{10}\{O_3P(CH_2)_2PO_3\}]$ (**2**). Each layer forms from $[Mo_4F_4O_{10}\{O_3P(CH_2)_2PO_3\}]^{4-}$ chains (**Figure 3.4b**) bridged by $\{Cu_2(bisterpy)(H_2O)_2\}^{4+}$ units. The $\{Mo_4F_4O_{10}\}$ clusters can be described as two dimers of edge-sharing $\{MoF_2O_4\}$ octahedra linked through bridging fluoride groups; the dimers are then attached via corner-sharing interactions between axial oxo groups. Each $\{PO_3\}$ terminus of the diphosphonate ligand shares two vertices with oxyfluoromolybdate octahedra. The clusters are then linked through the organic tether of the diphosphonate ligand.

Each distorted square octahedral Cu(II) site is defined by corner-sharing interactions with a phosphonate group through one bridging oxo group as well as three equatorially bonded nitrogen donors of the bisterpy ligand and one axially bonded aqua ligand. Adjacent sheets are perpendicular to each other, creating a dense structure containing no free solvent molecules.

Incorporation of the propylenediphosphonate ligand generated the only three-dimensional structure of the series. The framework of $[\{Cu_2(bisterpy)\}Mo_4F_6O_9\{O_3P(CH_2)_3PO_3\}]$ (**3**) is constructed from

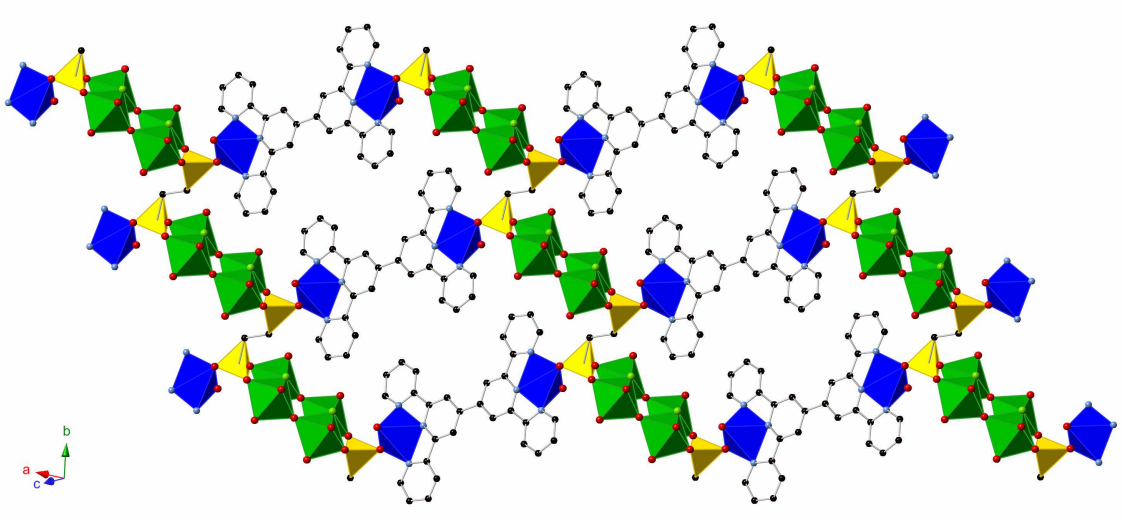

(a)

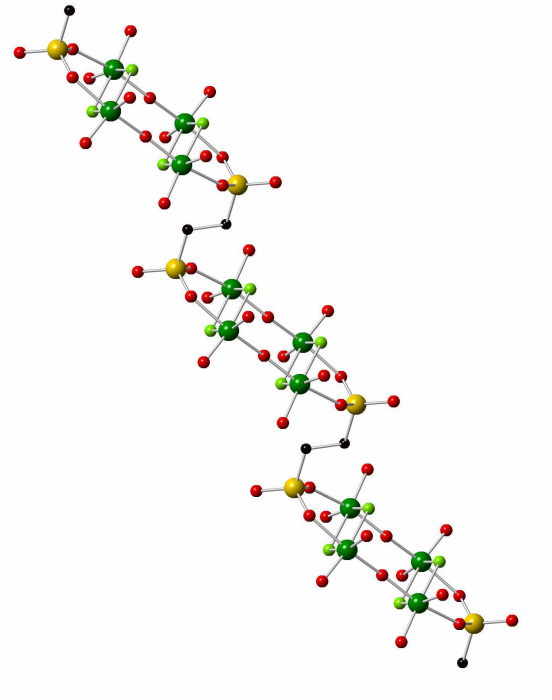

(b)

Figure 3.4. **(a)** Polyhedral representation of the two-dimensional structure of $[\{Cu_2(bisterpy)(H_2O)_2\}Mo_4F_4O_{10}\{O_3P(CH_2)_2PO_3\}]$ (**2**); **(b)** Ball and stick representation of one $\{Mo_4F_4O_{10}(O_3P(CH_2)_2PO_3)\}^{4-}$ chain.

$\{Mo_4F_6O_9(O_3P(CH_2)_3PO_3)\}_n^{4n-}$ and $\{Cu_2(bisterpy)\}_n^{4n+}$ chains linked through phosphonate groups (**Figure 3.5**). As in **2**, the oxyfluoromolybdate cluster can be described as two dimers of edge-sharing molybdenum octahedra coordinated through two bridging fluorides; however, these dimers form between a $\{MoF_2O_4\}$ and $\{MoF_3O_3\}$ units. The dimers then link through a single bridging axial oxo group to form the quarternuclear molybdate clusters, which link through the diphosphonate ligand to form staggered chains. Each cluster coordinates to two phosphonate groups, one to each dimer of the cluster through corner-sharing interactions with two phosphonate oxo groups.

In contrast to **1**•11H_2O and **2**, the copper-bisterpy unit of **3** forms $\{Cu_2(bisterpy)\}_n^{4n+}$ chains consisting of edge-sharing Cu(II) dimers linked through two phosphonate oxo groups that are then bridged by bisterpy ligands. Each distorted square pyramidal copper site links to one terpyridine end of a bisterpy ligand through the three nitrogen donors, and two triply bridging phosphonate oxo groups that provide the connectivity between the copper centers as well as to the molybdodiphosphonate chains. This structure may also be described as chains of $[Mo_4F_6O_9\{(O_3P)_2R\}]^{4-}$ clusters linked through Cu(II) dimers, with the organic ligands providing connectivity between the chains into three dimensions.

The remaining four compounds in this series display similar structural motifs; all form one-dimensional structures composed of chains of alternating molybdodiphosphonate units and copper-bisterpy units. While differences between the structures include the identity of the oxyfluoromolybdate cluster, protonation sites on the phosphonate groups, and the number of aqua ligands coordinated to the Cu(II) centers in addition to the diphosphonate ligand tether length, compounds incorporating the

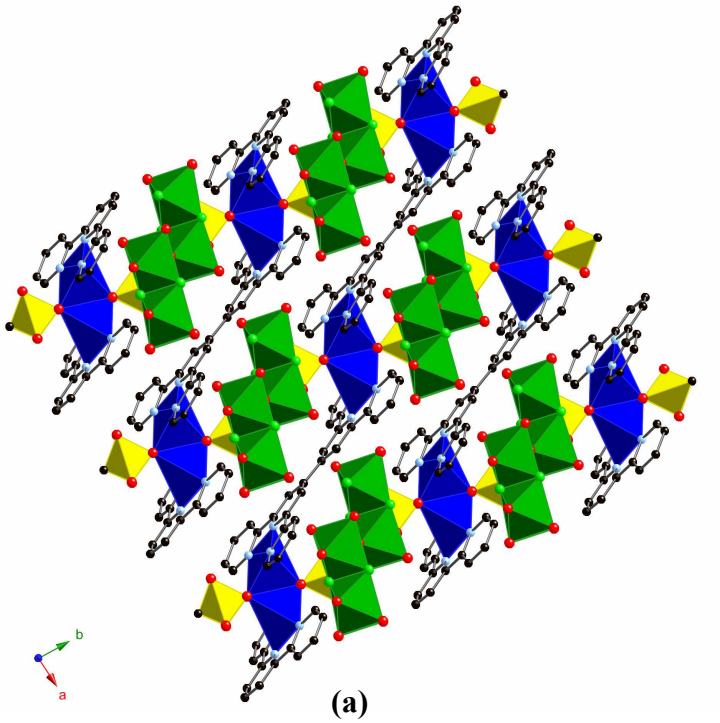

(a)

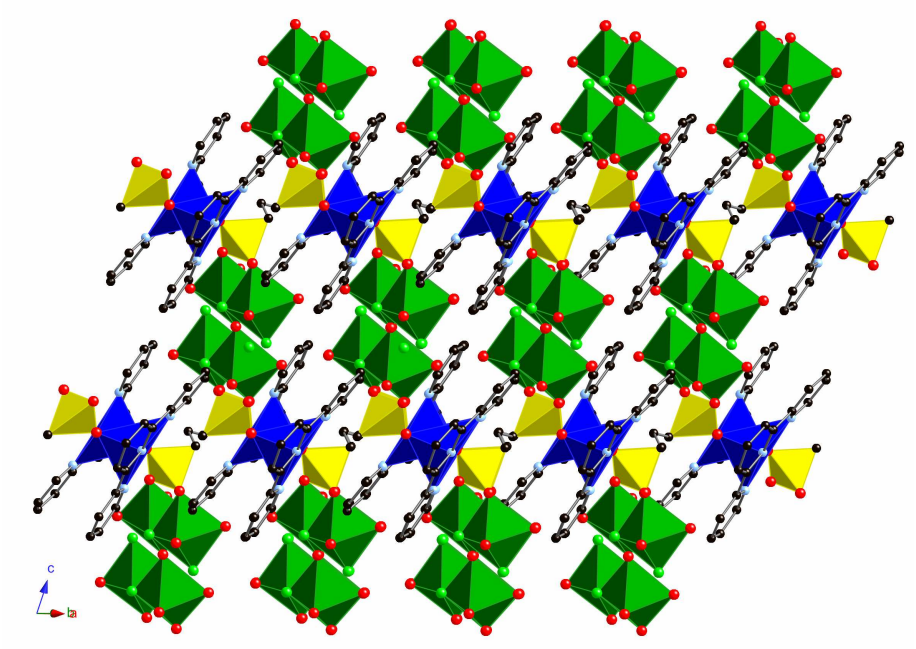

(b)

Figure 3.5. Polyhedral representations of [{Cu_2(bisterpy)}$Mo_4F_6O_9${$O_3P(CH_2)_3PO_3$}] (**3**) viewed **(a)** down the molybdodiphosphonate chains and **(b)** down the copper-bisterpy chains.

hexaylenediphosphonate and nonylenediphosphonate ligands display identical building units.

The molybdodiphosphonate unit of $[\{Cu_2(bisterpy)(H_2O)_2\}Mo_2F_6O_4\{HO_3P(CH_2)_4PO_3H\}]$ (**4**) consists of two $\{MoF_3O_3\}$ octahedra bridged by the butylenediphosphonate ligand through a corner-sharing interaction with one oxo group of each phosphonate end (**Figure 3.6**). Each Cu(II) site

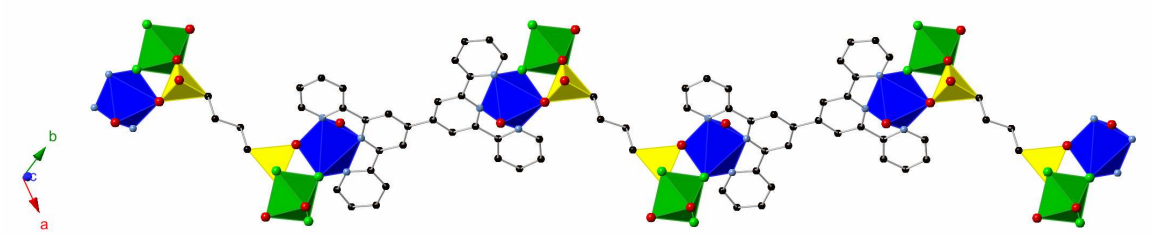

(a)

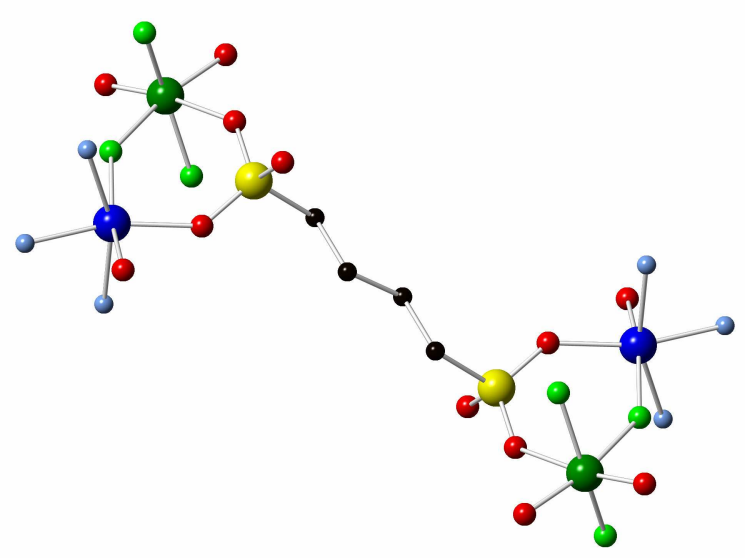

(b)

Figure 3.6. (a) Polyhedral representation of the one-dimensional structure of $[\{Cu_2(bisterpy)(H_2O)_2\}Mo_2F_6O_4\{HO_3P(CH_2)_4PO_3H\}]$ (**4**); **(b)** Ball and stick representation of the oxyfluoromolybdate unit.

links to one oxyfluoromolybdate octahedron through a bridging fluoride and one phosphonate end through a bridging oxo group, leaving one protonated phosphonate oxo group at each end of the ligand. The copper sites are bridged through the bisterpy ligand, and one equatorially coordinated aqua ligand completes the distorted octahedral environment of each copper center. Upon packing, both the coordinated aqua ligands and the protonated phosphonate oxo groups are directed between the chains.

The copper-bisterpy unit of $[\{Cu_2(bisterpy)\}Mo_2F_4O_4\{HO_3P(CH_2)_5PO_3H\}_2]\bullet 2H_2O$ (**5**•$2H_2O$) is similar to that found in **6**, displaying coordination between each Cu(II) site through corner-sharing interactions through a bridging fluoride to the molybdate unit and through a bridging oxo group to one phosphonate end of the diphosphonate ligand (**Figure 3.7**). These distorted square

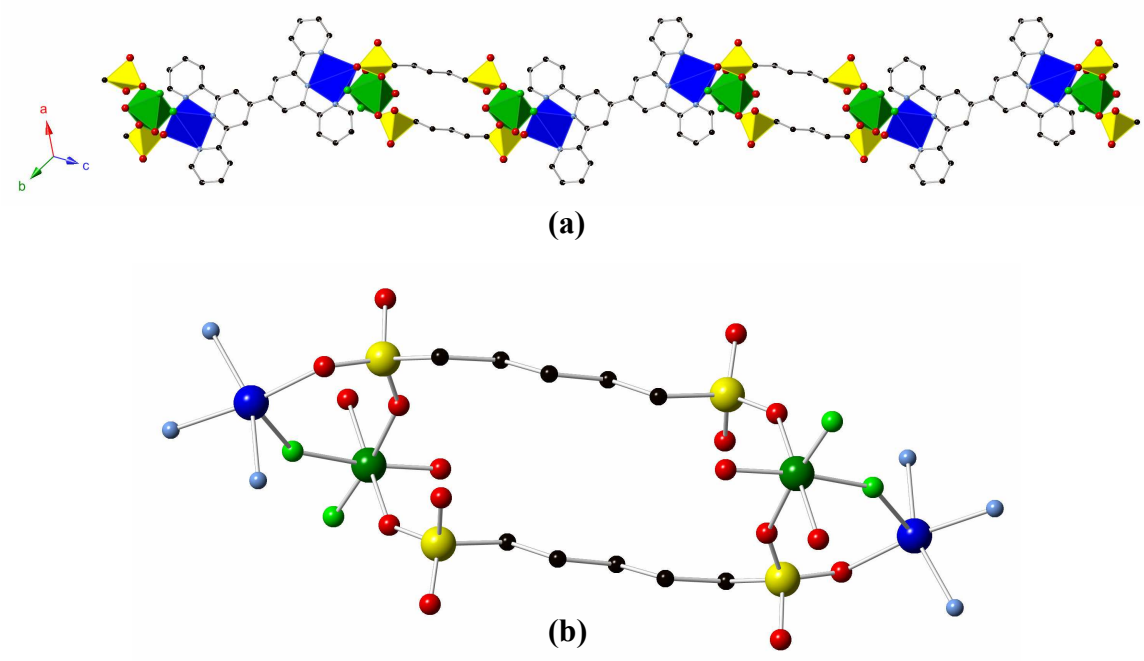

Figure 3.7. (a) Polyhedral representation of the one dimensional structure of $[\{Cu_2(bisterpy)\}Mo_2F_4O_4\{HO_3P(CH_2)_5PO_3H\}_2]\bullet 2H_2O$ (**5**•$2H_2O$); **(b)** Ball and stick representation of the oxyfluoromolybdate unit.

pyramidal Cu(II) centers are then bridged by the bisterpy ligand. The molybdodiphosphonate unit is composed of two $\{MoF_2O_4\}$ octahedra bridged by two pentylenediphosphonate ligands. Each Mo(VI) octahedron coordinates to two diphosphonate ligands through one bridging oxo group of each phosphonate terminus. The diphosphonate ligand contains three uncoordinated and protonated oxo groups, of which two are protonated.

As seen in **Figure 3.8**, the structures of $[\{Cu_2(bisterpy)(H_2O)_2\}Mo_4F_8O_8\{O_3P(CH_2)_6PO_3\}]\bullet 2H_2O$ (**6**$\bullet 2H_2O$) and $[\{Cu_2(bisterpy)(H_2O)_2\}Mo_4F_8O_8\{O_3P(CH_2)_9PO_3\}]$ (**7**) share the same copper-bisterpy and molybdodiphosphonate building units. The oxyfluoromolybdate clusters formed are edge-sharing $\{Mo_2F_4O_6\}$ dimers linked via two bridging fluorides and bridged by the diphosphonate ligand. Each phosphonate terminus coordinates to one oxyfluoromolybdate dimer through two bridging oxo groups. The remaining phosphonate oxo group coordinates to a distorted square pyramidal Cu(II) site, and the copper centers are bridged by the bisterpy ligand. As in **2** and **3**, there is no direct copper-molybdenum coordination in these two structures.

3.3.3 General Structural Observations

When fluoride is incorporated into the structures of copper-molybdate hybrid materials in the presence of diphosphonic acid ligands, the common pentanuclear molybdodiphosphonate clusters are not formed; instead, a variety of novel oxyfluoromolybdate clusters are produced (**Table 3.2**). While phosphonate groups will coordinate to a pentanuclear molybdate cluster through the three oxo groups, leaving the molybdate oxo groups as the only potentital copper coordination sites on the

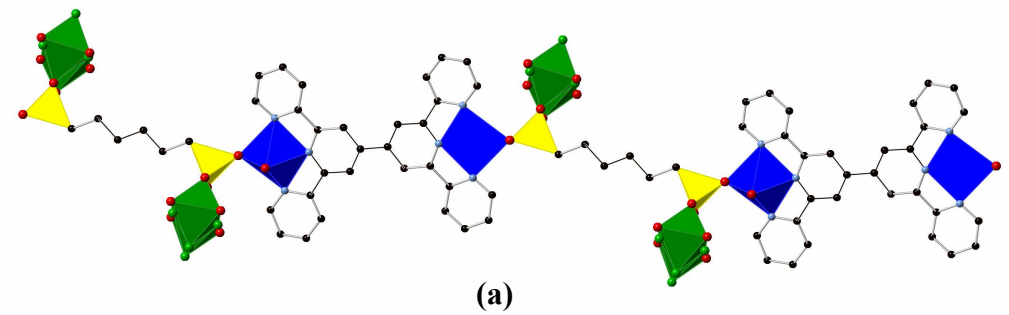

(a)

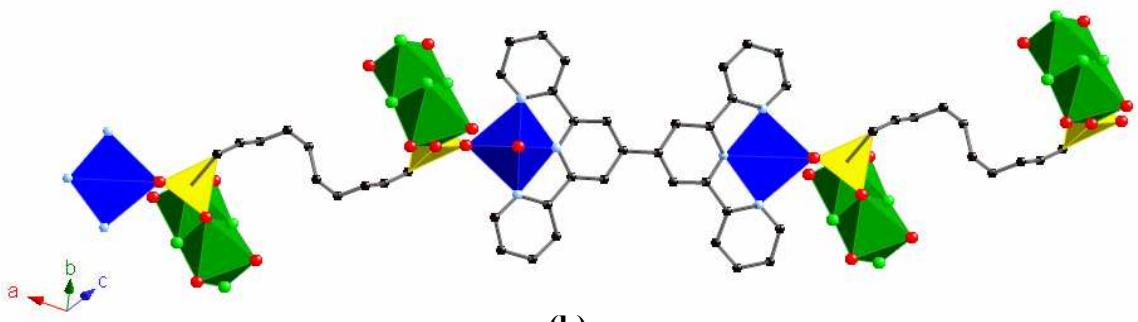

(b)

Figure 3.8. Polyhedral representations of the one-dimensional structures of **(a)** $[\{Cu_2(bisterpy)(H_2O)_2\}Mo_4F_8O_8\{O_3P(CH_2)_6PO_3\}]\bullet 2H_2O$ (**6**•$2H_2O$) and **(b)** $[\{Cu_2(bisterpy)(H_2O)_2\}Mo_4F_8O_8\{O_3P(CH_2)_9PO_3\}]$ (**7**); disorder in the carbon chain of the diphosphonate ligand in **9** around an inversion center leading to two half-occupied carbon atoms located in the center of the chain, thus appearing as 10 atoms instead of 9.

molybdodiphosphonate unit, **1**-**7** all exhibit coordination of copper centers to phosphonate groups with some structures involving additional coordination to molybdate octahedra. Due to the decreased number of potential copper coordination sites on the smaller molybdodiphosphonate units generated within this family of compounds, only one three-dimensional structure is produced while one-dimensional structures are most prevalent.

Table 3.2. Summary of structural characteristics of oxyfluoromolybdate materials.

Compound	Overall Dimensionality	Oxyfluoromolybdate Unit	Reference
$[\{Cu_2(bisterpy)(OH)\}Mo_2F_3O_4\{O_3P(CH_2)PO_3\}]\bullet 11H_2O$ (**1**•$11H_2O$)	2-D	$\{Mo_2F_3O_4(O_3P(CH_2)PO_3)\}^{3-}$ cluster	*a*
$[\{Cu_2(bisterpy)(H_2O)_2\}Mo_4F_4O_{10}\{O_3P(CH_2)_2PO_3\}]$ (**2**)	2-D	$\{Mo_4F_4O_{10}(O_3P(CH_2)_2PO_3)\}^{4-}$ chain	*a*
$[\{Cu_2(bisterpy)\}Mo_4F_6O_9\{O_3P(CH_2)_3PO_3\}]$ (**3**)	3-D	$\{Mo_4F_6O_9(O_3P(CH_2)_3PO_3)\}^{4-}$ chain	*a*
$[\{Cu_2(bisterpy)(H_2O)_2\}Mo_2F_6O_4\{HO_3P(CH_2)_4PO_3H\}]\bullet 2H_2O$ (**4**•$2H_2O$)	1-D	$\{MoF_3O_2(HO_3P(CH_2)_4PO_3H)MoF_3O_2\}^{4-}$ cluster	*a*
$[\{Cu_2(bisterpy)\}Mo_2F_4O_4\{HO_3P(CH_2)_5PO_3H\}_2]\bullet 2H_2O$ (**5**•$2H_2O$)	1-D	$\{MoF_2O_2(HO_3P(CH_2)_5PO_3H)_2MoF_2O_2\}^{4-}$ cluster	*a*
$[\{Cu_2(bisterpy)(H_2O)_2\}Mo_4F_8O_8\{O_3P(CH_2)_6PO_3\}]\bullet 2H_2O$ (**6**•$2H_2O$)	1-D	$\{Mo_2F_4O_4(O_3P(CH_2)_6PO_3)Mo_2F_4O_4\}^{4-}$ cluster	*a*
$[\{Cu_2(bisterpy)(H_2O)_2\}Mo_4F_8O_8\{O_3P(CH_2)_9PO_3\}]$ (**7**)	1-D	$\{Mo_2F_4O_4(O_3P(CH_2)_9PO_3)Mo_2F_4O_4\}^{4-}$ cluster	*a*
$Ni(tpyprz)_2]_2[Mo_4O_{12}F_2][Mo_6O_{19}]$	Molecular	$\{Mo_4O_{12}F_2\}^{2-}$ cluster	30
$[\{Ni_3(tpyprz)_2(H_2O)_2\}(Mo_5O_{15})(Mo_2O_4F_2)\{O_3P(CH_2)_3PO_3\}_2]$	3-D	$\{Mo_2O_4F_2(O_3PR)_2\}^{2-}$ units within molybdodiphosphonate chain	34
$[Cu_4(H_2O)_2(phenbisterpy)_2\{HO_3P(CH_2)_4POH_3\}]$ $[Mo_4FO_{12})_2\{O_3P(CH_2)_4PO_3\}]\bullet 6H_2O$	2-D	$[(Mo_4FO_{12})_2\{O_3P(CH_2)_4PO_3\}]^{6-}$ cluster	53

By altering the tether length of the diphosphonate ligand, a variety of complex, dense-phase materials were produced. Only **4**-**7** offer a direct comparison of the influence of diphosphonate tether lengths, as these compounds contain chains of similar composition. As the tether length is increased from a 4-carbon chain to a 6-carbon chain, the oxyfluoromolybdate clusters are further separated by the extended aliphatic chain. When the tether length is increased further in **7**, the carbon chain begins to fold and kink to provide less spacing between oxyfluoromolybdate clusters.

3.3.4 Magnetic Susceptibility Studies

Magnetic measurements were collected for all compounds. A representative plot of magnetic susceptibility and effective magnetic moment as a function of the temperature is shown in **Figure 3.9**. All compounds exhibit Curie-Weiss paramagnetism. The high temperature data were fit to the Curie-Weiss law:

$$\chi = \chi_h + TIP = \frac{\mu_{eff}^2}{8[T-\theta]} + TIP$$

$$\mu_{eff}^2 = g^2 S(S+1)$$

For these compounds, the paramagnetism is derived exclusively from the Cu(II)-d^9 sites. The data gave the following fits: **1**•11H_2O, θ = -3.2 K, TIP = -0.0009 cm^3/mol, μ_{eff} = 2.86; **2**, θ = -2.2 K, TIP = -0.00009 cm^3/mol, μ_{eff} = 2.75; **3**, θ = -1.1 K, TIP = -0.0003 cm^3/mol, μ_{eff} = 2.76; **4**, θ = -0.9 K, TIP = -0.0004 cm^3/mol, μ_{eff} = 2.78; **5**•2H_2O, θ = -0.54 K, TIP = 0.0001 cm^3/mol, μ_{eff} = 2.73; **6**•2H_2O, θ = -0.20 K, TIP = 0.0005 cm^3/mol, μ_{eff} = 2.85; **7**, θ = -0.20 K, TIP = 0.0005 cm^3/mol, μ_{eff} = 2.65. In each case, the effective magnetic moment is consistent with two Cu(II) sites per formula unit. The data show no evidence of antiferromagnetic ordering even at low temperatures, which is

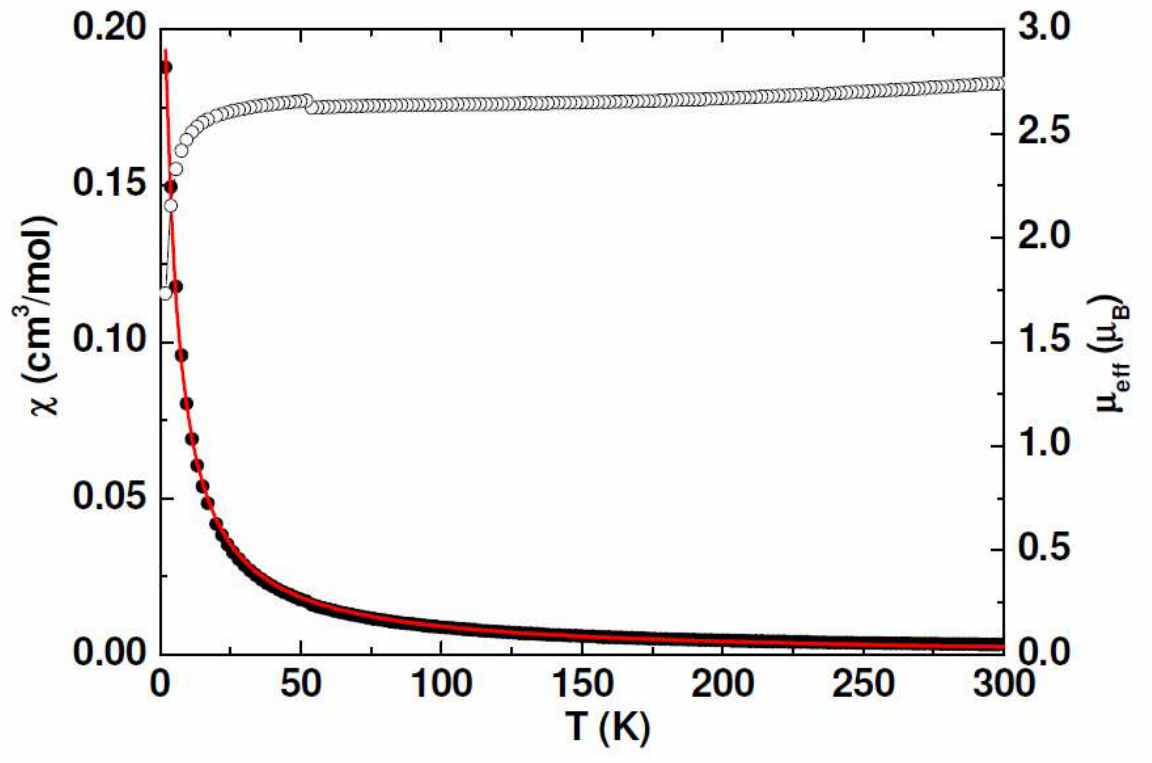

Figure 3.9. The dependence of the magnetic susceptibility χ (●) and effective magnetic moment μ_{eff} (○) of **1**•11H_2O on temperature T. The line drawn through the data is the fit to the Curie-Weiss law.

indicative of a lack of communication between electrons on neighboring copper centers through the bisterpy ligand. This observation can be attributed to the size of the ligand for **1**-**2**, and **4**-**7**, where the distance between metal centers diminishes any possible communication between the magnetic orbitals.

Contrary to the presence of copper(II) dimers in **3**, the magnetic analysis again shows no evidence of antiferromagnetic coupling between metal centers. To elucidate this lack of communication, a HOMO/LUMO molecular orbital determination was made using Gaussian 03w.[65] A simplified cluster containing only the copper centers bridged by oxygens was modeled. The ground state cluster was modeled using density functional

theory (DFT) using the B3LYP functional with a split-valence 6-31 g+(d,p) basis set. The geometric parameters were fixed by the crystallographic data. Within this copper dimer, a short bond (1.93 Å) links each copper to one oxo group while a longer interaction (2.42 Å) provides the axial bond of each copper linking it to the second oxo group. The HOMO and LUMO orbital diagrams of the dimer are illustrated in **Figure 3.10**. The HOMO level consists of the copper $d_{x^2-y^2}$ magnetic orbitals overlapping with

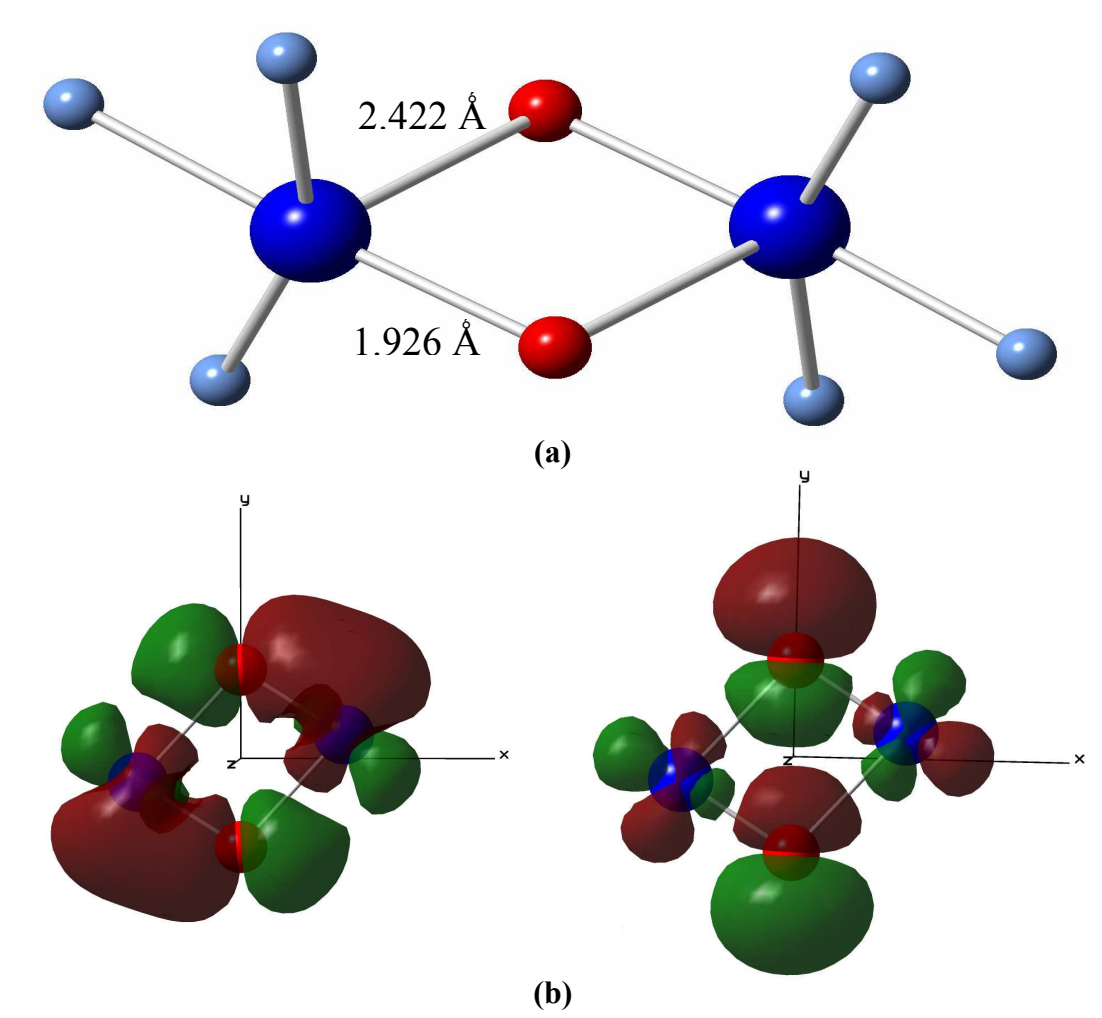

Figure 3.10. (a) Ball and stick representation of the copper(II) dimer of **5** with bond lengths labeled. **(b)** HOMO (left) and LUMO (right) molecular orbital plots of the Cu_2O_2 cluster of compound **5**.

the oxygen p_x orbitals over the short interaction, however the orbitals are too far apart over the longer interaction to allow for orbital overlap as suggested by the paramagnetic character displayed by the magnetic measurements.

3.3.5 Thermal Gravimetric Analysis

The thermal behavior of all compounds was investigated. The thermogravimetric profiles of **1-2** and **6-7** are characterized by an initial weight loss step within the 25-300 ^{o}C range that is attributed to the loss of water molecules of crystallization and aqua ligands. Step-wise decomposition of the organic groups follows up to 725-750 ^{o}C, as illustrated in **Figure 3.11**.

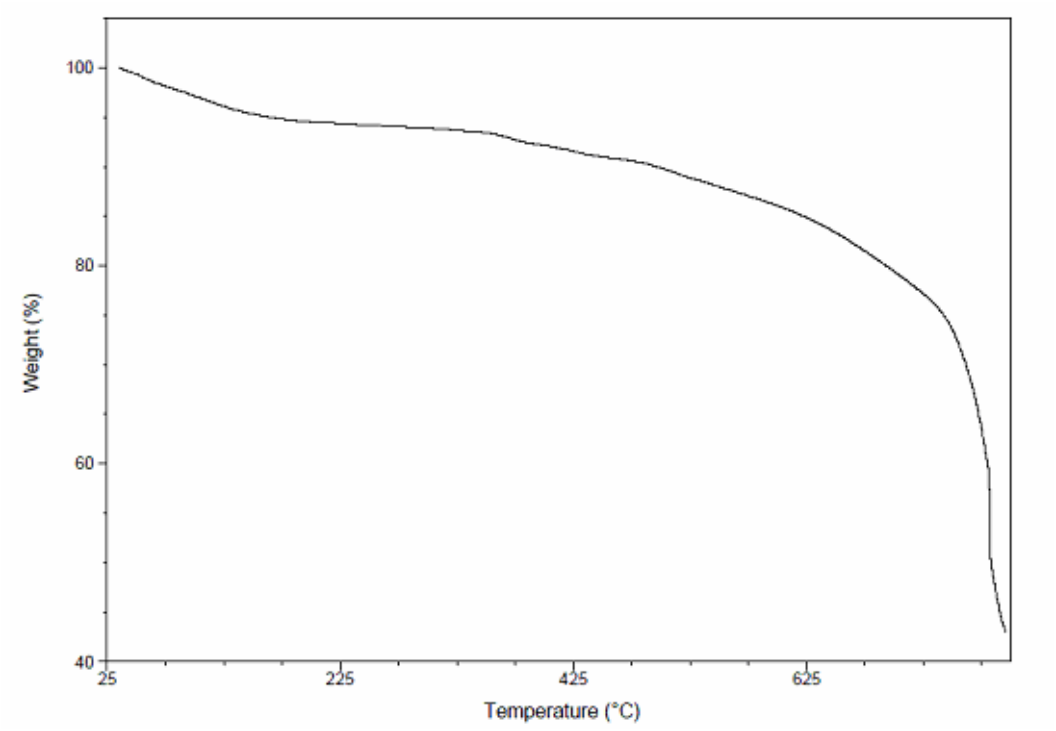

Figure 3.11. Thermogravimetric profile for **1** in the temperature range 25-800 ^{o}C.

Conversely, **4** and **5** display an initial weight loss associated with a simultaneous loss of water molecules of crystallization and aqua ligands, and partial decomposition of the organic groups. Additional weight loss to above 700 ^{o}C is due to the continued decomposition of the organic ligands (**Figure 3.12**).

Compound **3** shows remarkable stability between room temperature and 300 ^{o}C, with no weight loss seen in this range due to the absence of water of crystallization within the structure. A two-step weight loss of *ca.* 15% between 300 and 425 ^{o}C can be attributed to loss of the diphosphonate ligand, followed by a weight loss of *ca.* 25% attributed to the decomposition of the bisterpy ligands (**Figure 3.13**).

3.4 Conclusions

Incorporation of fluoride into copper-bisterpy/molybdodiphosphonate materials results in the formation of several unusual oxyfluoromolybdate clusters in which fluoride groups replace some molybdate oxo groups, affording the three-dimensional $[\{Cu_2(bisterpy)\}Mo_4F_6O_9\{O_3P(CH_2)_3PO_3\}]$ (**3**), the two-dimensional $[\{Cu_2(bisterpy)(OH)\}Mo_2F_3O_4\{O_3P(CH_2)PO_3\}]\bullet 11H_2O$ (**1**$\bullet 11H_2O$) and $[\{Cu_2(bisterpy)(H_2O)_2\}Mo_4F_4O_{10}\{O_3P(CH_2)_2PO_3\}]$ (**2**), and the one-dimensional $[\{Cu_2(bisterpy)(H_2O)_2\}Mo_2F_6O_4\{HO_3P(CH_2)_4PO_3H\}]$ (**4**), $\{Cu_2(bisterpy)\}Mo_2F_4O_4\{HO_3P(CH_2)_5PO_3H\}_2]\bullet 2H_2O$ (**5**$\bullet 2H_2O$), $[\{Cu_2(bisterpy)(H_2O)_2\}Mo_4F_8O_8\{O_3P(CH_2)_6PO_3\}]\bullet 2H_2O$ (**6**$\bullet 2H_2O$) and $[\{Cu_2(bisterpy)(H_2O)_2\}Mo_4F_8O_8\{O_3P(CH_2)_9PO_3\}]$ (**7**). Compounds **2** and **3** contain molybdodiphosphonate chains assembled from unique oxyfluoromolubdate clusters coordinated through the organic tether of the diphosphonate. The prevalent one-

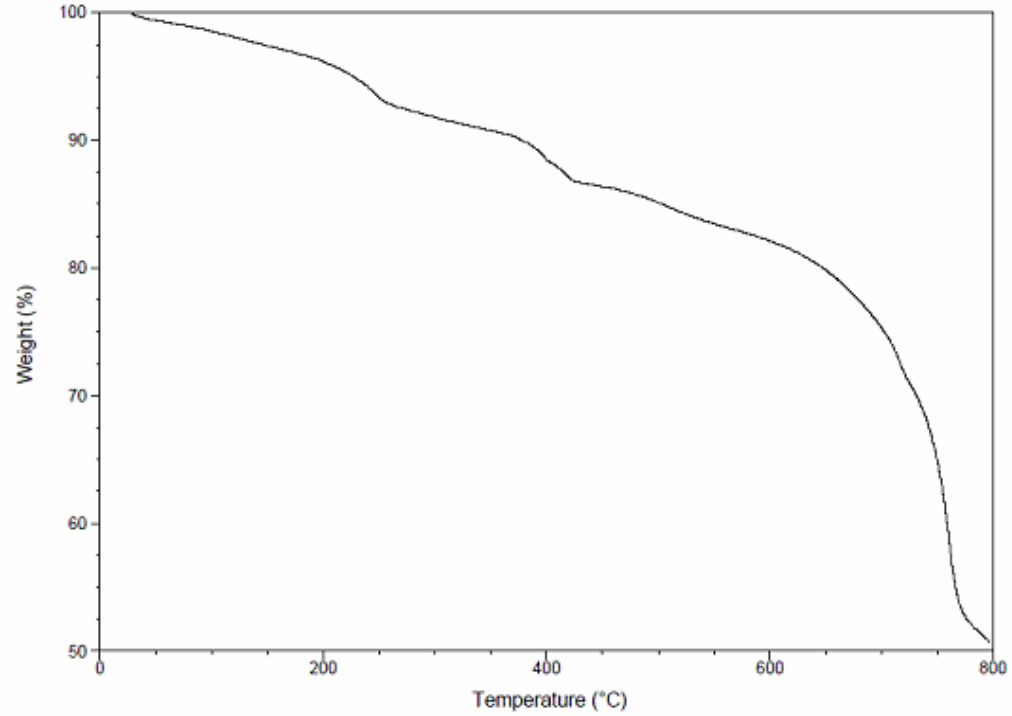

Figure 3.12. Thermogravimetric profile for **4** in the temperature range 25-750 ^{o}C.

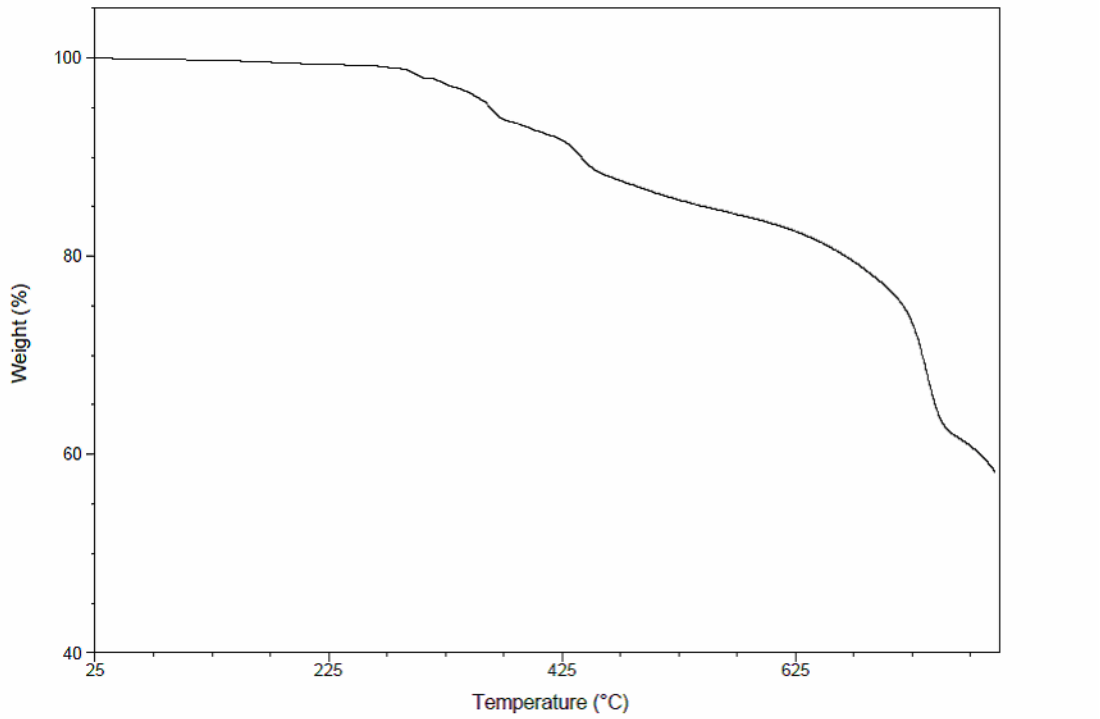

Figure 3.13. Thermogravimetric profile for [{Cu_2(bisterpy)}$Mo_4F_6O_9${$O_3P(CH_2)_3PO_3$}] (**3**) in the temperature range 25-775 ^{o}C.

dimensional structures do not contain distinct molybdodiphosphonate chains, but are instead constructed from isolated molybdodiphosphonate components linked through copper-bisterpy units. Of the fluorinated compounds, only **6**•$2H_2O$ and **7** contain the same oxyfluoromolybdate cluster. It is also noteworthy that the degree of fluorination in these compounds is not directly proportional to the amount of fluoride present in the reaction mixture.

In addition to the tether length of the diphosphonate ligands, it is apparent that the flexibility of the copper(II) centers and the central C-C bond of the bisterpy ligand, the irregular number of copper connection sites on each molybdate cluster, and the array of oxyfluoromolybdate clusters formed leads to the construction of unexpected structures of higher density, unpredictable dimensionality, and variable complexity.

3.5 Acknowledgement

This work was supported by a grant from the National Science Foundation, CHE-0242153.

3.6 References

[1] J. Darriet, W. Massa, J. Pebler and R. Stief, *Solid State Sci.*, 2002, **4**, 1499.

[2] W. Eerenstein, N. D. Mathur and J. F. Scott, *Nature*, 2006, **442**, 759.

[3] A. Tressaud, *Angew. Chem., Int. Ed.*, 2006, **45**, 6792.

[4] K. Adil, M. Leblanc, V. Maisonneuve and P. Lightfoot, *Dalton Trans.*, 2010, **39**, 5983.

[5] K. Scheurell, G. Scholz, E. Kernnity, *J. Solid State Chem*. **2007**, *180*, 749.

[6] M.E. Welk, C.L. Stern, K.R. Poeppelmeier, A.J. Norquist, *Cryst. Growth Des*. **2007**,

7, 956.

[7] M. Estermann, L. B. McCusker, C. Baerlocher, A.Merrouche and H. Kessler, *Nature*, 1991, **352**, 320.

[8] G. A. Senchyk, A. B. Lysenko, H. Krautscheid, K. V. Domasevitch, *Inorg. Chem. Comm*. **2011**, *14*, 1365.

[9] A. Michailovski, H. Ruegger, D. Sheptyakov, G. R. Patzke, *Inorg. Chem.* **2006**, *45*, 5641.

[10] A. Michailovski, J. B. Willems, N. Stock, G. R. Patzke, *Helv. Chim. Acta* **2005**, *88*, 2479.

[11] B. M. Gatehouse, P. Leverett, *J. Chem. Soc. A* **1971**, 2107.

[12] P. Hagenmuller, *Inorganic solid fluorides*, Academic Press, London, **1985**.

[13] F. H. Aidoudi, P. J. Byrne, P. K. Allan, S. J. Teat, P. Lightfoot, R. E. Morris, *Dalton Trans.* **2011**, *40*, 4324.

[14] T. Mahenthirarajah, Y. Li, P. Lightfoot, *Inorg. Chem*. **2008**, *47*, 9097.

[15] F. A. Himeur, P. K. Allan, S. J. Teat, R. J. Goff, R. E. Morris, P. Lightfoot, *Dalton Trans*. **2010**, *39*, 6018.

[16] D. W. Aldous, A. M. Z. Slawin, P. Lightfoot, *J. Solid State Chem*. **2008**, *181*, 3033.

[17] D. W. Aldous, N. F. Stephens, P. Lightfoot, *Dalton Trans*. **2007**, 4207.

[18] D.W. Aldous, N.F. Stephens, P. Lightfoot, *Dalton Trans*. **2007**, 2271.

[19] N. F. Stephens, M. Buck, P. Lightfoot, *J. Mater. Chem*. **2005**, *15*, 4298.

[20] P. A. Maggard, A. L. Kopf, C. L. Stern, K. R. Poeppelmeier, *Inorg. Chem*. **2002**, *41*, 4852.

[21] K.R. Heier, A.J. Norquist, C.G. Wilson, C.L. Stern, K.R. Poeppelmeier, *Inorg. Chem*. **1998**, *37*, 76.

[22] P. A. Maggard, C. L. Stern, K. R. Poeppelmeier, *J. Am. Chem. Soc.* **2001**, 13, 7742.

[23] P. A. Maggard, A. L. Kopf, C. L. Stern, K. R. Poeppelmeier, *Cryst. Eng. Comm.* **2004**, *6*, 451.

[24] T. Mahenthirarajah, Y. Li, P. Lightfoot, *Dalton Trans*. **2009**, 3280.

[25] T. Kanatani, K. Matsumoto, R. Hagiwara, *Eur. J. Inorg. Chem*. **2010**, *7*, 1049.

[26] J. E. Kirsch, H. K. Izumi, L. Stern, K. R. Poeppelmeier, *Inorg. Chem*. **2005**, *44*, 4586.

[27] E. Burkholder, J. Zubieta, *Inorg. Chim. Acta* **2004**, *357*, 279.

[28] B. Kamenar, B. Kaitner, N. Strukan, *Acta Cryst.***1990**, *C46*, 2249.

[29] A. K. Stover, J. R. Gutnick, A. N. Sarjeant, A. J. Norquist, *Inorg. Chem.* **2007**, *46*, 4389.

[30] E. Burkholder, V. Golub, C. J. O'Connor, J. Zubieta, *Inorg. Chem.* **2004**, *43*, 7014.

[31] D. Riou, G. Férey, *J. Solid State Chem*. **1994**, *111*, 422.

[32] D. Riou, F. Taulelle, G. Férey, *Inorg. Chem*. **1996**, *35*, 6392.

[33] G. Bonavia, R. C. Haushalter, J. Zubieta, *J. Solid State Chem*. **1996**, *126*, 292.

[34] W. Ouellette, V. Golub, C. J. O'Connor, J. Zubieta, *Dalton Trans*. **2005**, 291.

[35] W. Ouellette, V. Golub, C. J. O'Connor, J. Zubieta, *J. Solid State Chem*. **2007**, *180*, 2500.

[36] W. Ouellette, M. H. Yu, C. J. O'Connor, J. Zubieta, *Inorg. Chem*. **2006**, *45*, 7628.

[37] Y. Chunag, J. Zubieta, *Inorg. Chem* **1996**, *245*, 177.

[38] R. C. Finn, E. Burkholder, J. Zubieta, *Chem, Commun.* **2001**, 1852.

[39] W. Kwak, M. T. Pope, T. F. Scully, *J. Am. Chem. Soc.* **1975**, *97*, 5735.

[40] B. Hedman, *Acta Cryst.* **1980**, *B36*, 2241.

[41] W. Kwak, L. M. Rajkovic, J. K. Sralick, M. T. Pope, C. O. Quicksall, *Inorg. Chem.* **1976**, *15*, 2778.

[42] A. Vioux, J. LeBideau, P. H. Mutin, D. Leclercq, *Top. Curr. Chem.* **2004**, *232*, 145.

[43] A. Clearfield, *Curr. Opin. Solid State Mater. Sci.* **2002**, *6*, 495.

[44] G. Alberti, in *Comprehensive Supramolecular Chemistry*, J. L. Atwood, J. E. D. Davies, F. Vogel, eds., Pergamon Press, New York, **1966**, *9*, 152.

[45] A. Clearfield, in *Comprehensive Supramolecular Chemistry*; J. L. Atwood, J. E. D. Davies, F. Vogel, eds., Pergamon Press, New York, **1966**, *9*, 107.

[46] A. Clearfield, *Chem. Mater.* **1998**, *10*, 2801.

[47] L. A. Vermeulen, *Prog. Inorg. Chem.* **1997**, *44*, 143.

[48] S. Jones, H. Liu, W. Ouellette, K. Schmidtke, C. J. O'Connor, J. Zubieta, *Inorg. Chem. Comm.* **2010**, *13*, 491.

[49] S. Feng, R. Xu, *Acc. Chem. Res.* **2001**, *34*, 239.

[50] J. Zubieta, *Solid State Methods, Hydrothermal in Comprehensive CoordinationChemistry II*, **2003**, vol. *1*, 697.

[51] J. Gopalakrishnan, N. S. P. Bhuvanesh, K. K. Rangan, *Curr. Opin. Solid State Mater. Sci.* **1996**, *1*, 285.

[52] J. Gopalakrishnan, *Chem. Mater*. **1995**, *7*, 1265.

[53] A. Rabenau, *Angew. Chem., Int. Ed. Engl.* **1985**, *24*, 1026.

[54] A. Stein, S. W. Keller, T. E. Mallouk, *Science* **1993**, *259*, 1558.

[55] J. L. Guth, H. Kessler, R. Wey, Stud. *Surf. Sci. Catal*. **1986**, *28*, 121.

[56] D. W. Aldous, R. J. Goff, J. P. Attfield and P. Lightfoot, *Inorg. Chem.*, **2007**, *46*, 1277.

[57] D. W. Aldous and P. Lightfoot, *Solid State Sci.*, **2009**, *11*, 315.

[58] D. I. Arnold, X. Ouyang, A. Clearfield, *Chem. Mater.* **2002**, *14*, 2020.

[59] E. C. Constable, A. M. W. Cargill Thompson, *J. Chem. Soc. Dalton Trans.* **1992**, 3467.

[60] SMART, Data Collection Software, version 5.630, Bruker-AXS Inc., Madison, WI (1997-2002).

[61] SAINT plus, Data Reduction Software, version 6.45A, Bruker-AXS Inc., Madison, WI (1997-2002).

[62] G. M. Sheldrick, SADABS, University of Göttingen (1996).

[63] SHELXTL PC, version 6.12, Bruker-AXS Inc., Madison, WI (2002).

[64] O'Connor, C. J., *Prog. Inorg. Chem.* **1979**, *29*, 203.

[65] Gaussian 03, Revision B.03, M. J. Frisch, G. W. Trucks, H. B. Schlegel, G. E. Scuseria, M. A. Robb, J. R. Cheeseman, J. A. Montgomery, Jr., T. Vreven, K. N. Kudin, J. C. Burant, J. M. Millam, S. S. Iyengar, J. Tomasi, V. Barone, B. Mennucci, M. Cossi, G. Scalmani, N. Rega, G. A. Petersson, H. Nakatsuji, M. Hada, M. Ehara, K. Toyota, R. Fukuda, J. Hasegawa, M. Ishida, T. Nakajima, Y. Honda, O. Kitao, H. Nakai, M. Klene, X. Li, J. E. Knox, H. P. Hratchian, J. B. Cross, C. Adamo, J. Jaramillo, R. Gomperts, R. E. Stratmann, O. Yazyev, A. J. Austin, R. Cammi, C. Pomelli, J. W. Ochterski, P. Y. Ayala, K. Morokuma, G. A. Voth, P. Salvador, J. J. Dannenberg, V. G. Zakrzewski, S. Dapprich, A. D. Daniels, M. C. Strain, O. Farkas, D. K. Malick, A. D. Rabuck, K. Raghavachari, J. B. Foresman, J. V. Ortiz, Q. Cui, A. G. Baboul, S. Clifford, J. Cioslowski, B. B. Stefanov, G. Liu, A. Liashenko, P. Piskorz, I. Komaromi, R. L. Martin, D. J. Fox, T. Keith, M. A. Al-Laham, C. Y. Peng, A. Nanayakkara, M. Challacombe, P. M. W. Gill, B. Johnson, W. Chen, M. W. Wong, C. Gonzalez, and J. A. Pople, Gaussian, Inc., Pittsburgh PA, 2003.

Chapter 4

Solid State Coordination Chemistry of the Copper/4-Pyridyltetrazolate System

4.1 Introduction

Inorganic oxide materials have garnered much attention due to their vast compositional range and considerable structural diversity, characteristics related to a range of useful physical properties and applications.[1-11] The rational design of new oxide phases drives the development of synthetic strategies. One approach focuses on the use of organic components or metal cations to modify the structure and properties of the oxide produced.[12-19]

Polyoxometalate clusters provide chemically robust and structurally diverse building units around which metal-organic compounds can be constructed.[20-26] Complex structures have been derived from polyoxomolybdate clusters,[26] Anderson,[27-28] Keggin,[29-33] Silverton,[34] and Wells-Dawson and double Dawson type polyanions.[35-37] Of the class of materials constructed from polyoxomolybdate clusters, embedded octamolybdate clusters, $\{Mo_8O_{26}\}^{4-}$ are quite common.[38] An interesting feature of their structural chemistry is the observation of eight isomeric forms of octamolybdates, α through θ.[39-48] Such clusters may be arranged into chains, networks, and frameworks via bridging with secondary metal complexes, which also provide charge compensation for the crystallization of the anionic clusters (**Scheme 4.1**).[49-54]

Incorporation of diphosphonic acid ligands into polyoxomolybdate materials results in the occurrence of a persistent one-dimensional structural motif of the type $\{Mo_5O_{15}(O_3PR)_2\}^{4-}$.[55] In these cases, use of a secondary metal complex again provides charge compensation while displaying a binding affinity for the chain through molybdate oxo groups. A binucleating secondary ligand has the ability to coordinate to two metal centers, and therefore bridge chains to form networks and frameworks according to the

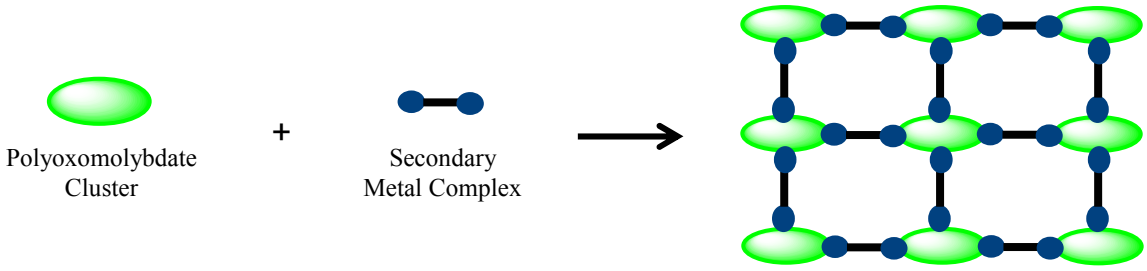

Scheme 4.1.

number of coordination sites on each cluster (**Scheme 4.2**). Examples of this type of connectivity are seen with the binucleating ligands bipyrimidine,[56] tetrapyridylpyrazine,[57] and bisterpy.[58]

A multi-nucleating secondary ligand offers a wider range of coordination chemistry due to the ability to coordinate to more than two metal centers.[59] Polyazaheteroaromatic ligands have been utilized in the construction of metal-organic materials that show promising hydrogen-storage and interesting magnetic properties.[60-63]

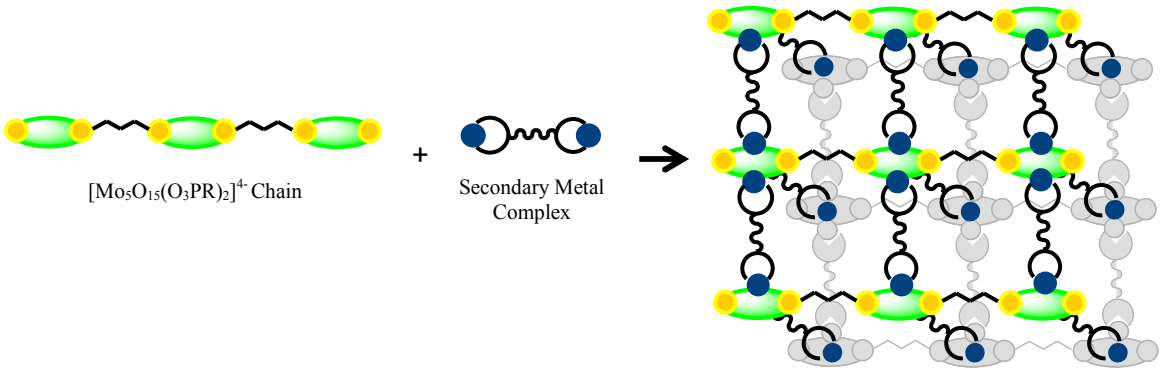

Scheme 4.2.

Analogous to the five-membered monocyclic pyrazole, imidazole, triazole, and tetrazole ligands, 5-(4'-pyridyl)tetrazole (4-pt) can exist in both the protonated neutral form and the anionic azolate form by deprotonation of the acidic N-H group (**Scheme 4.3**).[64] Anionic 4-pt may link metal centers through N2 and N3 positions to provide one-

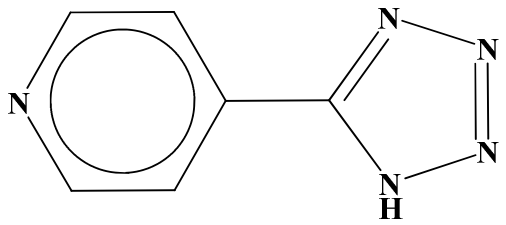

5-(4'-pyridyl)tetrazole

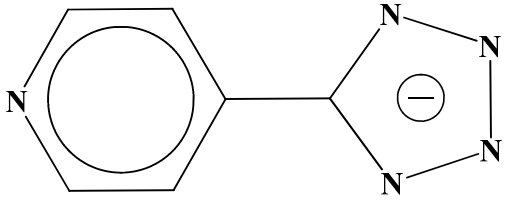

5-(4'-pyridyl)tetrazolate

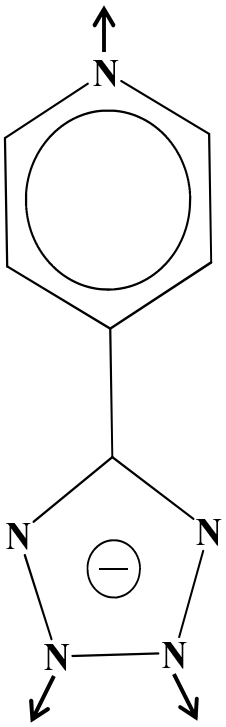

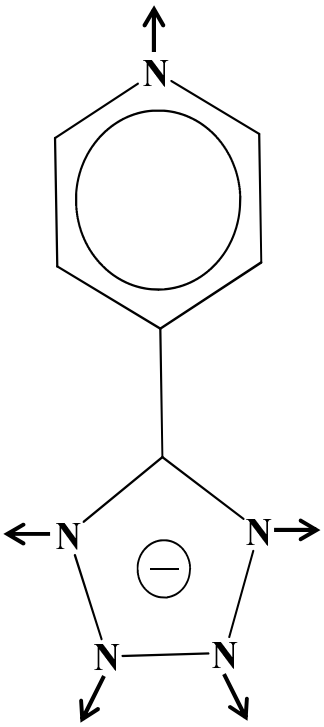

Scheme 4.3.

dimensional or oligomeric building blocks. These units can then be linked through the pyridyl nitrogen to expand the overall dimensionality of the structure. Additional coordination to the N1 and N4 tetrazolate nitrogens may also occur, further increasing the complexity of the secondary metal-ligand cationic component.

Hydrothermal conditions have been exploited in the synthesis of six novel copper/4-pt materials incorporating polyoxomolybdate building units. The two-dimensional $[\{Cu_3(4\text{-pt})_2(4\text{-Hpt})_2(H_2O)_2\}\{\beta\text{-}Mo_8O_{26}\}]\bullet 2H_2O$ (**1**•$2H_2O$), the three-dimensional $[\{Cu_{10}(4\text{-pt})_6(4\text{-Hpt})_2\}\{\beta\text{-}MoO_{26}\}]\bullet 2H_2O$ (**2**•$2H_2O$) and $[\{Cu_4(4\text{-Hpt})_3(H_2O)\}Mo_5O_{15}\{O_3P(CH_2)_2PO_3\}]\cdot 2.25H_2O$ (**3**·$2.25H_2O$), the one-dimensional $[Cu_6(4\text{-pt})_2(4\text{-Hpt})_2][PMo^{V}Mo^{VI}_{11}O_{40}]\cdot 2.5H_2O$ (**4**·$2.5H_2O$) and $[Cu_3(OH)(4\text{-pt})_2(4\text{-Hpt})_2(H_2O)_2][PMo_{12}O_{40}]\bullet 10.5H_2O$ (**5**•$10.5H_2O$), and the two-dimensional $[Cu_3(OH)(4\text{-pt})_3(4\text{-}H_2pt)(H_2O)][PMo_{12}O_{40}]\cdot 7.5H_2O$ (**6**·$7.5H_2O$) materials have been prepared.

4.2 Experimental Section

All chemicals were used as obtained without further purification. Molybdenum(VI) Oxide (99.5%) was purchased from Alfa Aesar. Cupric Acetate was purchased from Baker. The diphosphonate ligands 1,2-ethylenediphosphonic acid and 1,3-propylenediphosphonic acid were synthesized according to methods reported in the literature[19]. All syntheses were carried out in 23mL poly(tetrafluroethylene) lined stainless steel containers under autogenous pressure. The pH of the solutions were measured both prior to and following heating using *pHydrion*™ pH paper. Water was distilled above 3.0MΩ in-house using a Barnstead Model 525 Biopure Distilled Water Center.

4.2.1 Synthesis of 5-(4'-pyridyl)tetrazole

A mixture of 4-cyanopyridine (6.25g, 60mmol), NaN_3 (11.70g, 180mmol), and triethylamine hydrochloride (24.70g, 180mmol) in toluene (150mL) and methanol (30mL) was heated at reflux for 3 days. Upon cooling to room temperature, an aqueous solution of NaOH (1.0M, 100mL) was added and the mixture was stirred for 30 minutes. The aqueous layer was separated and treated with concentrated HCl until the solution reached pH 5.0. The white precipitate was collected by filtration and dried in air.

4.2.2 Synthesis of $[\{Cu_3(4\text{-pt})_2(4\text{-Hpt})_2(H_2O)_2\}\{\beta\text{-}Mo_8O_{26}\}]\bullet 2H_2O$ ($1\bullet 2H_2O$)

A solution of cupric acetate (0.136g, 0.6812mmol), molybdenum(VI) oxide (0.196g, 1.3617mmol), 4-Hpt (0.050g, 0.3401mmol), and H_2O (10.00g, 556mmol) with the mole ratio 2.00:4.00:1.00:1634.81 was stirred briefly before heating to 135^{o}C for 4 days with initial and final pH values of 5.0 and 3.5, respectively. Blue plate crystals were isolated in 85% yield that were suitable for X-ray diffraction. IR (KBr pellet, cm^{-1}): 3421(w), 1645(m), 1448(w), 1434(w), 945(s), 918(m), 885(s), 873(s), 846(m), 713(s), 536(w), 521(w).

4.2.3 Synthesis of $[\{Cu_{10}(4\text{-pt})_6(4\text{-Hpt})_2\}\{\beta\text{-}MoO_{26}\}]\bullet 2H_2O$ ($2\bullet 2H_2O$)

A solution of cupric acetate (0.136g, 0.6812mmol), molybdenum(VI) oxide (0.196g, 1.3617mmol), 4-Hpt (0.050g, 0.3401mmol), and H_2O (10.00g, 556mmol) with the mole ratio 2.00:4.00:1.00:1634.81 was stirred briefly before heating to 180^{o}C for 2 days with initial and final pH values of 5.2 and 3.2, respectively. Yellow plate crystals were isolated in 35% yield that were suitable for X-ray diffraction. IR (KBr pellet, cm^{-1}): 3447(s), 2923(w), 2854(w), 1655(s), 1637(s), 1625(s), 1509(m), 1438(m), 940(s), 910(s), 837(s), 669(s).

4.2.4 Synthesis of $[\{Cu_4(4\text{-Hpt})_3(H_2O)\}Mo_5O_{15}\{O_3P(CH_2)_2PO_3\}]\cdot 2.25H_2O$ $(3\cdot 2.25H_2O)$

A solution of cupric acetate (0.136g, 0.6812mmol), molybdenum(VI) oxide (0.196g, 1.3617mmol), 1,2-ethylenediphosphonic acid (0.129g, 0.6787mmol), 4-Hpt (0.050g, 0.3401mmol), and H_2O (10.00g, 556mmol) with the mole ratio 2.00:4.00:2.00:1.00:1634.81 was stirred briefly before heating to 180°C for 2 days with initial and final pH values of 2.5 and 1.5, respectively. Orange crystals were isolated in 20% yield that were suitable for X-ray diffraction. IR (KBr pellet, cm^{-1}): 3422(s), 1637(s), 1560(s), 1536(s), 1439(s), 1200(s), 1124(s), 1100(s), 1046(s), 967(s), 937(s), 910(s), 851(s), 752(s), 715(s), 529(m).

4.2.5 Synthesis of $[Cu_6(4\text{-pt})_2(4\text{-Hpt})_2][PMo^{V}Mo^{VI}_{11}O_{40}]\cdot 2.5H_2O$ $(4\cdot 2.5H_2O)$

A solution of cupric acetate (0.136g, 0.6812mmol), molybdenum(VI) oxide (0.196g, 1.3617mmol), 1,2-ethylenediphosphonic acid (0.129g, 0.6787mmol), 4-PT (0.050g, 0.3401mmol), H_2O (10.00g, 556mmol), and hydrofluoric acid (0.100mL, 5.79mmol) with the mole ratio 2.00:4.00:2.00:1.00:1634.81:17.02 was stirred briefly before heating to 180°C for 2 days with initial and final pH values of 1.8 and 1.5, respectively. Black crystals were isolated in 90% yield that were suitable for X-ray diffraction. IR (KBr pellet, cm^{-1}): 3448(s), 1638(s), 1525(s), 1439(s), 1055(s), 948(s), 905(m), 803(s).

4.2.6 Synthesis of $[Cu_3(OH)(4\text{-pt})_2(4\text{-Hpt})_2(H_2O)_2][PMo_{12}O_{40}]\bullet 10.5H_2O$ $(5\bullet 10.5H_2O)$

A solution of cupric acetate (0.138g, 0.6812mmol), molybdenum(VI) oxide (0.195g, 1.3655mmol), 1,3-propylenediphosphonic acid (0.139g, 0.7356mmol), 4-Hpt

(0.050g, 0.3401mmol), H_2O (10.00g, 556mmol), and hydrofluoric acid (0.100mL, 5.79mmol) with the mole ratio 2.00:4.01:2.16:1.00:1634.81:17.02 was stirred briefly before heating to 100°C for 4 days with initial and final pH values of 3.0 and 1.0, respectively. Green block crystals were isolated in 90% yield that were suitable for X-ray diffraction. IR (KBr pellet, cm^{-1}): 3422(s), 1638(s), 1543(s), 1523(m), 1439(m), 1064(s), 959(s), 881(s), 799(s), 745(w).

4.2.7 Synthesis of $[Cu_3(OH)(4\text{-pt})_3(4\text{-}H_2pt)(H_2O)][PMo_{12}O_{40}]\cdot 7.5H_2O$ ($6\cdot 7.5H_2O$)

A solution of cupric acetate (0.137g, 0.6862mmol), molybdenum(VI) oxide (0.197g, 1.3689mmol), 1,3-propylenediphosphonic acid (0.138g, 0.7304mmol), 4-Hpt (0.053g, 0.3605mmol), and H_2O (10.00g, 556mmol) with the mole ratio 1.90:3.78:2.03:1.00:1542.30 was stirred briefly before heating to 150°C for 4 days with initial and final pH values of 3.0 and 1.0, respectively. Green block crystals were isolated in 30% yield that were suitable for X-ray diffraction. IR (KBr pellet, cm^{-1}): 3422(s), 1638(s), 1543(s), 1524(s), 1437(m), 1203(m), 1063(s), 1016(w), 962(s), 880(s), 805(s), 755(w), 503(w).

4.2.8 X-ray Crystallography

Crystallographic data of all compounds were collected at low temperature (90K) on a Bruker P4 diffractometer using Mo-K_α radiation (λ = 0.71073Å) equipped with a SMART CCD system[20]. The data were corrected for Lorentz and polarization effects,[21] and adsorption corrections were made using SADABS[22]. The structures were solved by direct methods and refinements were made using the SHELXTL[23] crystallographic software. After first locating all of the nonhydrogen atoms from the initial solution of

each structure, the models were refined against F^2 using first isotropic and then anisotropic thermal displacement parameters until the final value of Δ/σ_{max} was less than 0.001. Hydrogen atoms were introduced in calculated positions and refined isotropically. Neutral atom scattering coefficients and anomalous dispersion corrections were taken from the *International Tables*, Vol. C. Crystallographic details for the structures of **1**-**6** are summarized in **Table 4.1**.

4.2.9 Magnetic Measurments

The magnetic data were recorded on a polycrystalline sample of $[\{Cu_3(4\text{-pt})_2(4\text{-Hpt})_2(H_2O)_2\}\{Mo_8O_{26}\}]\bullet 2H_2O$ (**1**$\bullet 2H_2O$) in the 2-300 K temperature range using a Quantum Design MPMS-5S SQUID spectrometer. The temperature dependent magnetic data were obtained at a magnetic field of H = 1000 Oe.

4.2.10 Thermal Gravimetric Analysis

Thermal gravimetric studies were performed using 10mg samples in an Auto TGA 2950 instrument under 50 mL/min flow of synthetic air. The temperature was ramped from 25 to 800^{o}C at a rate of 5^{o}C/min for the decomposition.

4.3 Results and Discussion

4.3.1 Synthesis and Infrared Spectroscopy

Compounds **1** and **2** were prepared by the hydrothermal reactions of $Cu(CH_3CO_2)_2\cdot H_2O$, MoO_3, and 5-(4'-pyridyl)tetrazole at pH 5.0-5.2. Compounds **3**-**6** also included a diphosphonic acid ligand, and their reactions occurred at pH 1.8-3.0. The stoichiometry of starting materials was held constant while the reaction temperature and pH were optimized for each compound. Compounds **1** and **5**-**6** formed between 100 ^{o}C

Table 4.1. Summary of crystallographic data for the structures of [{Cu_3(4-pt)$_2$(4-Hpt)$_2$(H_2O)$_2$}{β-Mo_8O_{26}}]•2H_2O (**1**•2H_2O), [{Cu_{10}(4-pt)$_6$(4-Hpt)$_2$}{β-MoO_{26}}]•2H_2O (**2**•2H_2O), [{Cu_4(4-Hpt)$_3$(H_2O)}Mo_5O_{15}{$O_3P(CH_2)_2PO_3$}]·2.25H_2O (**3**·2.25H_2O), [Cu_6(4-pt)$_2$(4-Hpt)$_2$][$PMo^{V}Mo^{VI}_{11}O_{40}$]·2.5$H_2O$ (**4**·2.5H_2O), [Cu_3(OH)(4-pt)$_2$(4-Hpt)$_2$(H_2O)$_2$][$PMo_{12}O_{40}$]•10.5H_2O (**5**•10.5H_2O), and [Cu_3(OH)(4-pt)$_3$(4-H_2pt)(H_2O)][$PMo_{12}O_{40}$]·7.5H_2O (**6**·7.5H_2O).

	1•2H_2O	**2**•2H_2O	**3**·2.25H_2O	**4**·2.5H_2O	**5**•10.5H_2O	**6**·7.5H_2O
Empirical Formula	$C_{12}H_{13}Cu_{1.50}Mo_4N_{10}O_{15}$	$C_{24}H_{19}Cu_5Mo_4N_{20}O_{14}$	$C_{20}H_{25.50}Cu_4Mo_5N_{15}O_{24.25}P_2$	$C_{18}H_{16.50}Cu_3Mo_6N_{15}O_{21.25}P_{0.50}$	$C_{24}H_{44}Cu_3Mo_{12}N_{20}O_{53.50}P$	$C_{24}H_{32}Cu_3Mo_{12}N_{20}O_{49.50}P$
FW	1016.39	1513.05	1659.85	1564.71	2841.66	2765.57
Crystal System	Monoclinic	Triclinic	Monoclinic	Triclinic	Monoclinic	Triclinic
Space Group	$P2_1/c$	$P\bar{1}$	$C2/c$	$P\bar{1}$	$P2_1/c$	$P\bar{1}$
a, Å	10.5475(11)	11.0227(7)	25.662(3)	12.0267(8)	23.001(2)	12.6659(18)
b, Å	18.2950(18)	11.6049(7)	15.9357(18)	12.2807(8)	12.9425(12)	12.6742(18)
c, Å	12.9152(13)	15.8019(10)	22.211(3)	13.9204(9)	25.023(2)	23.583(3)
α, deg	90	97.2190(10)	90	100.3050(10)	90	83.460(3)
β, deg	90.402(2)	102.5180(10)	114.353(2)	98.5230(10)	109.700(2)	84.445(3)
γ, deg	90	102.9640(10)	90	113.0350(10)	90	61.237(3)
V, Å^3	2492.1(4)	1890.4(2)	8274.8(16)	1806.7(2)	7013.2(11)	3293.3(8)
Z	4	2	8	2	4	2
D_{calcd}, g cm^{-1}	2.709	2.658	2.665	2.876	2.691	2.789
μ, mm^{-1}	3.306	4.130	3.661	3.869	3.102	3.294
T, K	90(2)	90(2)	90(2)	90(2)	90(2)	90(2)
λ, Å	0.71073	0.71073	0.71073	0.71073	0.71073	0.71073
R1[a]	0.0462	0.0379	0.0303	0.0475	0.0768	0.0698
wR2[b]	0.1144	0.0931	0.1166	0.0922	0.1844	0.1830

[a] $R1 = \Sigma||F_o| - |F_c||/\Sigma|F_o|$. [b] $wR2 = \{\Sigma[w(F_o^2 - F_c^2)^2]/\Sigma[w(F_o^2)^2]\}^{1/2}$.

and 150 ^{o}C while **2-4** required a higher temperature, 180 ^{o}C. The high temperature phases all exhibit reduction of the copper centers to Cu(I), which is a common result in the presence of nitrogenous ligands.

The infrared spectra of **1-6** are characterized by one to two strong bands between 900 and 975 cm^{-1} assigned to ν(Mo=O) and a strong band at 830-885 cm^{-1} assigned to ν(Mo-O-Mo). A series of bands in the range 1300-1645 cm^{-1} is attributed to the pyridyltetrazole ligand. Compound **3** exhibits a series of four strong bands between 1000 and 1200 cm^{-1} assigned to the 1,2-ethylenediphosphonate, while the spectra of **4-6** include a strong band at 1050-1060 cm^{-1} assigned to the keggin phosphate group.

4.3.2 X-ray Structures

As shown in **Figure 4.1(a)**, the structure of $[\{Cu_3(4\text{-pt})_2(4\text{-Hpt})_2(H_2O)_2\}\{\beta\text{-}Mo_8O_{26}\}]\bullet 2H_2O$ (**1**$\bullet 2H_2O$) is two-dimensional. The layer is constructed from $\{\beta\text{-}Mo_8O_{26}\}^{4-}$ clusters and a $\{Cu_3(4\text{-pt})_2(4\text{-Hpt})_2(H_2O)_2\}_n^{4n+}$ network. The β-octamolybdate cluster consists of a compact arrangement of eight edge-sharing $\{MoO_6\}$ octahedra. Six molybdenum sites exhibit two terminal oxo-groups, while the central pair of molybdenum sites exhibits a single terminal oxo-group. In total, there are six μ_2-, four μ_3- and two μ_5- oxo-groups. The $\{Mo_8O_{26}\}^{4-}$ clusters are embedded within the two-dimensional copper-pyridyltetrazole substructure.

The $\{Cu_3(4\text{-pt})_2(4\text{-Hpt})_2(H_2O)_2\}_n^{4n+}$ network consists of trinuclear units of corner-sharing copper octahedra linked through the dipodal 4-pt ligands (**Figure 4.1(b)**). The copper triads form from a linear arrangements of two peripheral '4+2' axially distorted $\{CuO_3N_3\}$ octahedra and a central $\{CuO_2N_4\}$ polyhedron. The central copper site is linked to each terminal copper center through two N2, N3-bridging tetrazolate groups and

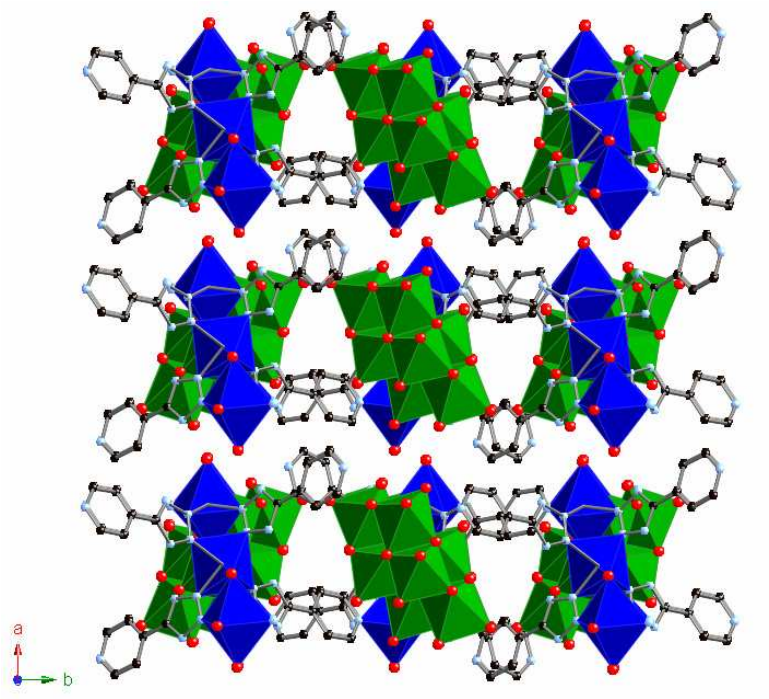

(a)

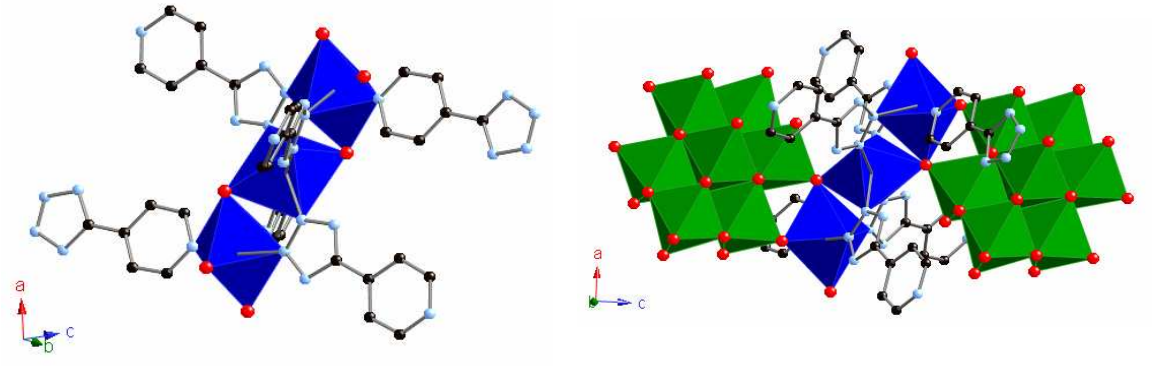

(b)

Figure 4.1. (a) A mixed polyhedral and ball and stick representation of the layer structure of $[\{Cu_3(4\text{-pt})_2(4\text{-Hpt})_2(H_2O)_2\}\{\beta\text{-}Mo_8O_{26}\}]\bullet 2H_2O$ (**1**•$2H_2O$) in the *ab* plane and **(b)** views of the copper/4-pt substructure of **1**•$2H_2O$, illustrating the trinuclear building unit with and without the $\{\beta\text{-}Mo_8O_{26}\}^{4-}$ clusters.

through an oxo-group from a neighboring cluster. The peripheral copper sites of the trinuclear unit also bond to an axial water molecule, an equatorial pyridyl nitrogen from a 4-pt ligand linking to an adjacent triad and to a terminal oxo-group of a molybdate cluster. As a consequence of this connectivity pattern, each molybdate cluster bonds to two copper clusters, while each $\{Cu_3(4\text{-pt})_2(4\text{-Hpt})_2(H_2O)_2\}^{4+}$ cluster is connected to four adjacent copper clusters through bridging 4-pt ligands. Two of the pyridyltetrazole groups of the copper clusters are protonated at the pyridyl nitrogen. These pendant 4-Hpt groups rest on the faces of the layers, while the coordinated water molecules project into the interlamellar domain. The water molecules of crystallization occupy the interlamellar domain and hydrogen bond to the pyridyl nitrogen hydrogen atom.

In contrast, the structure of $[\{Cu_{10}(4\text{-pt})_6(4\text{-Hpt})_2\}\{\beta\text{-}MoO_{26}\}]\bullet 2H_2O$ (**2**$\bullet 2H_2O$) is three-dimensional, as shown in **Figure 4.2**. In this case, the $\{\beta\text{-}Mo_8O_{26}\}^{4-}$ clusters are embedded in a three dimensional $\{Cu_{10}(4\text{-pt})_6(4\text{-Hpt})_2\}_n^{4n+}$ framework constructed from $\{CuN_4\}$ tetrahedra and $\{CuN_3\}$ and $\{CuN_2O\}$ trigonal planar sites. The copper substructure may be described as chains of copper tetrahedra and trigonal planes linked through tetrazolate groups bridging through the N2, N3, N4-donors. As shown in **Figure 4.2(b)**, each tetrazolate group bridges three copper sites. The pyridyltetrazole ligands are disposed so as to project the pyridyl termini outward from the chain. The nitrogen donors of half of these pyridyl groups bond to an exo-chain $\{CuN_2O\}$ site, each of which links two chains. The remaining pyridyl groups are protonated and non-coordinating (**Figure 4.2(c)**). The molybdate clusters populate the channels formed by the $\{Cu_{10}(4\text{-pt})_6(4\text{-Hpt})_2\}_n^{4n+}$ framework. Each cluster bonds through doubly-bridging oxo-groups to form

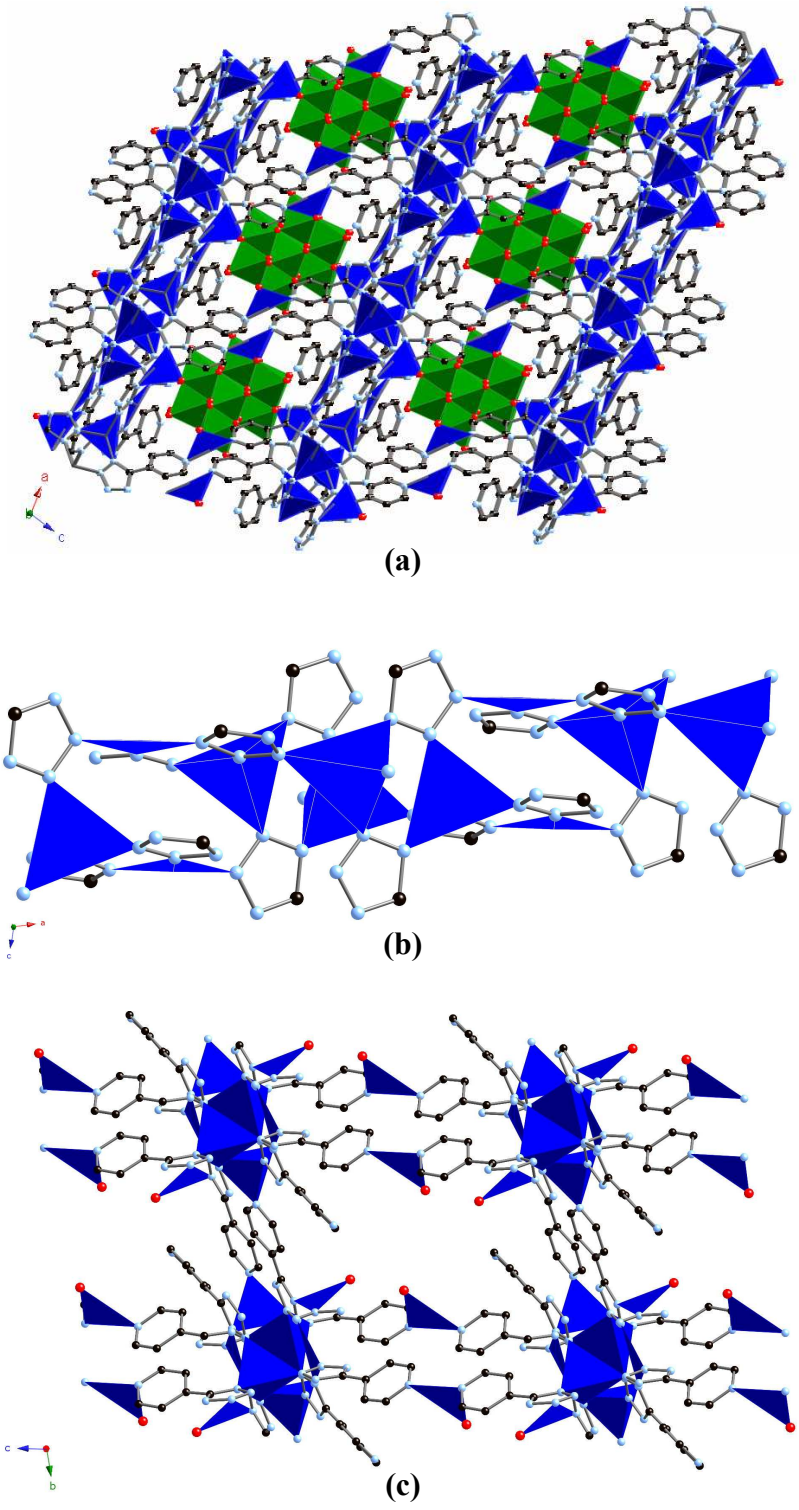

Figure 4.2. **(a)** A view of the three-dimensional structure of [{Cu_{10}(4-pt)$_6$(4-Hpt)$_2$} {β-MoO_{26}}]•2H_2O (**2**•2H_2O) in the *ac* plane; **(b)** the Cu/4-pt chain building block; and **(c)** a view parallel to the chain axes, showing the linking of chains through the exo-catenate copper sites (*bc* plane).

{CuN_2O} trigonal planar units, two associated with the copper chain substructures and two of the exo-catenate type.

The three-dimensional structure of [{Cu_4(4-Hpt)$_3$(H_2O)}Mo_5O_{15}{$O_3P(CH_2)_2PO_3$}]·2.25H_2O (**3**·2.25H_2O) contains {$Mo_5O_{15}(O_3PR)_2$}$_n^{4n-}$ chains embedded within a complex Cu(I)/4-pt framework (**Figure 4.3**). As seen in **Figure 4.3(b)**, the molybdodiphosphonate chain is composed of pentanuclear molybdate clusters linked through the organic tether of the 1,2-ethylenediphosphonate ligand.

The {Cu_4(4-Hpt)$_3$(H_2O)}$^{4+}$ framework contains four distinct Cu(I) tetrahedra linked through the tetrazolate ends of the 4-pt ligands (**Figure 4.3(c)**). Two copper centers are defined by three tetrazolate nitrogens and one molybdate oxo group, the third site coordinates to three tetrazolate nitrogens and one aqua ligand, and the fourth site links to four tetrazolate nitrogens. This results in coordination of either three or four of the tetrazolate nitrogens on each ligand to copper centers, while all pyridyl nitrogens are protonated. The framework forms two sets of orthogonal channels within which the molybdodiphosphonate chains are located (**Figure 4.3(d)**). The protonated pyridyl groups and aqua ligands are directed into the channels.

The structure of [Cu_6(4-pt)$_2$(4-Hpt)$_2$][$PMo^{V}Mo^{VI}_{11}O_{40}$]·2.5$H_2O$ (**4**·2.5H_2O) is formed by the arrangement of Cu(I)/4-pt chains around uncoordinated α-keggin clusters (**Figure 4.4**). The α-keggin cluster {$PMo^{V}Mo^{VI}_{11}O_{40}$}$^{4-}$ consists of eleven {$Mo^{VI}O_6$} and one {$Mo^{V}O_6$} octahedra that form four {Mo_3O_{13}} units arranged on a sphere and linked via twenty four bridging oxo groups. Each of the twelve molybdenum sites exhibits one terminal oxo group. The central phosphate tetrahedron coordinates to the cluster through

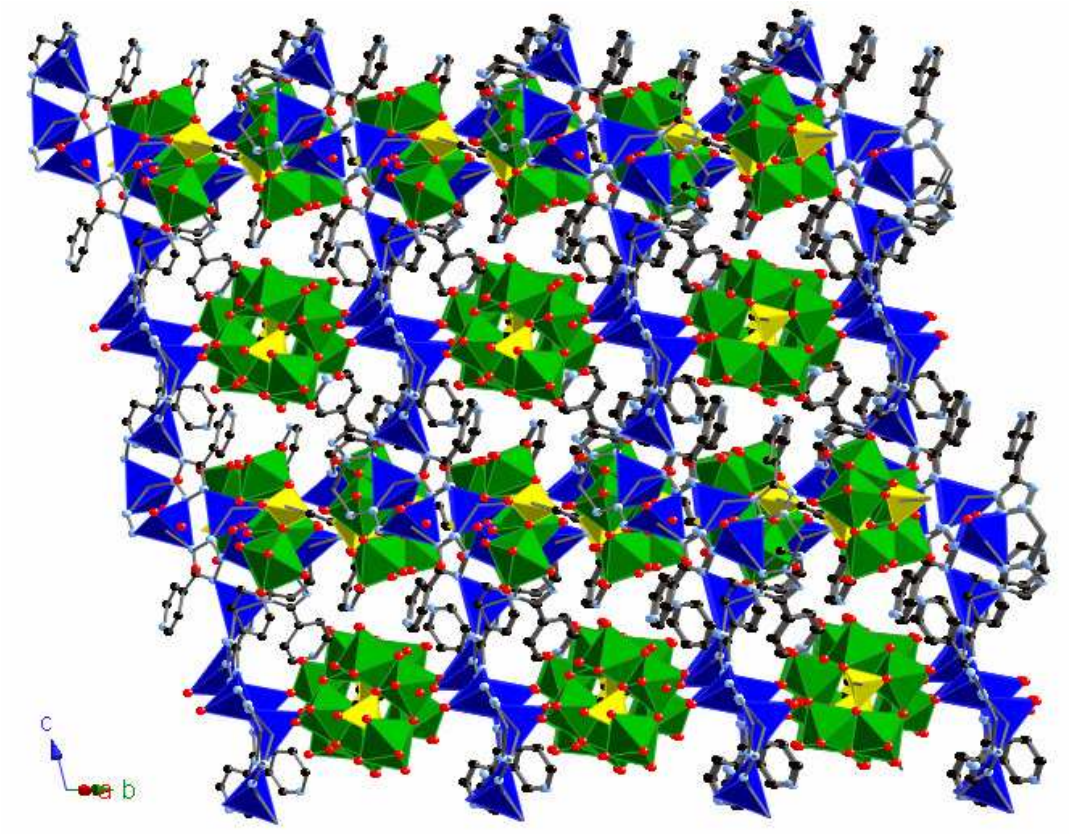

(a)

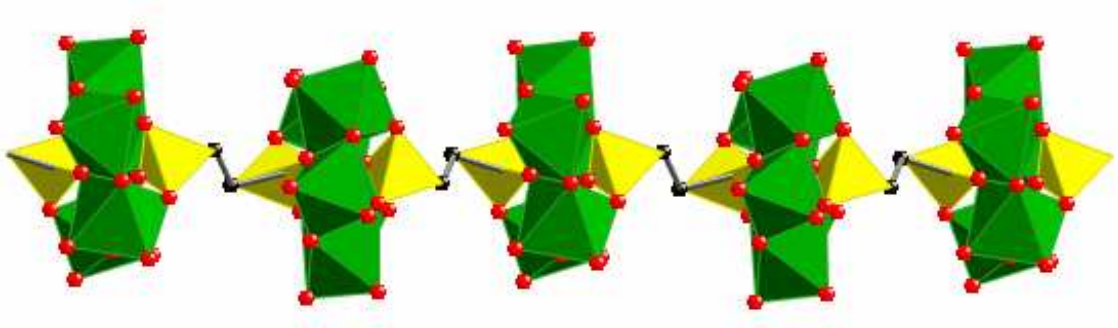

(b)

Figure 4.3. **(a)** A view of the three-dimensional structure of [{Cu_4(4-Hpt)$_3$(H_2O)}Mo_5O_{15}{$O_3P(CH_2)_2PO_3$}]·2H_2O (**3**·2H_2O); **(b)** the {Mo_5O_{15}{$O_3P(CH_2)_2PO_3$}$_n$}$^{4n-}$ chain.

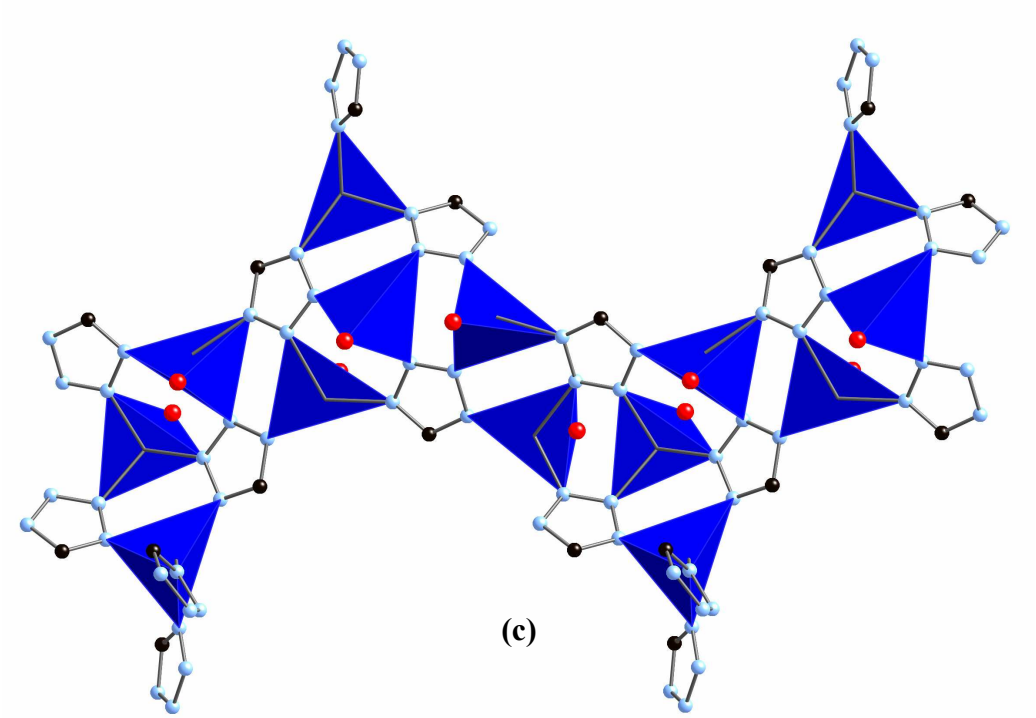

(c)

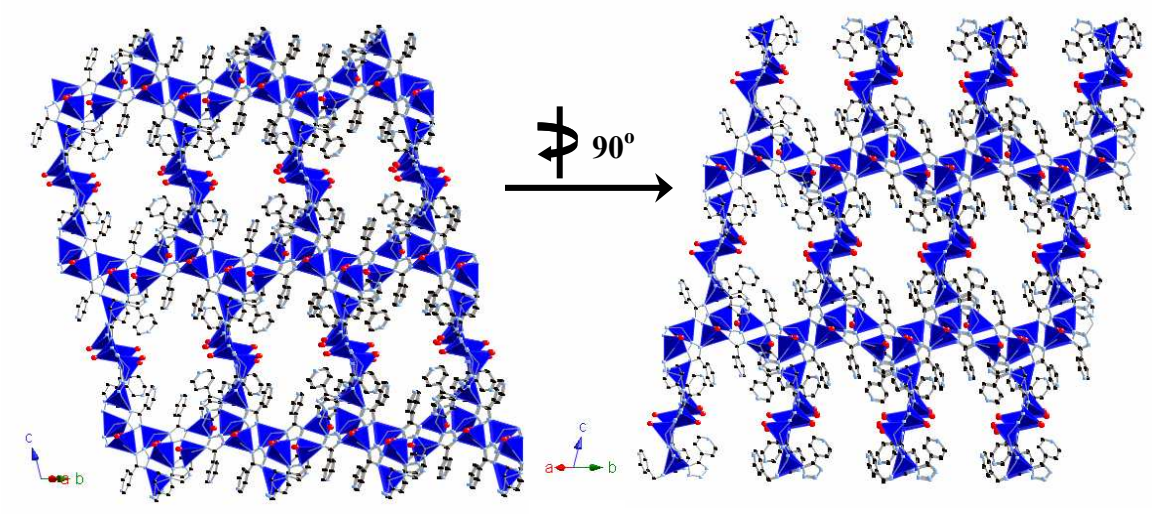

(d)

Figure 4.3 (cont.). **(c)** The Cu/4-pt component, pyridyl groups removed for clarity; and **(d)** the Cu/4-pt framework, molybdodiphosphonate chains removed, showing the orthogonal channels.

all four oxo groups. The $\{PMo^{V}Mo^{VI}_{11}O_{40}\}^{4-}$ clusters do not coordinate to the copper/4-pt chains, but instead act as structure-directing anions.

The $\{Cu_6(4\text{-pt})_2(4\text{-Hpt})_2\}_n^{4n+}$ chains are composed of trigonal planar Cu(I) sites linked into linear arrangements of six metal centers coordinated through the tetrazolate ends of the 4-pt ligands (**Figure 4.4(b)**). The hexameric units are terminated by one 4-pt ligand on each end to which there is no further copper coordination. These units extend into chains through coordination of two 4-pt ligands to neighboring units. Three distinct Cu(I) sites are present within the structure; two are defined by N1, N3, N4 tetrazolate nitrogens, and the second to N2, N2, N4 tetrazolate nitrogens. The third copper site coordinates to two tetrazolate ends through N3, N3 donors and one pyridyl nitrogen. The ligands along the center of the chain link three metal centers through three tetrazolate nitrogens, while pendant ligands along the sides of the chain link only two metal centers through the tetrazolate end. Protonated pyridyl groups are directed above and below the chain.

The one-dimensional structure of $[Cu_3(OH)(4\text{-pt})_2(4\text{-Hpt})_2(H_2O)_2][PMo_{12}O_{40}]\bullet 10.5H_2O$ (**5**•$10.5H_2O$) is composed of $\{Cu_3(OH)(4\text{-pt})_2(4\text{-Hpt})_2(H_2O)_2\}_n^{3n+}$ chains and $\{PMo_{12}O_{40}\}^{3-}$ α-keggin clusters (**Figure 4.5**). As in **4**·$2.5H_2O$, each $\{PMo_{12}O_{40}\}^{3-}$ cluster contains a central tetrahedral phosphate group linked to a spherical shell of twelve $\{MoO_6\}$ octahedra through bridging oxo groups. The α-keggin clusters are pendant to each Cu(II)/4-pt chain, each coordinating to one copper center through a single oxo group.

The Cu(II)/4-pt chain consists of trinuclear units of corner-sharing copper centers joined via a central hydroxo group in which two copper centers exhibit distorted square

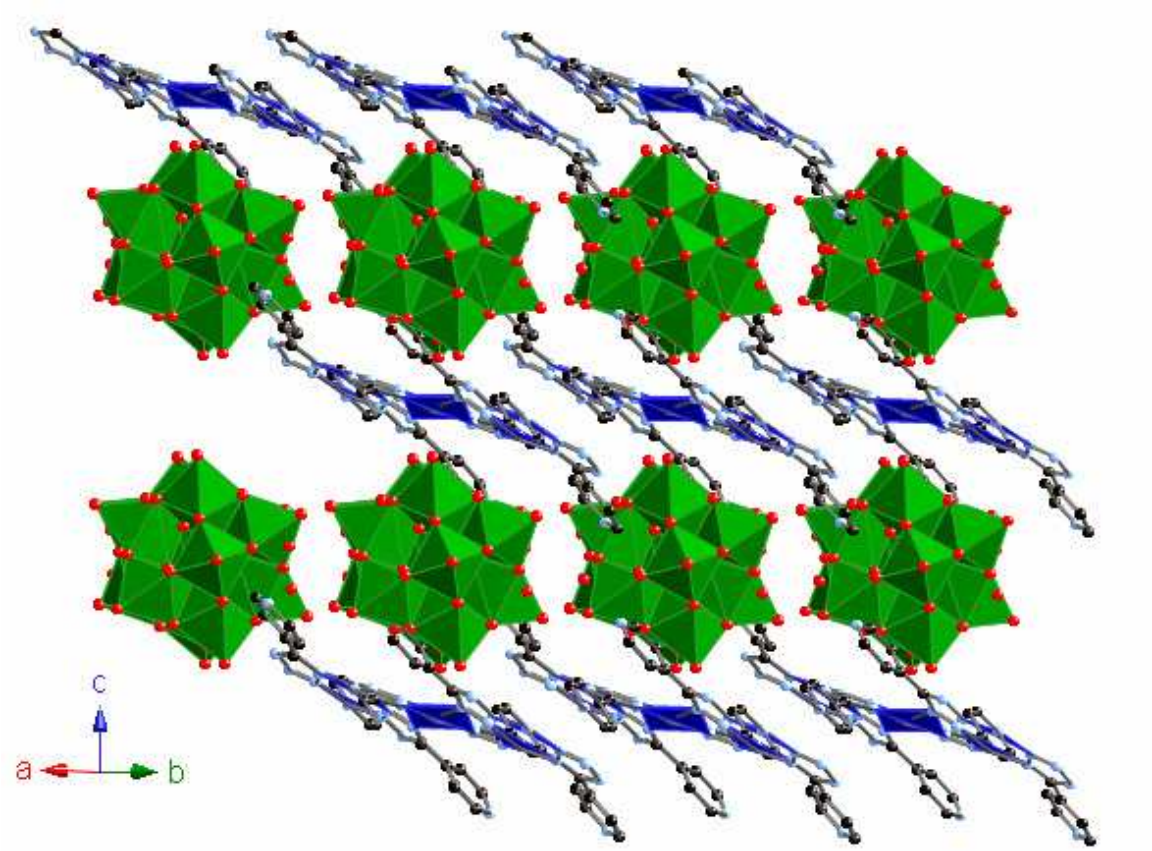

(a)

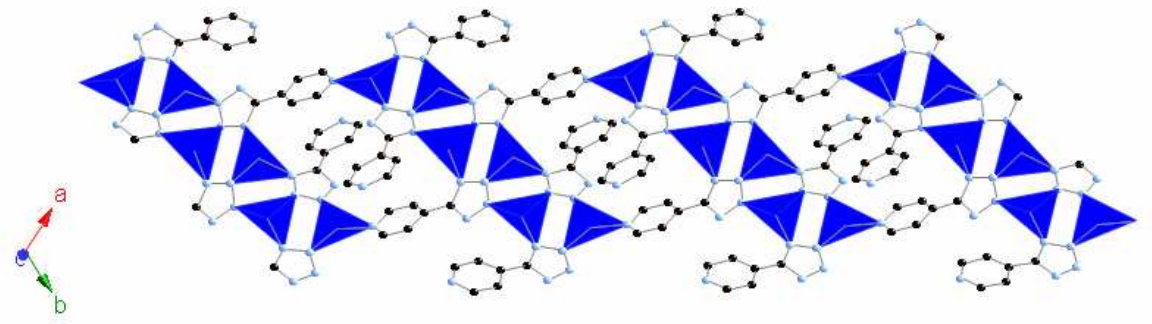

(b)

Figure 4.4. (a) A view of the arrangement of one-dimensional Cu/4-pt chains and α-keggin clusters in $[Cu_6(4\text{-pt})_2(4\text{-Hpt})_2][PMo^{V}Mo^{VI}_{11}O_{40}]\cdot 2.5H_2O$ (**4**·2.5H_2O); **(b)** the $\{Cu_6(4\text{-pt})_2(4\text{-Hpt})_2\}_n^{4n+}$ chain viewed in the *ab* plane.

pyramidal geometry and the third forms a distorted octahedron. Within each triad, one copper center is defined by two tetrazolate nitrogens, the μ_3-hydroxo group, and one aqua ligand in the basal plane and a third tetrazolate nitrogen in the apical position. The second 5-coordinate metal center coordinates to two tetrazolate nitrogens, one pyridyl nitrogen, and the μ_3-hydroxo group in the basal plane and a molybdate oxo group in the apical position. The octahedral copper binds to two tetrazolate nitrogens, one pyridyl nitrogen, and the bridging hydroxo group equatorially and a third tetrazolate nitrogen and an aqua ligand axially. Each triad coordinates to four 4-pt tetrazolate groups, of which two link neighboring triads through the pyridyl nitrogen and two are protonated at the pyridyl nitrogen and are directed away from the chain (**Figure 4.5(c)**).

The structure of $[Cu_3(OH)(4\text{-pt})_3(4\text{-}H_2pt)(H_2O)][PMo_{12}O_{40}]\cdot 7.5H_2O$ (**6**$\cdot 7.5H_2O$) consists of double layers containing two Cu(II)/4-pt sheets sandwiching coordinated α-keggin clusters that are then separated by additional uncoordinated α-keggins above and below each layer (**Figure 4.6**). The $\{PMo_{12}O_{40}\}^{3-}$ clusters are identical to those found in **5**$\cdot 12H_2O$.

The $\{Cu_3(OH)(4\text{-pt})_3(4\text{-}H_2pt)(H_2O)\}^{3+}$ network consists of copper triads (**Figure 4.6(b)**) similar to those seen in **5**$\cdot 10.5H_2O$. The square pyramidal copper sites are defined by two tetrazolate nitrogens, one pyridyl nitrogen, and the μ_3-hydroxo group in the basal plane and a third tetrazolate nitrogen in the apical position. The distorted octahedral copper site is defined by two tetrazolate nitrogens, one pyridyl nitrogen, and the hydroxo group in the equatorial plane, and one aqua ligand and one α-keggin oxo group in the axial positions. Each triad coordinates to four 4-pt ligands; three ligands are coorinated through tetrazolate ends which then link to neighboring triads through the

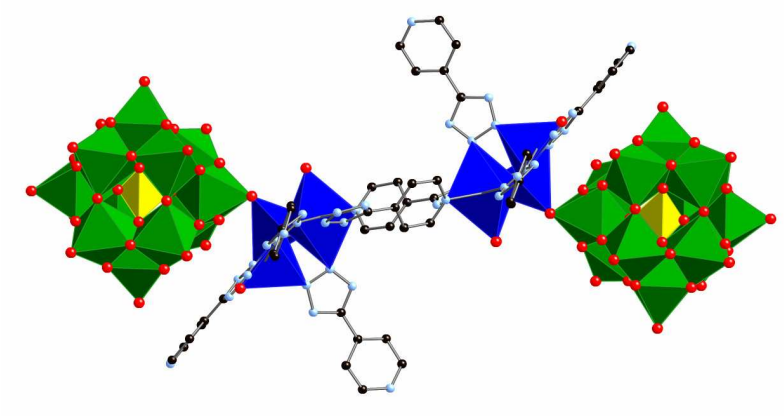

(a)

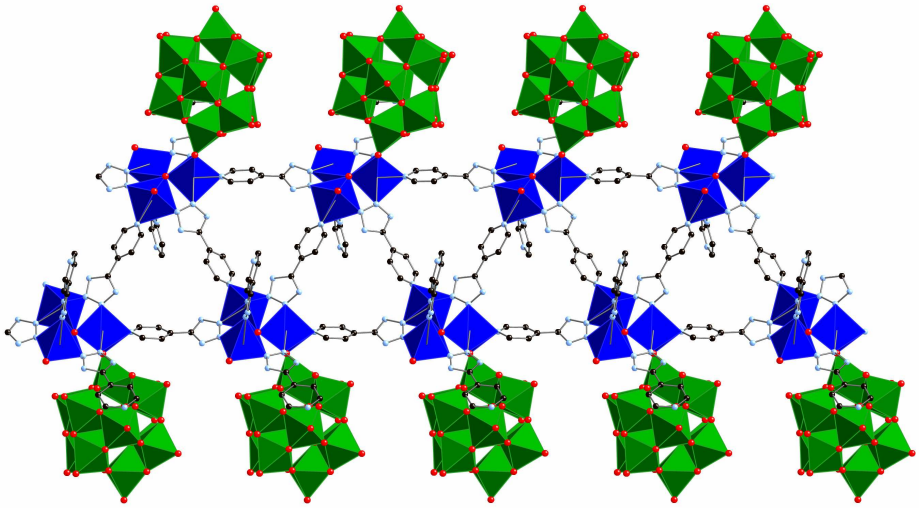

(b)

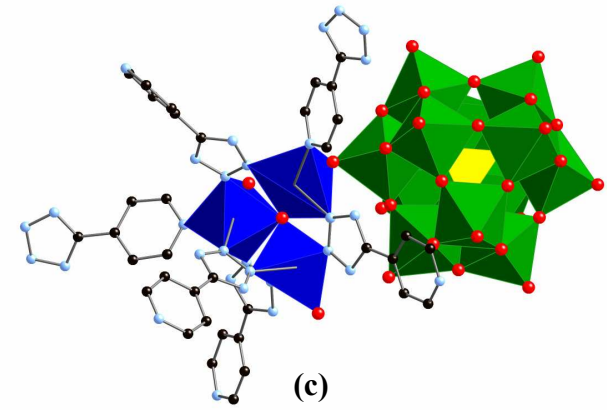

(c)

Figure 4.5. **(a)** A view of the one-dimensional structure of $[Cu_3(OH)(4\text{-pt})_2(4\text{-Hpt})_2(H_2O)_2][PMo_{12}O_{40}]\bullet 10.5H_2O$ (**5**•$10.5H_2O$) viewed down the Cu/4-pt chain (*ac* plane); **(b)** a view of the chain showing coordination of the α-keggin clusters to the Cu/4-pt chain; and **(c)** the copper triad showing 4-pt and α-keggin coordination.

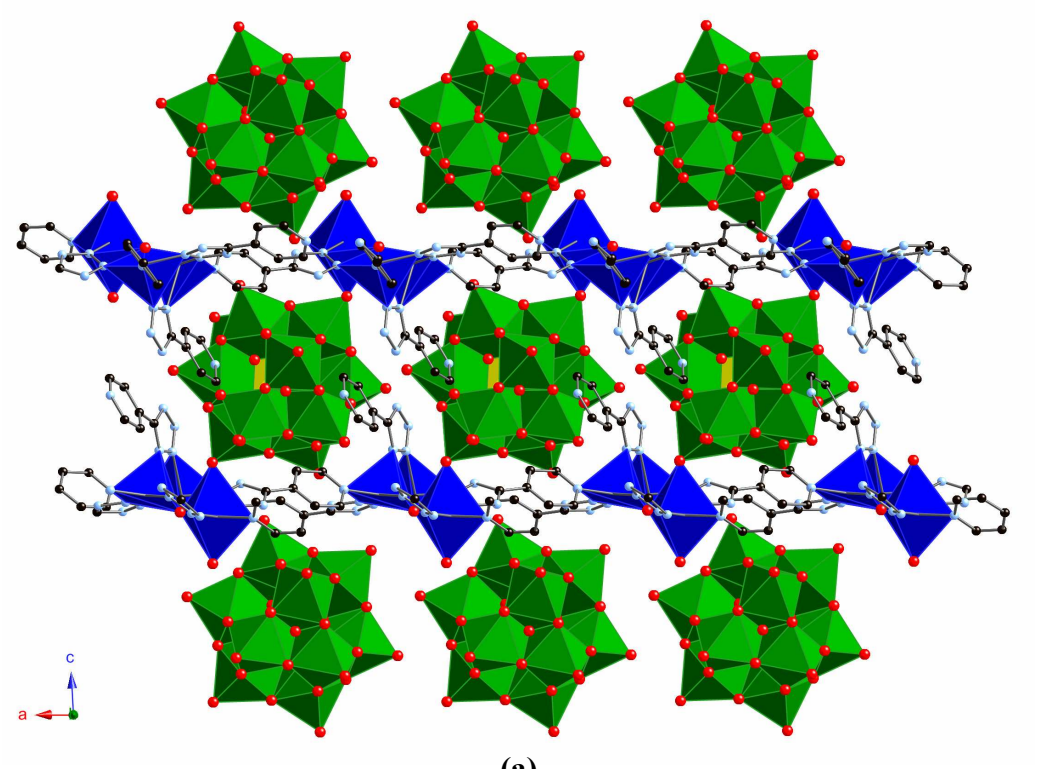

(a)

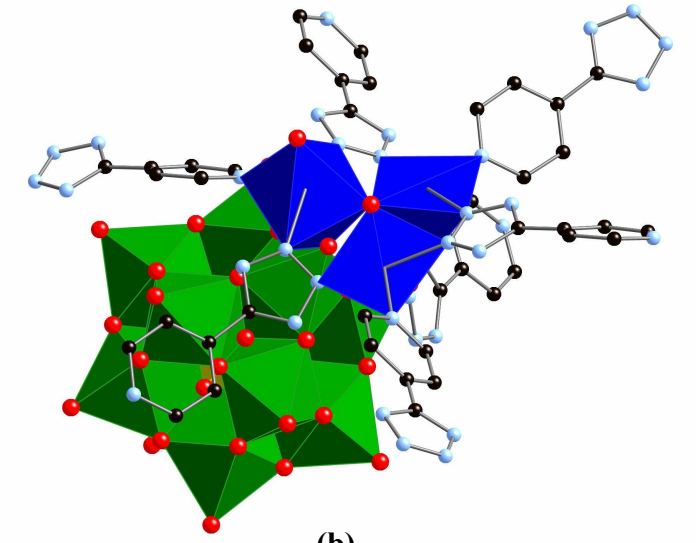

(b)

Figure 4.6. **(a)** A view of the double layer of $[Cu_3(OH)(4\text{-pt})_3(4\text{-}H_2pt)(H_2O)][PMo_{12}O_{40}]\cdot 7.5H_2O$ (**6**$\cdot 7.5H_2O$) in the *ac* plane with uncoordinated α-keggin cluster situated above and below; **(b)** the copper triad showing 4-pt and α-keggin coordination.

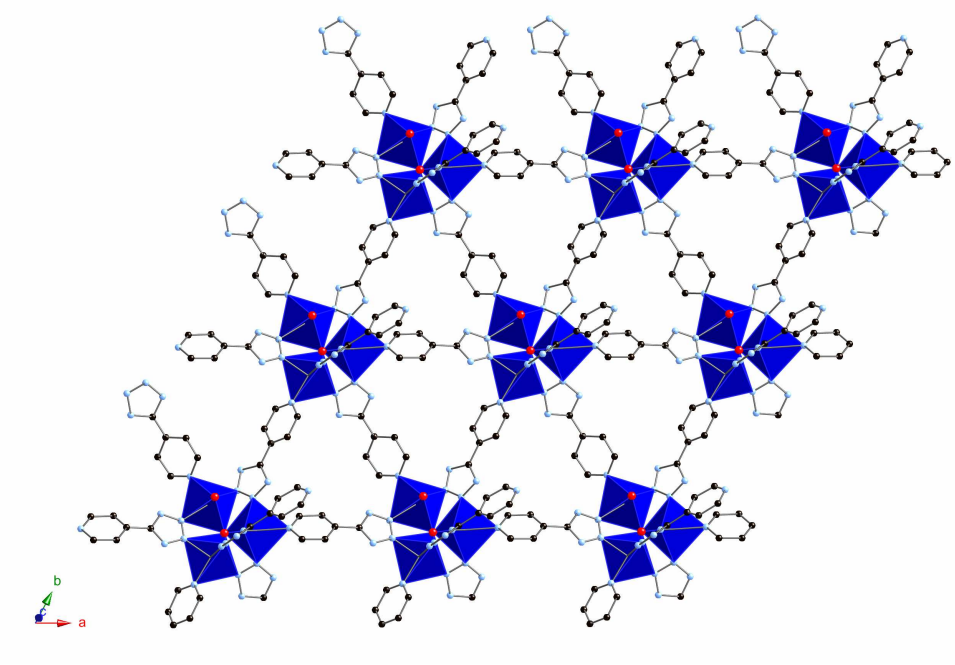

(c)

Figure 4.6 (cont.). (c) A view of one Cu/4-pt sheet viewed in the *ab* plane.

pyridyl nitrogen. The fourth ligand is doubly protonated, at both the N1 position of the tetrazole end and at the pyridyl nitrogen. The protonated pyridyl groups are directed below the layer.

Each double layer contains two copper/4-pt sheets related to each other by a two-fold rotation axis, between which the doubly coordinated $\{PMo_{12}O_{40}\}^{3-}$ clusters are located. **Figure 4.6(c)** shows the face of one Cu/4-pt sheet. Uncoordinated α-keggins flank each layer above and below.

4.3.3 General Structural Observations

The use of copper/4-pt cationic units in the construction of metal-organic materials demonstrates the structural variability afforded by this multi-nucleating ligand.

Compounds **1**-**2** and **4**-**6** adopt a coordination mode similar to the proposed scheme, in which metal centers bind to both the tetrazolate and pyridyl groups. However, this does not always result in an overall three-dimensional structure; **4** and **5** exhibit one-dimensional Cu/4-pt chains that are truncated in one direction by either unexpected termination of metal coordination to the ligand as in **4**, or binding of pendant molybdate clusters along the sides of the chain as in **5**. Conversely, **3** shows no metal coordination to the pyridyl group of the 4-pt ligand and instead achieves its three-dimensional structure through increased copper coordination to the tetrazolate end.

In copper(II) phases **1** and **5**-**6**, every tetrazolate group bonds to two metal centers. This results in a relatively simple Cu/4-pt array within each structure. The copper(I) phases **2**-**4** exhibit metal binding to between two and four tetrazolate nitrogens, with each structure demonstrating two different tetrazolate binding modes, leading to more complicated assemblies. It is noteworthy that this increased metal coordination does not necessarily influence the dimensionality of the structure, as the Cu/4-pt configuration of **4** is one-dimensional.

The presence of 1,2-ethylenediphosphonate in **3** produces the typical $\{Mo_5O_{15}(O_3P(CH_2)_2PO_3\}_n^{4n-}$ chains within a very complex copper/4-pt framework. The appearance of keggin clusters in **4**-**6** suggests the diphosphonate ligands in each synthesis degraded to provide a phosphate source for the formation of the clusters as opposed to integrating into the structure. The keggin anion is a highly stable structural unit that forms readily from a molybdate solution in the presence of a phosphate source.

4.3.4 Magnetic Susceptibility Studies

The temperature dependent magnetic data for compound **1**•$2H_2O$ were recorded at a magnetic field 1000 Oe in the 2 - 300 K temperature range after zero field cooling using a Quantum Design MPMS-XL-7 SQUID magnetometer. As shown in **Figure 4.7**, the magnetic data conformed to the linear trimer model with interaction Hamiltonian $H = -2J(S_1S_2 + S_2S_3) - 2J_0S_1S_3$, following equation 1 below:

$$\chi = \chi_0 + \chi_{TI} = \frac{Ng^2\mu_B{}^2}{4kT} \frac{\exp(-2J/kT) + \exp(-2J_0/kT) + 10\exp(J/kT)}{\exp(-2J/kT) + \exp(-2J_0/kT) + 2\exp(J/kT)} + \chi_{TI} \qquad (1)$$

The best fit gives g = 2.10, J/k = -5.76 K, J_0/k = 0, and χ_{TI} = 0.00114 emu/mol. At 300 K, the effective moment $\mu_{eff} = (8\chi_0T)^{1/2}$ of 3.14 μ_B (μ_{eff} = 3.00 μ_B , calculated) is consistent with three Cu(II) sites per formula. A small degree of coupling is seen between metal centers within each trimer, as demonstrated by the value of J/k. However, communication does not extend through the 4-pt ligands between trimers. The magnetic properties of **5** and **6** are under investigation.

4.3.5 Thermal Analysis

The thermogravimetric profile of **1**•$2H_2O$ (**Figure 4.8**) is quite distinct from those of **2**-**6**. Compound **1** exhibits a sharp weight loss of *ca.* 3.5% at 250 ^oC, corresponding to the loss of water of crystallization and the weakly coordinated water molecules, followed almost immediately by ligand decomposition between 265 and 330 ^oC. On the other hand, **2**-**5** have a gradual weight loss to 250-270 ^oC attributed to the loss of water of crystallization and aqua ligands. Compound **2** has a region of stability to 320 ^oC, followed by multi-step ligand decomposition between 320 ^oC and 650 ^oC (**Figure 4.9**). Compounds **3**-**5** show almost immediate ligand decomposition that occurs in multiple

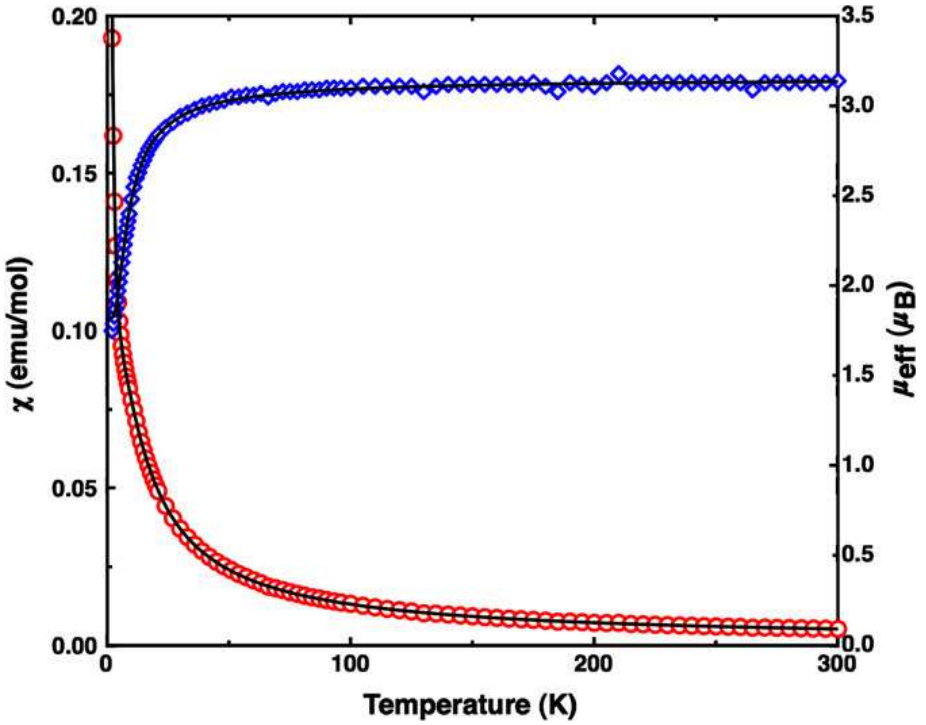

Figure 4.7. The temperature dependence of the magnetic susceptibility χ (red circles) and of the effective magnetic moment μ_{eff} (blue diamonds) of **1**. The solid line drawn through the data is the fit to the linear trimer model.

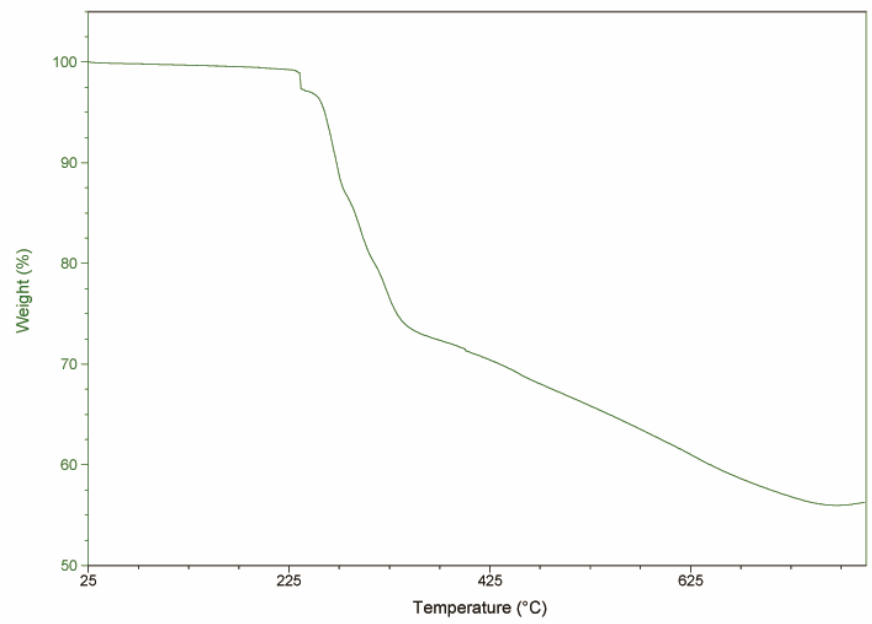

Figure 4.8. The thermogravimetric profile of **1** in the temperature range 25 – 800 ^{o}C.

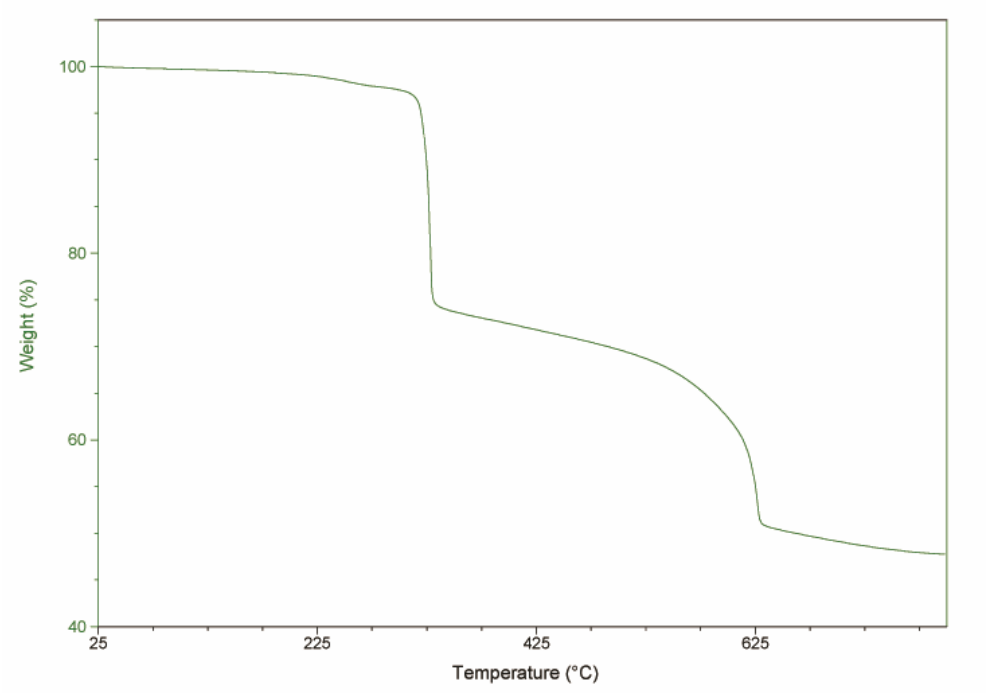

Figure 4.9. The thermogravimetric profile of **2** in the temperature range 25 – 800 ^{o}C.

steps between 270 ^{o}C and 750 ^{o}C. Compound **6** exhibits a gradual weight loss of *ca.* 3% between room temperature and 150 ^{o}C due to the loss of some water of crystallization, followed by a region of stability to 250 ^{o}C before a sharp weight loss of *ca.* 5% between 250 ^{o}C and 270 ^{o}C corresponding to the remaining water of crystallization and aqua ligands. Ligand decomposition occurs in multiple steps between 270 ^{o}C and 800 ^{o}C. In all cases, the product of the thermal decomposition is an amorphous gray powder.

4.4 Conclusions

Hydrothermal methods have been exploited in the construction of metal-organic materials containing copper/4-pt cationic structural units. Increased reaction temperature has resulted in the reduction of copper sites by the 4-pt ligands, affording three Cu(I)

phases. A direct comparison may be made between the structures of **1** and **2** of which the syntheses vary only in the reaction temperature; copper reduction produces a completely different and more complex Cu/4-pt substructure. This increased structural complexity is also demonstrated in **3** and **4**, where all three Cu(I) phases exhibit increased copper-tetrazolate coordination. Reduction of copper in the presence of polyazaheterocyclic ligands has been previously reported.[65]

The overall structures are generated in a synergistic interaction between the copper/4-pt cationic component and the molybdate anion. Anion control is a recurrent theme of this chemistry,[66] and each compound contains an oxide cluster that must be accommodated within the cationic frameworks. The most pronounced example is the complex Cu/4-pt framework of **3**, which contains channels large enough to hold the anionic molybdodiphosphonate chains.

4.5 Acknowledgement

This work was supported by a grant from the National Science Foundation, CHE-0242153.

4.6 References

[1] N. N. Greenwood, A. Earnshaw, *Chemistry of the Elements*, Pergamon Press, New York, **1984**.

[2] A. F. Wells, *Structural Inorganic Chemistry, 4th ed.*, Oxford University Press, Oxford, **1978**.

[3] W. H. McCarroll, *Encyclopedia of Inorganic Chemistry*, R. B. King, ed., John Wiley & Sons, New York, **1994**, *6*, 2903.

[4] D. W. Bruce, D. O'Hare, eds., *Inorganic Materials*, Wiley, Chichester, **1992**.

[5] A. K. Cheetham, *Science* **1964**, *264*, 794.

[6] B. Cockayne, D. W. James, eds., *Modern Oxide Materials*, Academic Press, New York, **1972**.

[7] W. Büchner, R. Schliebs, G. Winter, K. H. Büchel, *Industrial Inorganic Chemistry*, VCH, New York, **1989**.

[8] T. Okuhara, M. Misono, *Encyclopedia of Inorganic Chemistry*. John Wiley and Sons, New York, **1994**, *6*, 2889.

[9] A. Clearfield, *Chem. Rev*. **1988**, *88*, 125.

[10] J. M. Newsam, *Solid State Compounds; Clarendon Press*, Oxford, **1992**, 234.

[11] M. V. Landau, *Transition Metal Oxides, in Handbook of Porous Solids*, Wiley-VCH, Weinheim, **2002**, *3*, 1677.

[12] H. Maekawa, *Materia* **2006**, *45*, 359.

[13] S. L. Suib, *Ann. Rev. Mater. Sci*. **1996**, *26*, 135.

[14] M. E. Davis, *CATTECH* **1997**, *1*, 19.

[15] R. F. Lobo, S. I. Zones, M. E. Davis, *J. Inclusion Phenom. Mol. Recog. Chem.* **1995**, *21*, 47.

[16] C. R. Kagan, D. B. Mitzi, C. D. Dimitrakopoulos, *Science* **1999**, *286*, 945.

[17] (a) D. B. Mitzi, *J. Chem. Soc., Dalton Trans*. **2001**, 1; (b) D. B. Mitzi, *Inorg. Chem*. **2000**, *39*, 6107.

[18] (a) S. I. Stupp, P. V. Braun, *Science* **1997**, *277*, 1242; (b) M. E. Davis, A. Katz, W. R. Ahmad, *Chem. Mater.* **1996**, *8*, 1820.

[19] P. J. Hagrman, D. Hagrman, J. Zubieta, *Angew. Chem. Int. Ed. Engl.* **1999**, *38*, 2639.

[20] M. T. Pope, *Heteropoly and Isopoly Oxometalates,* Springer, New York, 1983.

[21] Special thematic issue on polyoxometalates: C. L. Hill, ed., *Chem. Rev*., **1998**, *98*, 1.

[22] *Polyoxometalate Chemistry: From Topology Via Self-Assembly to Applications*, M. T. Pope, A. Müller, eds., Kluwer Academic, Dordrecht, The Netherlands, **2001**.

[23] *Polyoxometalates: From Platonic Solids to Anti-Retroviral Activity*, M.T. Pope, A.

Müller, eds., Kluwer Academic, Dordrecht, The Netherlands, **1994**.

[24] J. P. Jolivet, *Metal Oxide Chemistry and Synthesis: From Solution to Solid State*, John Wiley, New York, **2000**.

[25] D. E. Katsoulis, *Chem. Rev*. **1998**, *98*, 359.

[26] K. Pavani, S. E. Lofland, K. V. Ramanujachary, A. Ramanan, *Eur. J. Inorg. Chem.* **2007**, 568.

[27] H. Y. An, Y. G. Li, D. R. Xiao, E. B. Wang, C. Y. Sun, *Cryst. Growth Des*. **2006**, *6*, 1107.

[28] R. G. Cao, S. X. Liu, L. H. Xie, Y. B. Pan, J. F. Cao, Y. H. Ren, L. Xu, *Inorg. Chem.* **2007**, *46*, 3541.

[29] Y. Xu, J. Q. Xu, K. L. Zhang, Y. Zhang, X. Z. You, *Chem. Commun*. **2000**, 153.

[30] N. Nyman, F. Bonhomme, T. M. Alam, A. M. Rodriguez, B. R. Cherry, J. L. Krumhansl, T. M. Nenoff, A. M. Sattler, *Science* **2002**, *297*, 996.

[31] C. Ritchie, E. Burkholder, P. Kögerler, L. Cronin, *Dalton Trans*. **2006**, 1712.

[32] R. N. Devi, E. Burkholder, J. Zubieta, *Inorg. Chim. Acta* **2003**, *348*, 150.

[33] P. Q. Zheng, Y. P. Ren, L. S. Long, R. B. Huang, L. S. Zheng, *Inorg. Chem*. **2005**, *44*, 1190.

[34] C. D. Wu, C. Z. Lu, H. H. Zhuang, J. S. Huang, *J. Am. Chem. Soc*. **2002**, *124*, 3836.

[35] Y. Lu, Y. Xu, Y. G. Li, E. B. Wang, X. X. Xu, Y. Ma, *Inorg. Chem*. **2006**, *45*, 2055.

[36] J. Y. Niu,D. J. Guo, J. W. Zhao, J. P. Wang, *New J. Chem*. **2004**, *28*, 980.

[37] B. B. Yan, Y. Xu, X. H. Bu, N. Goh, L. S. Chia, G. D. Stucky, *J. Chem. Soc., Dalton Trans*. **2001**, 2009.

[38] D. G. Allis, R. S. Rarig, E. Burkholder, J. Zubieta, *J. Mol. Structure* **2004**, *688*, 11.

[39] α-molybdate: (a) V. W. Day, M. F. Fredrich, W. G. Klemperer, W. Shum, *J. Am. Chem. Soc*. **1977**, *99*, 952; (b) W. Yang, C. Lu, H. Zhuang, *J. Chem. Soc., Dalton Trans.* **2002**, 2879.

[40] β-molybdate: (a) X. M. Lu, W. J. Li, X. A. Mao, *Jiegou Huaxe* **2000**, *19*, 163; (b) R. Z. Wang, J. Q. Xu; G. Y. Yang, W. M. Bu, Y. H. Xing, D. M. Li, S. Q. Liu, L. Ye, Y. G. Fan, *Polish J. Of Chem*. **1999**, *73*, 1909; (c) X. M. Lu, S. C. Liu, Y. Liu,

X. H. Bu, S. L. Hong, *Huaxue Xuebao* **1997**, *55*, 1009; (d) A. Kitamura, T. Ozeki, A. Yagasaki, *Inorg. Chem*. **1997**, *36*, 4275; (e) C. J. Gomez-Garcia, E. Coronado, S. Triki, L. Ouahab, P. Delhar, *Adv. Mater*. **1993**, *5*, 283; (f) D. Attanasio, M. Bonamico, V. Fores, L. Suber, *J. Chem. Soc., Dalton Trans*. **1992**, 2523; (g) X. Wang, X. Xu, Q. Wang, Y. Zhai, *Polyhedron* **1992**, *11*, 1423; (h) J. Fuchs, I. Bruedgam, *Z. Naturforsch. B* **1977**, *32B*, 853; (i) W. G. Klemperer, W. Shum, *J. Am. Chem. Soc.* **1976**, *98*, 8291; (j) J. Fuchs, H. Hartl, *Angew. Chem.* **1976**, *88*, 385.

[41] γ-molybdate: (a) M. C. Niven, J. J. Cruywagen, J. B. B. Heyns, *J. Chem. Soc., Dalton Trans*. **1991**, 2007; (b) M. Inoue, T. Yamase, *Bull. Chem. Soc. Japan* **1995**, *68*, 3055.

[42] δ-molybdate: R. Xi, B. Wang, K. Isobe, T. Nishioka, K. Toriumi, Y. Ozawa, *Inorg. Chem.* **1994**, *33*, 833.

[43] R. N. Devi, J. Zubieta, *Inorg. Chim. Acta* **2002**, *332*, 72.

[44] R. S. Rarig, J. Zubieta, *J. Solid State Chem*. **2002**, *167*, 370.

[45] C. Z. Lui, C. D. Wu, H. H. Zhuang, J. S. Huang, *Chem. Mater.* **2002**, *14*, 2649.

[46] R. S. Rarig, L. Bewley, E. Burkholder, J. Zubieta, *Ind. J. Chem*. **2003**, *42A*, 2235.

[47] J. Q. Xu, R. Z. Wang, G. Y. Yang, Y. H. Xing, D. M. Li, W. M. Bu, L. Ye, Y. G. Fan, G. D. Yang, Y. Xing, Y. H. Lin, H. Q. Jia, *Chem. Commun.* **1999**, 983.

[48] D. G. Allis, E. Burkholder, J. Zubieta, *Polyhedron* **2004**, *23*, 1145.

[49] D. Hagrman, C. Zubieta, R. C. Haushalter, J. Zubieta, *Angew. Chem., Int. Ed. Engl.* **1997**, *36*, 873.

[50] D. Hagrman, C. Sangregorio, C. J. O'Connor, J. Zubieta, *J. Chem. Soc., Dalton Trans.* **1998**, 3707.

[51] D. Hagrman, P. Hagrman, J. Zubieta, *Inorg. Chim. Acta* **2000**, *300-302*, 212.

[52] J. R. D. DeBord, R. C. Haushalter, L. M. Meyer, D. J. Rose, P. . Zapf, J. Zubieta, *Inorg. Chim. Acta* **1997**, *256*, 165.

[53] D. Hagrman, P. J. Zapf, J. Zubieta, *Chem. Commun.* **1998**, 1283.

[54] D. Hagrman, J. Zubieta, *C. R. Acad. Sci., Ser. IIc* **2000**, *3*, 231.

[55] W. Kwak, M. T. Pope, T. F. Scully, *J. Am. Chem. Soc.* **1975**, *97*, 5735.

[56] N. G. Armatas, W. Ouellette, K. Whitenack, J. Pelcher, H. Liu, E. Romaine, C. J.

O'Connor, J. Zubieta, *Inorg. Chem.* **2009,** *48*, 8897.

[57] (a) N. G. Armatas, D. G. Allis, A. Prosvirin, G. Carnutu, C. J. O'Connor, K. Dunbar, J. Zubieta, *Inorg. Chem.* **2008**, *47*, 832; (b) E. Burkholder, V. Golub, C. J. O'Connor, J. Zubieta, *Inorg. Chem.* **2004**, *43*, 7014; (c) E. Burkholder, J. Zubieta, *Chem. Commun.* **2001**, 2056.

[58] S. Jones, J. M. Vargas, C. J. O'Connor, J. Zubieta, *submitted*.

[59] M. Dinca, A. F. Yu, J. R. Long, *J. Am. Chem. Soc.* **2006**, *128*, 8904.

[60] W. Ouellette, A. V. Prosvirin, K. Whitenack, K. R. Dunbar, J. Zubieta, *Angew. Chem.* **2009**, *121*, 2174.

[61] J. H. Zhou, R. M. Cheng, Y. Song, Y. Z. Li, Z. Yu, X. T. Chen, Z. L. Xue, X. Z. You, *Inorg. Chem.* **2005**, *44*, 8011, and references therein.

[62] Z. S. Meng, L. Yun, W. X. Zhang, C. G. Hong, R. Herchel, Y. C. Ou, J. D. Leng, M. X. Peng, Z. J. Lin, M. L. Tong, *Dalton Trans.*, **2009**, 10284.

[63] S. Ferrer, P. J. van Koningsbruggen, J. G. Haasnoot, J. Reedijk, H. Kooijman, A. L. Spek, L. Lezama, A. M. Arif, J. S. Miller, *J. Chem. Soc., Dalton Trans*. **1999**, 4269.

[64] P. J. Steel, *Coord. Chem. Rev*. **1990**, *106*, 227.

[65] W. Ouellette, A. V. Prosvirin, V. Chieffo, K. R. Dunbar, B. Hudson, J. Zubieta, *Inorg. Chem*. **2006**, *45*, 9346.

[66] W. Ouellette, H. Liu, C. J. O'Connor, J. Zubieta, *Inorg. Chem*. **2009**, *48*, 4658.

Chapter 5

Synthesis of Anionic Polyoxomolybdate Clusters Based on Spherical Mo-132

5.1 Introduction

The rational design of complex functional systems relies on the organization of well-defined building blocks across multiple length scales.[1-3] Although simple assemblies of nanoparticles have attracted a great deal of interest, the focus of nanoscience and nanotechnology research has shifted to the construction of larger architectures consisting of ordered arrays of various types of nanoscopic components.[4-7] Many strategies utilized in the preparation of such nanoparticle assemblies depend on molecular interactions, dispersion forces, and differences in particle sizes. Yet electronic forces involved in the formation of these materials remains relatively unexplored.[5,8-11]

The electrostatic interaction between charged entities in solution, as well as the properties of their aggregates, is dependent upon their size regime.[12] On the molecular scale, oppositely charged ions will remain stable in solution until a specific concentration ratio is achieved, at which point precipitation occurs. Conversely, a solution of charged microparticles will continuously precipitate due to instability caused by residual van der Waals forces and the poor solvation of larger aggregates.[13] In the intermediate nanoscale size range, a mixture of oppositely charged metal nanoparticles displays stability similar to that of ionic solutions and does not precipitate until the point of overall electroneutrality is reached.[3-5,10-11,14-16] Investigations into the behavior and stability of more complex nanoscopic entities reveals electrostatic interactions between positively charged metal nanoparticles and negatively charged proteins,[6] and between negatively charged metal nanoparticles and positively charged small biomolecules.[17] However, limited work has focused on charge balancing effects on the stability of mixtures of proteins, polymers, or other charged nanoscopic entities with nanoparticles or

microparticles.[3-6,10-17] The understanding of charge-balanced precipitation in these mixtures is hindered by the directional electrostatic forces often exhibited by such particles due to broad and random charge distributions.

Polyoxometalates (POMs) provide an attractive building block for functional materials due to the range of structures and topologies that can form, as well as their properties. Due to their sizes, structures, and properties, POMs are considered intermediates between small molecules and oxide solids. Of particular interest are the nanoscaled $\{Mo_{11}\}_n$ class of polyoxomolybdates, of which the spherical-ball (n = 12) and the wheel-shaped (n = 14) anions such as $(NH_4)_{42}[Mo^{VI}_{72}Mo^{V}_{60}O_{372}(C_2H_3O_2)_{30}(H_2O)_{72}]$ (Mo-132) and $Na_{21}[Mo^{VI}_{126}Mo^{V}_{28}O_{462}H_{14}(H_2O)_{54}(H_2PO_4)_7]$, respectively, are representative.[2]

Mo-132 is a molecular cluster with a nanoscopic diameter of 2.9 nm and a quantized 42 negative charges per cluster in aqueous solution, and crystallizes as the $(NH_4)_{42}[\{(Mo^{VI})Mo^{VI}_5O_{21}(H_2O)_6\}_{12}\{Mo^{V}_2O_4(O_2C_2H_3)\}_{30}]\cdot \approx 300H_2O + \approx 10C_2H_3O_2NH_4$ ammonium salt.[18-19] This compound exhibits unique solution properties such as spontaneous self-assembly into "blackberry-type" supramolecular structures.[20] Additionally, its surface properties and charge can be modified through encapsulation with a precise number of cationic surfactants. The $\{Mo_{11}\}$ units that make up the molybdenum oxide shell of the cluster consist of a central 7-coordinate molybdenum(VI) atom surrounded by five molybdenum(VI) octahedra coordinated through edge-sharing interactions around the equatorial plane. Five molybdenum(V) octahedra then coordinate around the edge through corner-sharing interactions (**Figure 5.1**). The structure may also be described as twelve pentagonal $\{(Mo^{VI})Mo^{VI}_5O_{21}(H_2O)_6\}^{6-}$ units located on the

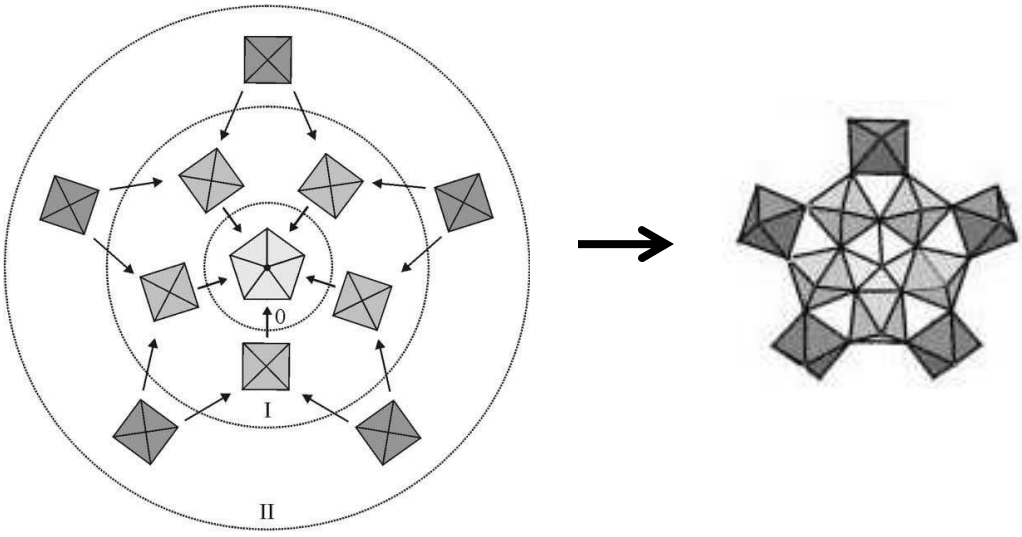

Figure 5.1. Formation of the $\{Mo_{11}\}$ structural unit of Mo-132.[19]

vertices of an icosahedron connected by thirty $\{Mo^{V}_{2}O_4(O_2C_2H_3)\}^{+}$ bridges located on the icosahedral edges (**Figure 5.2**). The acetate oxygens link the edge-sharing $\{Mo^{V}_{2}\}$ units with the acetate methyl groups directed inside the cluster, forming a hydrophobic inner surface. The cluster contains 20 $\{Mo_9O_9\}$ pores with the ability to expand to allow the transfer of ions larger than the latent pore size (**Figure 5.3**).[21] Mo-132 is readily synthesized by the partial reduction of an acidic molybdate solution in the presence of acetic acid followed by room temperature cyrstallization.[22]

The size and charge of the $\{Pentagon\}_{12}\{Linker\}_{30}$ scaffold can be altered by varying the identity of both the metal and the ligand of the linker unit, thereby offering an array of analogous nanoscopic particles for investigation. The diatomic $\{Mo^{V}_{2}O_4\}$ bridge can be replaced by monatomic $\{Fe^{III}_{30}\}$ bridges to form the structurally analogous $[\{(Mo^{VI})Mo^{VI}_{5}O_{21}\}_{12}Fe^{III}_{30}]$ cluster with a diameter of 2.3 nm and an overall 18+ charge

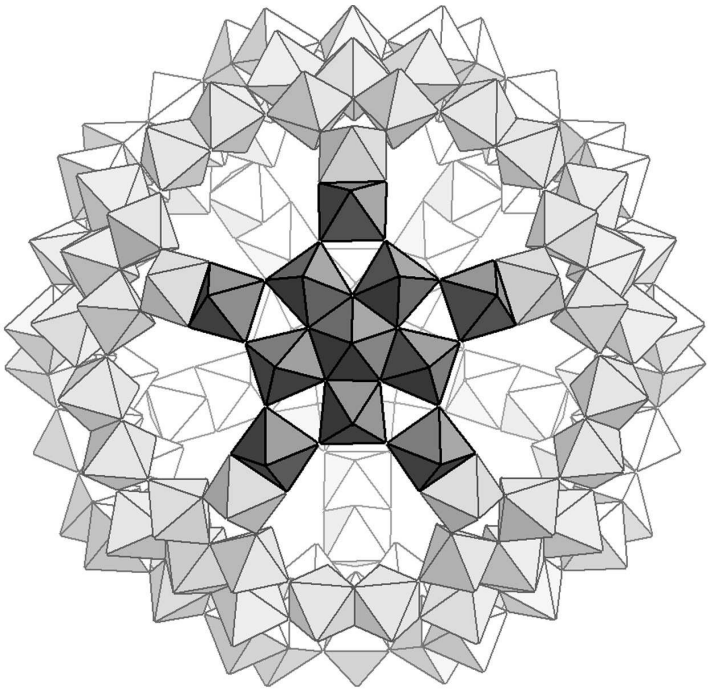

Figure 5.2. A polyhedral representation of the molybdenum scaffold of Mo-132 viewed down the C_5 symmetry axis.[22]

Figure 5.3. A ball-and-stick representation of the $\{Mo_9O_9\}$ pore present in Mo-132. Blue spheres – molybdenum; red spheres – oxygen.[21]

(Figure 5.4).[23-24] Replacement of the acetate groups within the $\{Mo^{V}_2O_4(O_2C_2H_3)\}$ linker units with alternate ligands instead produces clusters of the same size as the Mo-

132 acetate cluster with variable charges. Exchange of every acetate group for a sulfate group decreases the cluster charge to 72- and results in a hydrophilic inner surface allowing the formation of highly ordered hydrogen bonded water networks within the cluster cavity.[15-26] An intermediate charge of 60- can be achieved through partial ligand exchange, resulting in the $(NH_4)_{60}[\{(Mo^{VI})Mo^{VI}_5O_{21}(H_2O)_6\}_{12}\{Mo^{V}_2O_4(SO_4)\}_{18}\{Mo^{V}_2O_4(CH_3COO)\}_{12}] \cdot \approx 300H_2O$ cluster containing twelve acetate groups and 18 sulfate groups coordinated to linker units distributed throughout the shell.[26] Introduction of oxalic acid or sodium dihydrogen phosphate to a solution of Mo-132 acetate clusters leads to the full exchange of acetate ligands with protonated oxalate groups[27] or protonated phosphate groups[28], respectively, producing clusters of the same 42- charge as the Mo-132 acetate cluster.

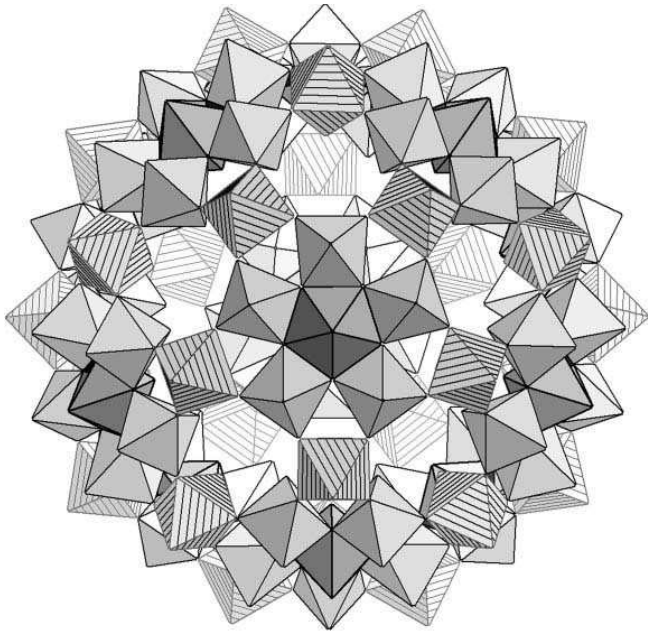

Figure 5.4. A polyhedral representation of the molybdenum/iron scaffold of $\{Mo_{72}Fe_{30}\}$ viewed down the C_5 symmetry axis. Gray polyhedra – molybdenum; hatched polyhedra – iron.[19]

In order to gain a full understanding of how electrostatic interactions affect the solution stability and precipitation of a mixture of polyoxomolybdate clusters with metal nanoparticles, a range of clusters varying in size and charge should be investigated. In addition to the synthesis of the Mo-132 acetate cluster $(NH_4)_{42}[\{(Mo^{VI})Mo^{VI}_5O_{21}(H_2O)_6\}_{12}\{Mo^{V}_2O_4(O_2C_2H_3)\}_{30}]\cdot \approx 300H_2O + \approx 10C_2H_3O_2NH_4$ (Mo-132a), the sulfate cluster $(NH_4)_{72-n}[(H_2O)_{81-n} + (NH_4)_n \subset \{(Mo^{VI})Mo^{VI}_5O_{21}(H_2O)_6\}_{12}\{Mo^{V}_2O_4(SO_4)\}_{30}] \cdot \approx 200H_2O$ (Mo-132b), and the mixed-ligand cluster $(NH_4)_{60}[\{(Mo^{VI})Mo^{VI}_5O_{21}(H_2O)_6\}_{12}\{Mo^{V}_2O_4(SO_4)\}_{18}\{Mo^{V}_2O_4(CH_3COO)\}_{12}] \cdot \approx 300H_2O$ (Mo-132c) according to procedures outlined in the literature, a series of acetate/sulfate mixed-ligand clusters were synthesized exhibiting additional acetate:sulfate ligand ratios to that previously reported.

5.2 Experimental Section

All chemicals were used as obtained without further purification. Ammonium heptamolybdate was purchased from Mallinckrodt Chemicals. Ammonium acetate and concentrated acetic acid, sulfuric acid and hydrochloric acid were purchased from Fisher Scientific. Ammonium sulfate was purchased from VWR. Hydrazinium sulfate was purchased from Aldrich Chemical Company. The pH of the solutions were measured using a Hanna Checker pH meter. Water was distilled above 3.0 MΩ in-house using a Barnstead Model 525 Biopure Distilled Water Center.

5.2.1 Synthesis of $(NH_4)_{42}[\{(Mo^{VI})Mo^{VI}_5O_{21}(H_2O)_6\}_{12}\{Mo^{V}_2O_4(C_2H_3O_2)\}_{30}] \cdot \approx 300H_2O \cdot \approx 10CH_3COONH_4$ (Mo132a)

Prepared according to the literature[22]:

To a solution of $(NH_4)_6Mo_7O_{24}\cdot 4H_2O$ (5.6 g, 4.5 mmol) and CH_3COONH_4 (12.5 g, 162.2 mmol) in water (250 mL) was added $N_2H_6\cdot SO_4$ (0.8 g, 6.1 mmol) followed by stirring for 10 min, after which 50% (v/v) CH_3COOH (83 mL) was added with stirring. The green solution was stored in an open 500-mL Erlenmeyer flask at 20 ^oC for 4 days, during which a slow color change to dark brown occurred. The precipitated brown crystals were filtered off through a glass frit and washed with 90% ethanol and diethyl ether and dried in air. Yield: 3.7 g (54% based on Mo). The product was recrystallized from a concentrated aqueous solution. Characteristic IR bands (KBr pellet): ν = 1620 (m, δ (H_2O)), 1541 (m, ν_{as} (COO)), *ca.* 1440 (sh), 1402 (m, δ (CH_3), ν_s (COO), δ_{as} (NH_4^+)), 968 (m), 936 (w, ν (Mo=O)), 855 (w), 795 (s), 725 (s), 567 cm^{-1} (m). Elemental analysis (%) calcd: C 3.4, H 3.8, N 2.6; found: C 3.4, H 3.8, N 2.6.

5.2.2 Synthesis of $(NH_4)_{72-n}[(H_2O)_{81-n} + (NH_4)_n \subset \{(Mo^{VI})Mo^{VI}_5O_{21}(H_2O)_6\}_{12}\{Mo^{V}_2O_4(SO_4)\}_{30}] \cdot \approx 200H_2O$ (Mo-132b)

Prepared according to the literature[25]:

To a solution of $(NH_4)_{42}[Mo_{132}O_{372}(H_2O)_{72}(C_2H_3O_2)_{30}] \cdot \approx 300H_2O + \approx 10CH_3COONH_4$ (2.0 g, 0.07 mmol) in water (160 mL) was added $(NH_4)_2SO_4$ (8.0 g, 60.5 mmol) followed by H_2SO_4 (21 mL, 2 M) with stirring. The solution was stored in an open 400-mL beaker at 20 ^oC for two weeks, after which the precipitated brown crystals were filtered off through a glass frit, washed with *ca.* 4 mL of cold 2-propanol followed by *ca.* 4 mL of diethyl ether and dried in air. Yield: 1.8 g (88% based on Mo).

Characteristic IR bands (KBr pellet): ν = 1628 (m, δ (H_2O)), 1400 (s, δ_{as} (NH_4^+)), 1186 (w), 1132 (m), 1040 (m, ν_{as} (SO_4)), 966 (s), *ca.* 950 (sh), 855 (w), 799 (s), 727 (s), 619 (w), 573 cm^{-1} (m). Elemental analysis (%) calcd: N 3.5; found: N 3.5. Crystal data: Space group $R\bar{3}$, a = 32.67, c = 72.72 Å, V = 67231 $Å^3$.

5.2.3 Synthesis of $(NH_4)_{60}[\{(Mo^{VI})Mo^{VI}_5O_{21}(H_2O)_6\}_{12}\{Mo^{V}_2O_4(SO_4)\}_{18}\{Mo^{V}_2O_4(CH_3COO)\}_{12}] \cdot \approx 300H_2O$ (Mo-132c)

Prepared using a modified synthesis from the literature[26]:

A solution of $(NH_4)_{42}[Mo_{132}O_{372}(H_2O)_{72}(C_2H_3O_2)_{30}] \cdot \approx 300H_2O$ + $\approx 10CH_3COONH_4$ (5.0 g, 0.17 mmol) and $(NH_4)_2SO_4$ (20.0 g, 151 mmol) was adjusted to pH ≈ 3 with 1 N HCl (*ca.* 2.7 mL). The solution was stirred at 20 °C for 2 h and purified by filtration. The dark brown filtrate was stored in an open 600-mL beaker at 20 °C for 11 days, followed by 3 days in a fume hood to promote evaporation of the reaction solution and crystallization of the product. The precipitated brown crystals were filtered off through a glass frit, washed with a small amount of cold 2-propanol and dried in air. Yield: 2.3 g (49% based on Mo). Characteristic IR bands (KBr pellet): ν = 1618 (m, δ (H_2O)), 1539 (m, ν_{as} (COO)), *ca.* 1425 (sh), 1406 (s, δ_{as} (NH_4^+)), 1182 (w, ν (SO_4)), 1127 (m, ν (SO_4)), 1044 (m, ν_{as} (SO_4)), 970 (s), 937 (w, ν (Mo=O)), 856 (s), 799 (s), 727 (s), 633 (m), 573 cm^{-1} (w). Elemental analysis (%) calcd: C 1.07, N 2.96, S 2.14; found: C 2.8, N 3.1, S 1.8. Crystal data: Space group $R\bar{3}$, a = 32.780, c = 73.682 Å, V = 68564 $Å^3$.

5.2.4 Syntheses of Various Acetate/Sulfate Mixed-Ligand Clusters

To a solution of $(NH_4)_{42}[Mo_{132}O_{372}(H_2O)_{72}(C_2H_3O_2)_{30}] \cdot \approx 300H_2O$ + $\approx 10CH_3COONH_4$ (2.0 g, 0.07 mmol) in water (160 mL) was added $(NH_4)_2SO_4$ (8.0 g,

60.5 mmol) followed by H_2SO_4 to adjust to pH 1.5 (≈ 3.2 mL, 2 M) with stirring. The solution was stored in an open 400-mL beaker at 20 ^oC for two weeks, after which the precipitated brown crystals were filtered off through a glass frit, washed with *ca.* 4 mL of cold 2-propanol followed by *ca.* 4 mL of diethyl ether and dried in air.

Additional syntheses varied the pH of the reaction solution by varying the amount of 2 M H_2SO_4: pH 2.0, ≈ 1.0 mL; pH 2.5, ≈ 0.5 mL; pH 3.0, ≈ 0.4 mL; pH 3.5, ≈ 0.2 mL. Yield: pH 1.5, 1.66 g; pH 2.0, 1.29 g; pH 2.5, 1.14 g; pH 3.0, 0.61g; pH 3.5, 0.82g. Characteristic IR bands (KBr pellet): ν = 1610-1620 (m, δ (H_2O)), 1530-1545 (w-m, ν_{as} (COO)), *ca.* 1425 (sh), 1400-1405 (s, δ_{as} (NH_4^+)), 1180-1190 (w-m, ν (SO_4)), 1115-1140 (m, ν (SO_4)), 1035-1045 (m, ν_{as} (SO_4)), 965-970 (s), 935-940 (w, ν (Mo=O)), 850-860 (s), 795-805 (s), 720-730 (s), 620-635 (m), 570-575 cm^{-1} (s). Elemental analysis (%) found: pH 1.5 – C 0.05, N 3.9, S 3.90; pH 2.0 – C 0.43, N 3.51, S 3.77; pH 2.5 – C 1.15, N 3.22, S 2.58; pH 3.0 – C 1.19, N 3.1, S 2.60; pH 3.5 – C 1.53, N 3.13, S 2.41.

5.3 Results and Discussion

The clusters Mo-132a and Mo-132b were successfully synthesized according to the literature.[22,25] These compounds are clearly characterized by their distinctive IR spectra. In addition to persistent peaks arising from the molybdenum oxide shell, the IR spectrum of Mo-132a shows two characteristic acetate peaks at 1541 and 1402 cm^{-1}, while that of Mo-132b instead shows three peaks in the range 1200-1000 cm^{-1} corresponding to S – O stretches of the sulfate groups (**Figure 5.5**). Elemental analysis results agree with the calculated values for carbon, hydrogen, and nitrogen in Mo-132a. Nitrogen analysis of Mo-132b agrees with the calculated value suggesting the number of

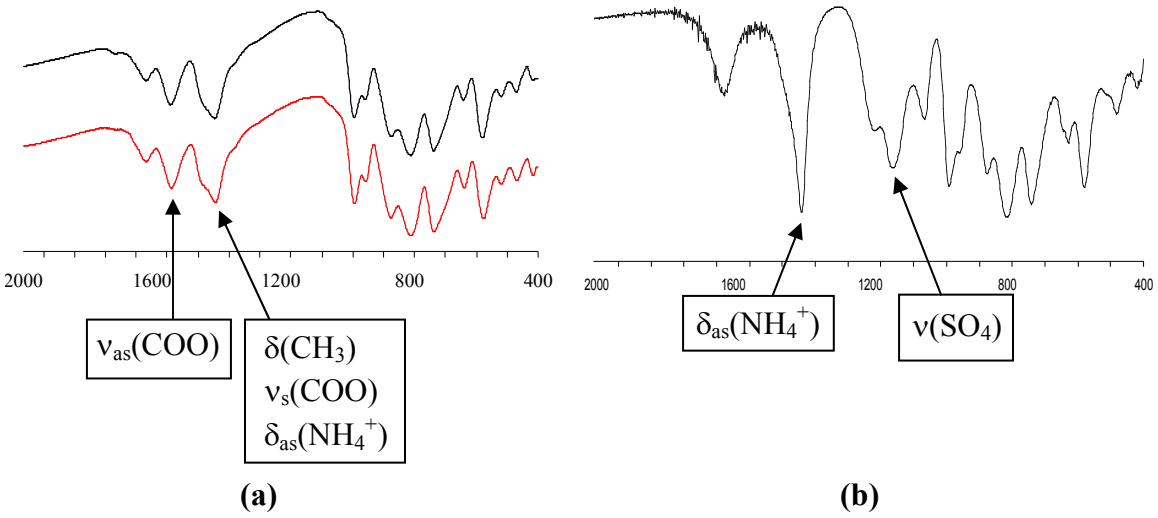

Figure 5.5. Infrared spectra of **(a)** the Mo-132 acetate cluster showing the characteristic acetate bands (original product – black line, recrystallized product – red line) and **(b)** the Mo-132 sulfate cluster showing the characteristic sulfate band.

ammonium cations, and therefore the cluster charge, is consistent with full ligand exchange in accordance with the assigned formula. The proton NMR spectrum of Mo-132b also shows no evidence of residual acetate in the cluster through a lack of peaks from the acetate methyl group (**Figure 5.6**).

The acetate/sulfate mixed ligand cluster Mo-132c was synthesized by careful adjustment of the pH of the reaction solution. Increasing the proton concentration of a solution of Mo-132a in the presence of sulfate ions promotes protonation of the acetate groups causing their dissociation from the molybdenum scaffold, followed by replacement with sulfate groups. The formation of Mo-132b requires an extremely low pH, while Mo-132c crystallizes at pH ≈ 3.0. Mo-132c was characterized by IR and proton NMR spectroscopy; as expected, the IR spectrum displays characteristic stretching

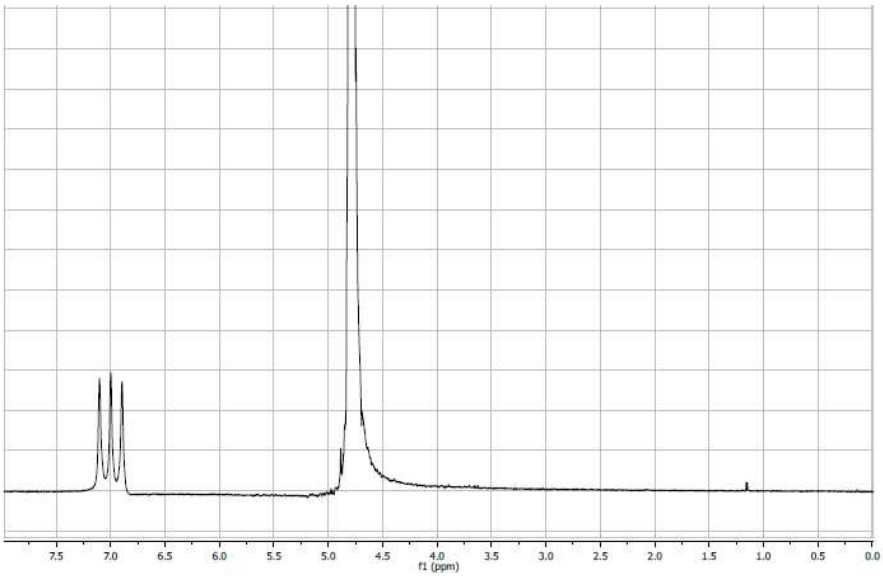

Figure 5.6. Nuclear magnetic resonance spectrum (in D_2O) of the Mo-132 sulfate cluster showing a triplet at 7.00 ppm corresponding to NH_4^+ most likely still trapped within the cluster. A weak doublet at 1.16 ppm is due to 2-propanol used to wash the product during filtering.

frequencies of both acetate and sulfate groups, and acetate CH_3 peaks are present in the NMR spectrum (**Figure 5.7**). Elemental analysis results agree with the calculated percentage of nitrogen in the product, and the sulfur analysis value falls within the experimental error limit of the analysis of the calculated value. While the experimental carbon value is higher than expected, the NMR shows peaks from residual propanol used to wash the product during filtering, to which the increased amount of carbon is attributed.

As the degree of sulfate substitution in Mo-132a is directly related to the pH of the reaction solution, the pH was further varied to allow the formation of clusters with a

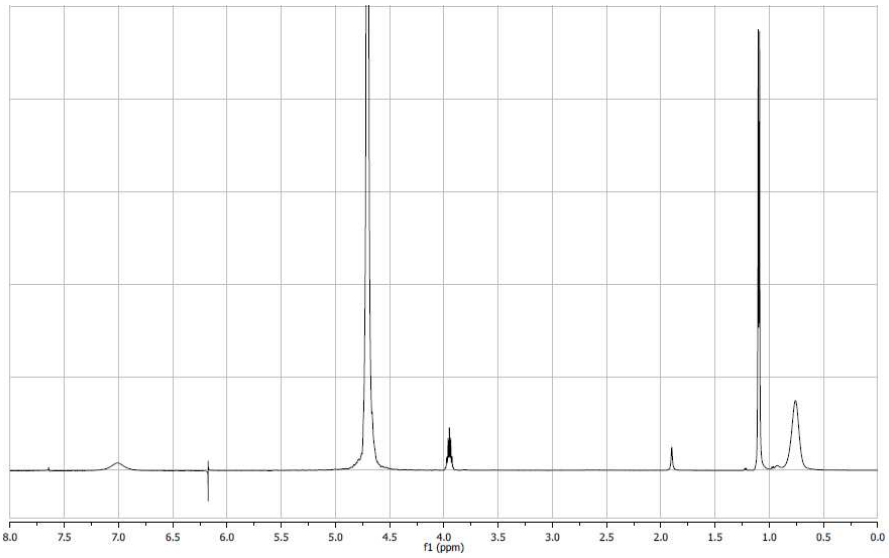

Figure 5.7. NMR spectrum (in D_2O) of the Mo-132 acetate/sulfate mixed ligand cluster showing two singlets at 0.76 ppm and 1.89 ppm corresponding to free and coordinated acetate groups, respectively. A very weak singlet at 7.00 ppm corresponds to free NH^{4+} present in the solution. A doublet at 1.09 ppm and a septet at 3.95 ppm are due to 2-propanol used to wash the product during filtering.

range of intermediate charges between those of Mo-132a and Mo-132b. A solution of Mo-132a in water was found to have a pH ≈ 4.0 prior to addition of ammonium sulfate and sulfuric acid, while the reaction solution of Mo-132b has a pH ≈ 1.0. Elemental analysis values for reactions of Mo-132a with ammonium sulfate as the sulfate source and sulfuric acid as the proton source at pH = 1.5, 2.0, 2.5, 3.0, and 3.5 show an increase in the percentage of carbon and a decrease in the percentage of sulfur and nitrogen as the pH increases. The carbon and nitrogen analyses for the pH = 3.0 cluster agree with the formulation of Mo-132c, showing no effect on cluster formation when a different proton source is used. These results demonstrate that reactions at lower pH will produce clusters containing larger numbers of NH_4^+ counterions due to the increased negative charge of

the cluster anion resulting from the increased number of sulfate groups present. Conversely, clusters formed at lower pH values contain fewer sulfate ligand substitutions and therefore comparatively low nitrogen percentages.

5.4 Conclusions

Polyoxomolybdate clusters of the type $\{Mo_{11}\}_n$ crystallize in various shapes, sizes, and charges dictated by the degree of reduction of molybdenum centers and the identity of certain structural components. The Mo-132 spherical-ball cluster shows great versatility through ligand exchange to form clusters exhibiting a range of anionic charges while maintaining the same overall dimensions. In addition to the acetate, sulfate, phosphate, and oxalate analogs reported in the literature, it is possible to crystallize mixed-ligand clusters of varying charges through control of the reaction pH. While elemental analysis can aid in the determination of the cluster charge, determination of an exact formula would require structural determination through x-ray diffraction to elucidate the presence and number of ordered water molecules within the cluster cavity.

Due to their nanoscopic dimensions and precise number of charges, Mo-132 clusters are an excellent candidate for a novel anionic mediator in the electrostatic self-assembly of charged metal nanoparticles to facilitate the study of the effect of electrostatic interactions on the precipitation point of such mixtures. UV-visible spectroscopy (UV-vis), dynamic light scattering (DLS) and zeta-potential (ξ-potential) measurements can be used to study the solution stability and precipitation point of these solutions. Oppositely charged metal nanoparticles form core-shell clusters in solution that are characterized by their unusual optical properties; the resonance absorption band

of the shell particles is enhanced, while that of the core particles is suppressed.[5] Addition of Mo-132 anion clusters to a solution of positively charged functionalized metal nanoparticles should result in a similar phenomenon that can be tracked through UV-vis spectroscopy. A sharp decrease in adsorption would be attributed to a specific precipitation point whereas continuously decreasing adsorption corresponds to continuous precipitation. DLS measurements track the size of aggregates in solution; the precipitation point would coincide with a sharp increase in aggregate size. The ξ-potential measurements denote at what point the system has reached a point of electroneutrality. These measurements can be compared with the adsorption and DLS measurements to determine if precipitation occurs at the point of electroneutrality as is observed for simpler nanoparticle mixtures. Such a point may also lead to the use of Mo-132 clusters as probes for the precise determination of charges on other nanoscopic entities.

5.5 Acknowledgement

This work was supported by a grant from the National Science Foundation, CHE-0242153.

5.6 References

[1] D. L. Long, R. Tsunashima, L. Cronin, *Angew. Chem. Int. Ed. Engl*. **2010**, *49*, 1736.

[2] A. Müller, S. Roy, *The Chemistry of Nanomaterials*: *Syntheses, Properties and Applications*, C. N. R. Rao, A. Müller, A. K. Cheetham, eds., Wiley-NCH Verlag GmbH & Co. K Ga A, Weinheim, **2004**, 452.

[3] R. Shenhar, V. M. Rotello, *Acc. Chem. Res.* **2003**, *36*, 549.

[4] K. J. M. Bishop, C. E. Wilmer, S. Soh, B. A. Grzybowski, *Small* **2009**, *5*, 1600.

[5] A. M. Kalsin, A. O. Pinchuk, S. K. Smoukov, M. Paszewski, G. C. Schatz, B. A. Grzybowski, *Nano Lett.* **2006**, *6*, 1896.

[6] C. C. You, M. De, V. M. Rotello, *Curr. Opin. Chem. Biol.* **2005**, *9*, 639.

[7] F. Stellaci, *Nat. Mater*. **2005**, *4*, 113.

[8] D. A. Walker, B. Kowalczyk, M. O. de la Cruz, B. A. Grzybowski, *Nanoscale* **2011** *3*, 1316 and references therein.

[9] E. V. Shevchenko, D. V. Talapin, N. A. Kotov, S. O'Brien, C. B. Murray, *Nature* **2006**, *439*, 55.

[10] M. E. Leunissen, C. G. Christova, A. P. Hynninen, C. P. Royall, A. I. Campbell, A. Imhof, M. Dijkstra, R. van Roiz, A. van Blaaderen, *Nature* **2005**, *437*, 235.

[11] A. M. Kalsin, M. Fialkowski, M. Paszewski, S. K. Smoukov, K. J. M. Bishop, B. A. Grzybowski, *Science* **2006**, *312*, 420.

[12] A. M. Kalsin, B. Kowalczyk, S. K. Smoukov, R. Klajn, B. A. Grzybowski, *JACS* **2006**, *128*, 15046.

[13] D. P. Yates, G. V. Franks, S. Biggs, G. J. Jameson, *J. Colloids Surf. A* **2005**, *255*, 85.

[14] J. Kolny, A. Kornowski, H. Weller, *Nano Lett.* **2002**, *2*, 361.

[15] M. C. Daniel, D. Astruc, *Chem, Rev.* **2004**, *104*, 293.

[16] O. D. Velev, *Science* **2006**, *312*, 376.

[17] M. Sastry, M. Rao, K. N. Ganesh, *Acc. Chem. Res.* **2002**, *35*, 847.

[18] A. Müller, E. Krickemeyer, H. Bögge, M. Schmidtmann, F. Peters, *Angew. Chem. Int. Ed.* **1998**, *37*, 3360.

[19] A. Müller, P. Kögerler, H. Bögge, *Structure and Bonding* **2000**, *96*, 203.

[20] M. L. Kistler, A. Bhatt, G. Liu, D. Casa, T. Liu, *J. Am. Chem. Soc.* **2007**, *129*, 6453.

[21] P. Gouzerh, M. Che, *L'Actualité Chimique* **2006**, 9.

[22] A. Müller, S. K. Das, E. Krickemeyer, C. Kuhlmann, *Inorg. Synth.* **2004**, *34*, 191.

[23] A. Müller, S. Sarkar, S. Q. N. Shah, H. Bögge, M. Schmidtmann, S. Sarkar, P. Kögerler, B. Hauptfleisch, A. X. Trautwein, V. Schünemann, *Angew. Chem. Int. Ed.* **1999**, *38*, 3238.

[24] A. Müller, H. Bögge, F. L. Sousa, M. Schmidtmann, D. G. Kurth, D. Volkmer, J. van Slageren, M. Dressel, M. L. Kistler, T. Liu, *Small* **2007**, *3*, 986.

[25] A. Müller, Y. Zhou, H. Bögge, M. Schmidtmann, T. Mitra, E. K. T. Haupt, A. Berkle, *Angew. Chem.* **2006**, *118*, 474.

[26] A. Müller, E. Krickemeyer, H. Bögge, M. Schmidtmann, B. Botar, M. O. Talismanova, *Angew. Chem. Int. Ed.* **2003**, *42*, 2085.

[27] A. Müller, L. Toma, H. Bögge, M. Henry, T. K. Haupt, A. Mix, F. L. Sousa, *Chem. Commun.* **2006**, 3396.

[28] A. Müller, S. K. Das, S. R. Talismanov, E. Beckmann, H. Bögge, M. Schmidtmann, A. Merca, A. Berkle, L. Allouche, Y. Zhou, L. Zhang, *Angew. Chem. Int. Ed.* **2003**, *42*, 5039.

Chapter 6

Conclusions

6.1 Conclusions

The scope of this research includes the detailed investigation of the design and synthesis of hybrid organic-inorganic materials of the oxomolybdenum-organodiphosphonate family incorporating Cu(II)/bisterpy and Cu(I,II)/4-pyridyltetrazole cationic units. The vast structural versatility of this class of compounds reflects the effects of the tether length of the organic component, number of available coordination sites on the oxide cluster, number of donor groups and flexibility of the secondary ligand, oxidation state of the metal cation, and the anionic oxide type and size. Furthermore, we have shown that variation in the hydrothermal reactions conditions, such as temperature, may influence the identity of the product. The synthesis and ligand-exchange capacity of the giant polyoxomolybdate cluster $[\{(Mo^{VI})Mo^{VI}_5O_{21}(H_2O)_6\}_{12}\{Mo^{V}_2O_4(O_2C_2H_3)\}_{30}]^{42-}$ were also studied, resulting in the preparation of clusters exhibiting a range of anionic charges.

6.2 The Oxomolybdenum Diphosphonate System

In order to elucidate the structural variability of this system, we have focused on the influence of specific variables such as tether length of the diphosphonate ligand and incorporation of fluoride into the oxide structure on the products formed.

6.2.1 Variations in Tether Length of Alkyldiphosphonates in the Cu(II)/Bisterpy/Molybdodiphosphonate System

The prototypical one-dimensional molybdodiphosphonate structure is observed in compounds incorporating 1,4-butylenediphosphonic acid and 1,5-pentylenediphosphonic acid ligands in the form of $\{Mo_5O_{15}(O_3P(CH_2)_nPO_3\}^{4-}$ chains. The increase in length of

the tether from $n = 4$ to $n = 5$ results in increased space between pentanuclear molybdate clusters while maintaining the chain structure and composition.

The introduction of Cu(II)/bisterpy (bisterpy = 2,2':4',4":2",2"'-quarterpyridyl-6',6"-di-2-pyridine) cationic secondary metal-ligand units provide coordination of the molybdodiphosphonate chains via bonding of the metal cation through molybdate oxo groups. However, the overall dimensionality of the structure is dictated by the number of coordination sites on the molybdate cluster as well as the orientation of the bisterpy ligand. The $n = 4$ compound $[\{Cu_2(bisterpy)(H_2O)\}Mo_5O_{15}\{O_3P(CH_2)_4PO_3\}]\bullet 4.5H_2O$ forms a three-dimensional structure with three metal coordination points per cluster. Yet **Figure 2.1(b)** clearly shows an accordian-type orientation of the bisterpy ligands in relation to the molybdodiphosphonate chains, resulting in reduced void space when compared to the rectangular grid structure predicted in **Scheme 2.1**. The $n = 5$ compound $[\{Cu_2(bisterpy)(H_2O)_2\}Mo_5O_{15}\{O_3P(CH_2)_5PO_3\}]$ forms ladder-type chains despite two metal coordination sites per molybdate cluster (**Figure 2.2(a)**). Pairs of $\{Cu_2(bisterpy)(H_2O)_2\}^{4+}$ units link two molybdate clusters of neighboring molybdodiphosphonate chains, resulting in the coordination of each chain to only one other. Further accomodation is made for the bisterpy ligands between the two single chains, allowing close proximity of neighboring molybdodiphosphonate chains within each ladder-type chain, by rotation along the central C-C bond of the ligand.

6.2.2 Fluoride Incorporation in the Cu(II)/Bisterpy/Molybdodiphosphonate System

The incorporation of fluoride anions into these materials results in the replacement of oxo groups by fluoride ions with profound structural consequences. As

opposed to the $\{Mo_5O_{15}(O_3PR)_2\}^{4-}$ clusters seen prevalently in molybdophosphonate chemistry, a variety of new oxyfluoromolybdate clusters are incorporated into these complexes (**Figure 6.1**). These clusters range from pairs of isolated oxyfluoromolybdate octahedra to binuclear and tetranuclear units. Though the molar ratio of molybdate starting material was kept constant in each reaction, the clusters formed contain anywhere from two to four total molybdenum centers.

Only two structures maintain a type of molybdodiphosphonate chain motif; the two-dimensional $[\{Cu_2(bisterpy)(H_2O)_2\}Mo_4F_4O_{10}\{O_3P(CH_2)_2PO_3\}]$ and the three-dimensional $[\{Cu_2(bisterpy)\}Mo_4F_6O_9\{O_3P(CH_2)_3PO_3\}]$ contain clusters to which the phosphonate ends of two different ligands are coordinated, directed away from each other (**Figure 6.1(b), (c)**). The one-dimensional structures formed from n = 4-6, 9 alkyldiphosphonate ligands all contain similar molybdophosphonate units in which the diphosphonate ligand is sandwiched between the oxyfluoromolybdate units of one cluster as opposed to providing coordination to neighboring clusters (**Figure 6.1(d)-(f)**). Cationic $\{Cu_2(bisterpy)\}^{4+}$ units then link the molybdophosphonate clusters into chains (**Figures 3.6-3.8**). The two-dimensional structure of $[\{Cu_2(bisterpy)(OH)\}Mo_2F_3O_4\{O_3P(CH_2)PO_3\}]\bullet 11H_2O$ provides the only example in this series of a multi-dimensional material forming from discrete molybdophosphonate clusters between which the diphosphonate ligand does not contribute coordination. It is common for methylenediphosphonate to chelate the same molybdate cluster as opposed to linking neighboring clusters due to its decreased spacer length. As shown in **Figure 3.3(a)**, the metal cations provide connectivity between molybdophosphonate clusters to form dimers, which are then linked by the bisterpy ligands to form the layer.

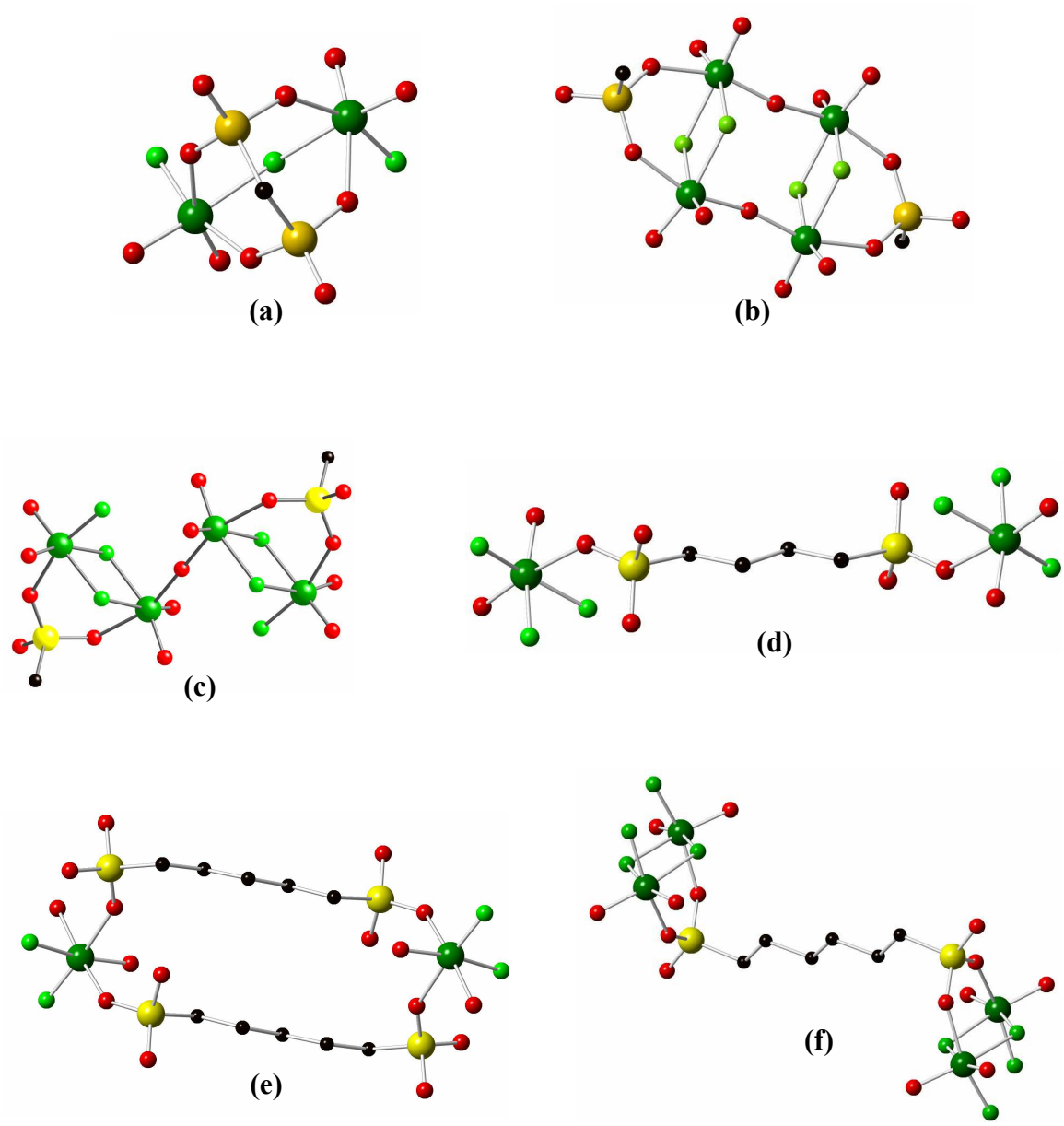

Figure 6.1. The new oxyfluoromolybdate clusters present in **(a)** [{Cu_2(bisterpy)(OH)}$Mo_2F_3O_4${$O_3P(CH_2)PO_3$}]•11H_2O, **(b)** [{Cu_2(bisterpy)(H_2O)$_2$}$Mo_4F_4O_{10}${$O_3P(CH_2)_2PO_3$}], **(c)** [{Cu_2(bisterpy)}$Mo_4F_6O_9${$O_3P(CH_2)_3PO_3$}], **(d)** [{Cu_2(bisterpy)(H_2O)$_2$}$Mo_2F_6O_4${$HO_3P(CH_2)_4PO_3H$}], **(e)** [{Cu_2(bisterpy)}$Mo_2F_4O_4${$HO_3P(CH_2)_5PO_3H$}$_2$]•2H_2O, and **(f)** [{Cu_2(bisterpy)(H_2O)$_2$}$Mo_4F_8O_8${$O_3P(CH_2)_6PO_3$}]•2H_2O and [{Cu_2(bisterpy)(H_2O)$_2$}$Mo_4F_8O_8${$O_3P(CH_2)_9PO_3$}].

A noteworthy aspect of this chemistry is the lack of correlation between the ratios of molybdate to fluoride starting materials and the resulting molybdenum to fluoride ion ratio in the product clusters, as shown in **Table 6.1**.

Table 6.1. Comparison of mole ratios of molybdenum to fluoride in reactions and products for $[\{Cu_2(bisterpy)(OH)\}Mo_2F_3O_4\{O_3P(CH_2)PO_3\}]\bullet 11H_2O$, $[\{Cu_2(bisterpy)(H_2O)_2\}Mo_4F_4O_{10}\{O_3P(CH_2)_2PO_3\}]$, $[\{Cu_2(bisterpy)\}Mo_4F_6O_9\{O_3P(CH_2)_3PO_3\}]$, $[\{Cu_2(bisterpy)(H_2O)_2\}Mo_2F_6O_4\{HO_3P(CH_2)_4PO_3H\}]$, $[\{Cu_2(bisterpy)\}Mo_2F_4O_4\{HO_3P(CH_2)_5PO_3H\}_2]\bullet 2H_2O$, $[\{Cu_2(bisterpy)(H_2O)_2\}Mo_4F_8O_8\{O_3P(CH_2)_6PO_3\}]\bullet 2H_2O$ and $[\{Cu_2(bisterpy)(H_2O)_2\}Mo_4F_8O_8\{O_3P(CH_2)_9PO_3\}]$.

	MoO_3:HF Ratio in Reaction	Mo:F Ratio in Product
$\{Mo_2F_3O_4(O_3P(CH_2)PO_3)\}^{3-}$	1:38	1:1.5
$\{Mo_4F_4O_{10}(O_3PR)_2\}^{4-}$	1:19	1:1
$\{Mo_4F_6O_9(O_3PR)_2\}^{4-}$	1:19	1:1.5
$\{MoF_3O_2(HO_3P(CH_2)_4PO_3H)MoF_3O_2\}^{4-}$	1:29	1:3
$\{MoF_2O_2(HO_3P(CH_2)_5PO_3H)_2MoF_2O_2\}^{4-}$	1:29	1:2
$\{Mo_2F_4O_4(O_3P(CH_2)_6PO_3)Mo_2F_4O_4\}^{4-}$	1:29	1:2
$\{Mo_2F_4O_4(O_3P(CH_2)_9PO_3)Mo_2F_4O_4\}^{4-}$	1:38	1:2

6.2.3 Future Work

In addition to variations in the tether length of alkyldiphosphonate ligands, the structural implications of the inclusion of aromatic diphosphonate ligands in the oxomolybdenum-organodiphosphonate system can be explored. Such as those shown in **Figure 6.2**, xylene-based ligands combine the added rigidity of aromatic rings with ease of synthesis as phosphonate addition onto the bromide starting material can occur in the same simple one-pot preparation used for the production of the alkyldiphosphonates.[1]

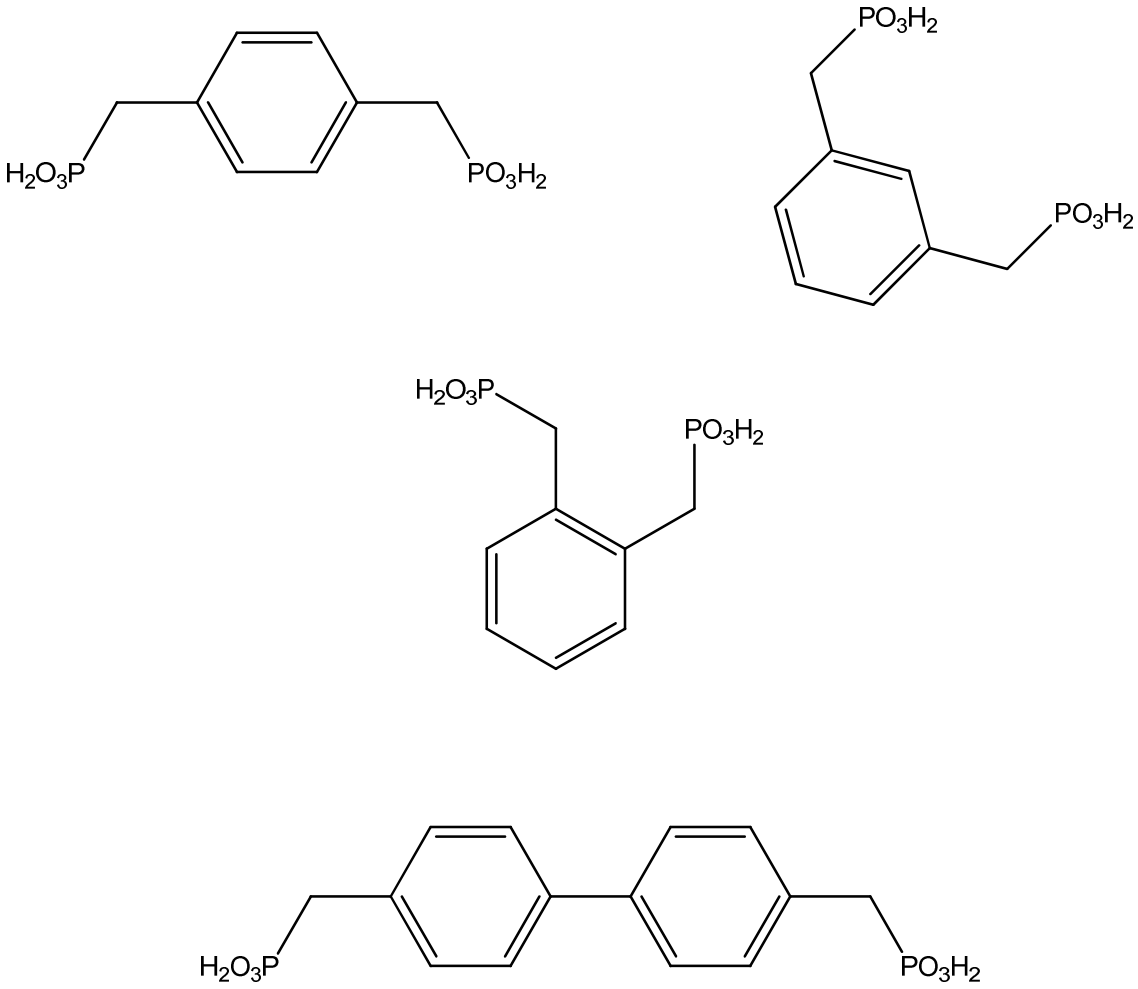

Figure 6.2. Various xylene-based diphosphonate ligands for incorporation into hybrid metal oxide materials.

A preliminary study incorporating p-xylenediphosphonic acid as the organic linker in the Cu(II)/bipyridine/molybdodiphosphonate system[2] produces the three-dimensional $[\{Cu(bpy)\}_2Mo_4O_{10}(O_3PCH_2C_6H_4CH_2PO_3)_2]$. While this compound contains molybdodiphosphonate chains linked through the organic tether of the diphosphonate ligand, the molybdate clusters are not of the persistent $\{Mo_5O_{15}(O_3PR)_2\}^{4-}$

type. Instead, inorganic molydophosphonate chains run along the *c* axis (**Figure 6.3**) and are linked through the p-xylene tethers extending from the phosphonate tetrahedral. This observation supports the suggestion that the diphosphonate ligand acts as a structural determinant in the formation of the phosphomolybdate substructures of these materials, as no fluoride is present to account for the altered molybdate motif. Further investigations using rigid aromatic diphosphonate ligands in the presence of larger, and eventually binucleating, secondary ligands as well as various metal cations may uncover a new persistent molybdate unit dictated by the specific nature of the diphosphonate ligand.

Due to the wide variety of new oxyfluoromolybdate clusters formed in the Cu(II)/bisterpy/molybdodiphosphonate system, the structural influence of fluoride inclusion on the molybdodiphosphonate systems incorporating M(II)/bipyrimidine[3] and M(II)/tetra-2-pyridylpyrazine[4] secondary building blocks can also be explored. Though it is clear that one cluster type does not prevail over a variety of structures, the formation of the same cluster within $[\{Cu_2(bisterpy)(H_2O)_2\}Mo_4F_8O_8\{O_3P(CH_2)_6PO_3\}]\bullet 2H_2O$ and $[\{Cu_2(bisterpy)(H_2O)_2\}Mo_4F_8O_8\{O_3P(CH_2)_9PO_3\}]$ suggests the possibility of control over the cluster composition dependent upon other synthetic parameters.

6.3 Structural Influence of Anion Incorporation in the Cu(I,II)/4-Pyridyltetrazole System

The introduction of 4-pyridyltetrazole (4-pt) as the secondary ligand in a multi-component construction scheme offers increased complexity of the cationic metal-ligand framework due to the presence of several nitrogen donors to which more metal centers

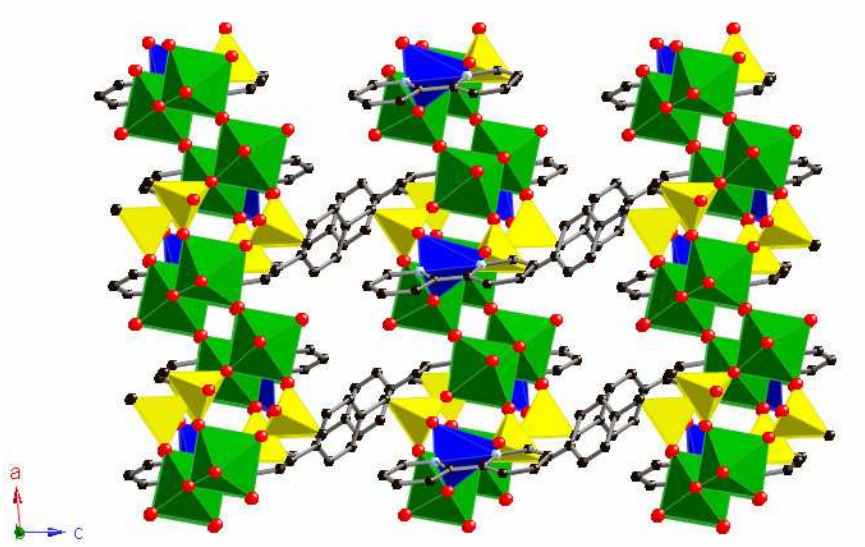

(a)

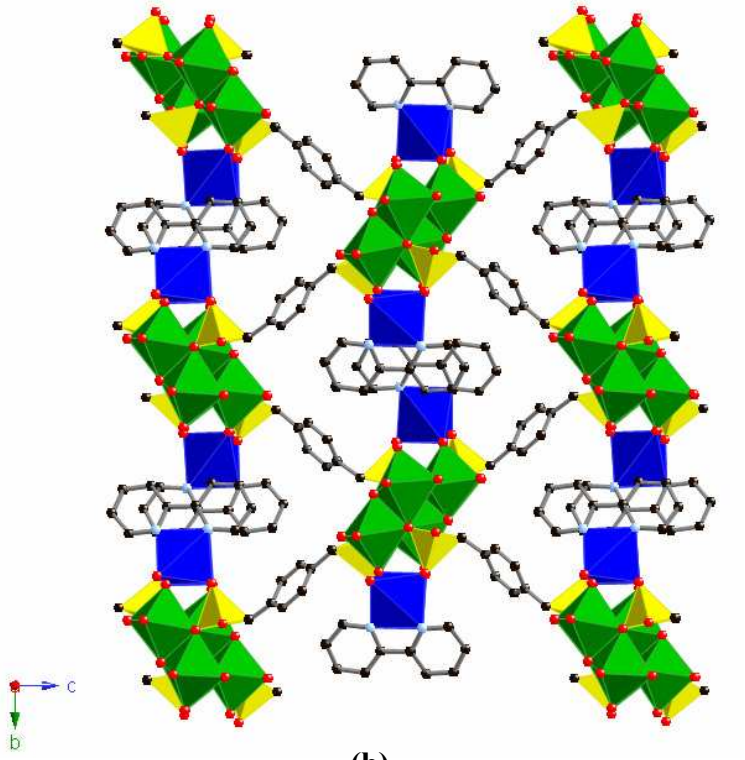

(b)

Figure 6.3. Polyhedral representation of the structure of $[\{Cu(bpy)\}_2Mo_4O_{10}(O_3PCH_2C_6H_4CH_2PO_3)_2]$ **(a)** in the *ac* plane and **(b)** the *bc* plane, parallel to the molybdophosphonate chains.[2]

may coordinate. This ligand has the ability to form three-dimensional structures with a metal cation by adopting the N2,N3 bridging mode at the tetrazolate end in addition to further metal coordination through the pyridyl nitrogen as shown in **Scheme 4.3.** Additional metal coordination through the N1 and N4 donors of the tetrazolate end forms a more complex multi-dimensional cationic structure. These coordination modes have been adopted by 4-pt in the presence of a metal cation and various anions including Cl^-, I^-, OH^-, and SO_4^{2-}[5].

Through incorporation of a variety of molybdate anions, we have shown additional anionic control of the metal/4-pt structure. The two-dimensional structure of $[\{Cu_3(4\text{-pt})_2(4\text{-Hpt})_2(H_2O)_2\}\{\beta\text{-}Mo_8O_{26}\}]\bullet 2H_2O$ and the three-dimensional $[\{Cu_{10}(4\text{-pt})_6(4\text{-Hpt})_2\}\{\beta\text{-}MoO_{26}\}]\bullet 2H_2O$ demonstrate the ways in which the copper/4-pt structure accommodates the larger octamolybdate anion (**Figures 4.1-4.2**). In both cases, the cationic structure dictates the dimensionality of the compound and forms cavities in which the molybdate clusters are located. Introduction of the 1,2-ethylenediphosphonate ligand into this system forms the prototypical one-dimensional $\{Mo_5O_{15}(O_3P(CH_2)_2PO_3\}^{4-}$ molybdodiphosphonate chains within the three-dimensional $[\{Cu_4(4\text{-Hpt})_3(H_2O)\}Mo_5O_{15}\{O_3P(CH_2)_2PO_3\}]\cdot 2H_2O$. Again, channels form within the complicated Cu(I)/4-pt framework to accommodate the molybdodiphosphonate chains (**Figure 4.3**).

When the diphosphonate ligand degrades under the hydrothermal conditions, we see phosphate incorporation into the molybdate clusters to form α-Keggin anions. These slightly larger clusters are not easily integrated into the surrounding copper/4-pt network, and we instead observe Cu/4-pt chains or layers surrounded by these clusters. The

structure of $[Cu_6(4\text{-pt})_2(4\text{-Hpt})_2][PMo^{V}Mo^{VI}_{11}O_{40}]\cdot 2.5H_2O$ contains $\{Cu_6(4\text{-pt})_2(4\text{-Hpt})_2\}^{4+}$ chains separated by Keggin clusters along the *c* axis (**Figure 4.4**). One-dimensional Cu/4-pt chains are also observed in $[Cu_3(OH)(4\text{-pt})_2(4\text{-Hpt})_2(H_2O)_2][PMo_{12}O_{40}]\bullet 10.5H_2O$, where the Keggin clusters are pendant to the chains (**Figure 4.5**). The two-dimensional structure of $[Cu_3(OH)(4\text{-pt})_3(4\text{-H}_2\text{pt})(H_2O)][PMo_{12}O_{40}]\cdot 7.5H_2O$ contains Cu/4-pt layers sandwiching coordinated Keggin clusters, and sandwiched by uncoordinated Keggin clusters (**Figure 4.6**). The formation of Keggin clusters as opposed to molybdodiphosphonate chains appears to be independent of reaction temperature, crystallization time, and pH as there is no delineation between these synthetic parameters for these compounds.

Throughout this project, the reduction of the copper(II) starting material to copper(I) in the final products is dependent upon the reaction temperature. Those compounds crystallized at temperatures between 100 ^{o}C and 150 ^{o}C contain copper(II) centers while compounds crystallized at 180 ^{o}C exhibit reduction of the copper sites. This variation in oxidation state of the metal cation is shown to influence the complexity of the Cu/4-pt networks within these compounds. While copper(II) centers prefer coordination to two tetrazolate nitrogen donors and the pyridyl nitrogen, the reduction to copper(I) causes increased coordination to the tetrazolate end of the ligand leading to the formation of highly complex cationic networks and frameworks.

6.3.1 Future Work

The structural influences of two reaction parameters remain relatively unexplored. Although the reduction of the copper centers by the 4-pt ligand appears dependent upon the reaction temperature, a precise temperature at which reduction occurs has not been

determined. Further syntheses carried out in the 150-180 ^{o}C range will aid in the elucidation of the point of reduction. Further investigation of this and other nitrogen-containing ligands as potential reducing agents may uncover other synthetic conditions required for the reduction of metal centers in this system. The reaction conditions that cause the degradation of the diphosphonate ligand leading to the formation of Keggin-type anions are also unclear at this point. There is no distinct difference in the reaction temperature, the crystal growth time, or the pH of these reactions as opposed to that of $[\{Cu_4(4\text{-Hpt})_3(H_2O)\}Mo_5O_{15}\{O_3P(CH_2)_2PO_3\}]\cdot 2H_2O$. Through careful variation of these conditions, it may be possible to determine the precise cause of diphosphonate ligand decomposition. This understanding will support the preparation of Cu/4-pt/molybdodiphosphonate compounds incorporating a variety of alkyldiphosphonate ligands to determine the overall structural effects of increasing the organic tether length of the ligand.

6.4 Synthesis and Ligand-Exchange Capacity of Giant Polyoxomolybdate Cluster Mo-132

The room-temperature crystallization following the reduction of an acidic molybdate solution in the presence of acetate and sulfate ligands has resulted in the preparation of several Mo-132 clusters containing various ratios of acetate to sulfate ligands and therefore exhibiting a variety of anionic charges. Based on elemental analysis results, the clusters exhibit anionic charges ranging from the 42- charge of the acetate cluster to the 72- charge of the sulfate cluster through various degrees of ligand exchange. As the pH of the reaction solution is decreased, the number of acetate ligands

exchanged for sulfate ligands increases. This causes a decrease in the cluster charge and therefore an increase in the number of ammonium cations associated with the cluster for purposes of charge compensation. Accordingly, the values obtained from sulfur and nitrogen analysis indicate the relative number of sulfate ligands and ammonium cations associated with each cluster, and therefore the relative charges of the clusters.

6.4.1 Future Work

In order to fully elucidate the number of acetate versus sulfate ligands present in each cluster, and therefore the overall cluster charge, x-ray diffraction experiements should be conducted. The published structures of the acetate and sulfate clusters show a difference in the number of water molecules associated with each, as the acetate cluster exhibits a hydrophobic inner surface excluding water molecules from crystallizing within the cluster cavity while the sulfate cluster exhibits ordered arrays of water molecules within the hydrophilic inner surface. This causes a degree of ambiguity in the prediction of the formula of mixed-ligand clusters, and therefore difficulty in interpreting the elemental analysis data. Due to the high symmetry of these compounds, it can be difficult to successfully assign exact positions for every atom of each ligand. However, the difference in electron density between the sulfur atom and the carbon atom will determine definitively which ligands are acetate groups and which are sulfate groups.

These nanoscopic clusters provide an ideal anionic mediator in the assembly of metal nanoparticles to study the electrostatic interactions on a mixture containing charged nanoscopic entities due to their size and precise charge. A preliminary study to determine the effect of electrostatic interactions on the precipitation point of a solution containing Mo-132 acetate clusters and positively charged functionalized gold

nanoparticles (AuNPs) reveals precipitation at the point of electroneutrality.[6] The interaction of positively and negatively charged gold nanoparticles with the Mo-132 clusters was studied by monitoring solutions of various Mo-132:AuNP ratios for aggregate size and charge of the aggregates *in-situ* with dynamic light scattering (DLS), ζ-potential, and ultraviolet-visible (UV-vis) spectroscopy. The UV-vis results (**Figure 6.4(a)**) show a sharp decrease in adsorbance of the positively charged gold nanoparticles at 6:1 attributed to the assembly of Mo-132 clusters surrounding each nanoparticle and, thus blocking the absorbance of the AuNP, prior to precipitation. DLS results (**Figure 6.4(b)**) show a sharp increase in aggregate size at 10:1, which is in agreement with the ζ-potential results (**Figure 6.4(c)**) showing the point of electroneutrality also at the 10:1 ratio. These results support the dependence of the precipitation point on the point of electroneutrality in such mixtures. Testing of additional clusters with a variety of charges would further indicate such a correlation.

6.5 General Conclusions

The hybrid organic-inorganic structures reported here result from the integration of functional organic molecules and specific inorganic moieties to form novel materials. Several structural determinants have been identified including the tether length, geometry, and orientation of organic components, the identity of the molybdate anionic unit, the oxidation state of the metal cation, the number of donor groups on the secondary ligand, and the incorporation of fluoride ions into the oxide component. The fine tuning of polyoxomolybdate cluster charge has been achieved through ligand exchange, affording the possibility of generating a library of clusters based on the Mo-132

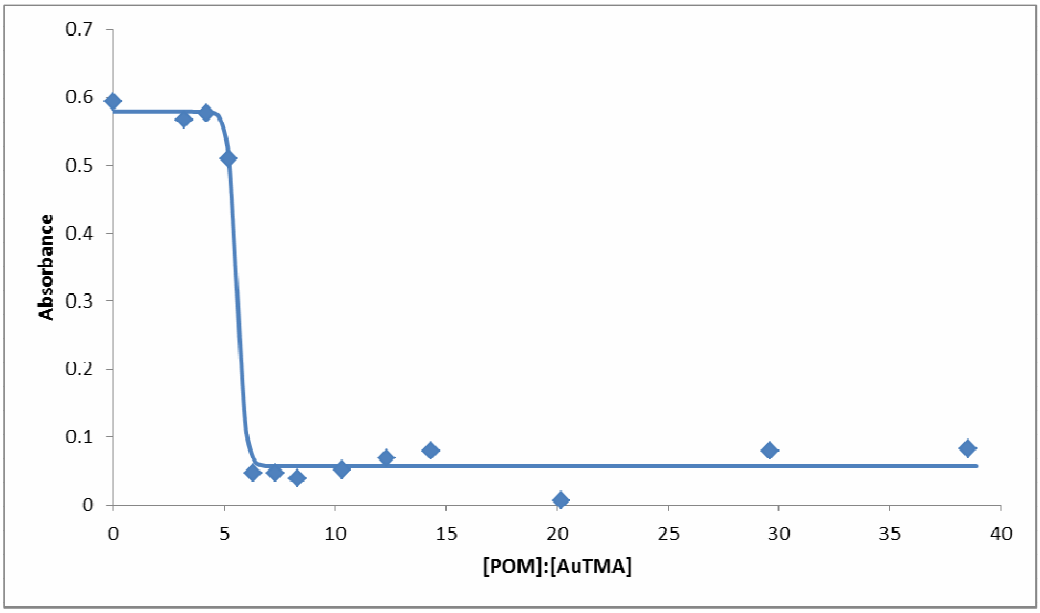

(a)

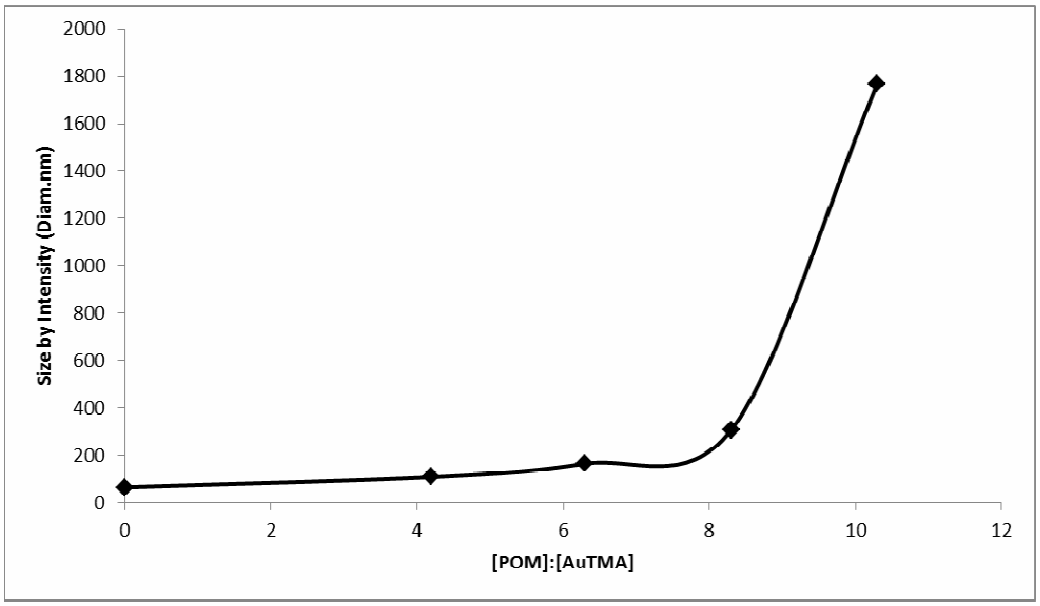

(b)

Figure 6.4. **(a)** The absorbance of AuTMA upon addition of Mo-132; **(b)** DLS measurements, showing a sharp increase in aggregate size upon the precipitation point.[6]

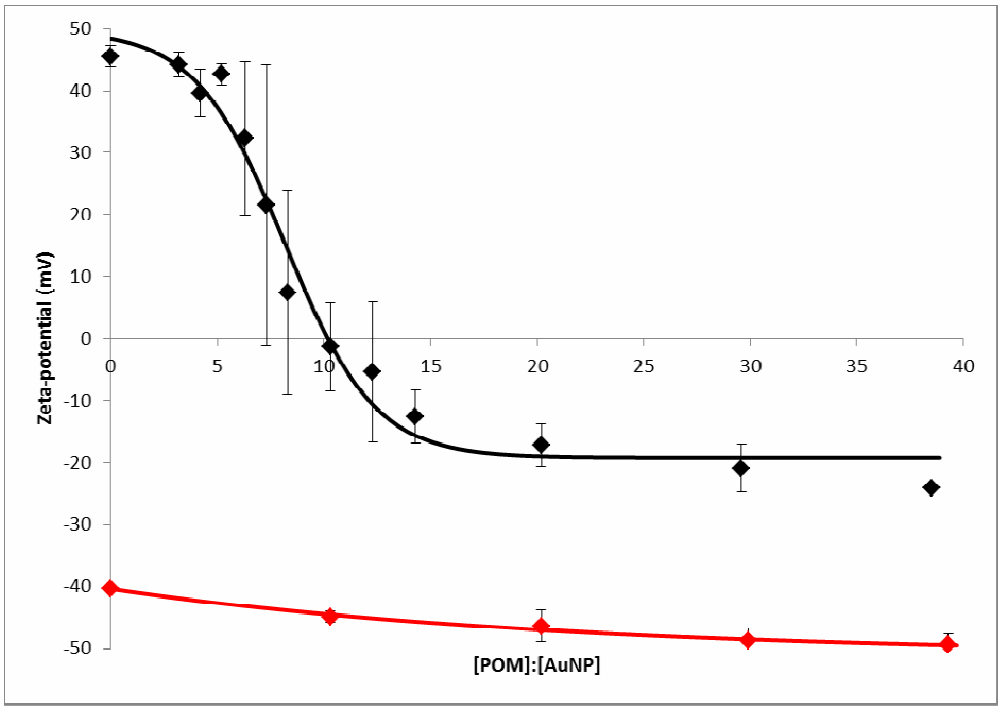

(c)

Figure 6.4 (cont.). (c) ξ-potential values for positively charged AuNPs titrated with Mo-132 (black line) and ξ -potential values for negatively charged AuNPs titrated with Mo-132 (red line).[6]

molybdate framework containing a variety of coordinated ligands and internal surface characteristics.

A wide range of new structural motifs and building blocks have been observed, suggesting that there remains much to be explored in order to increase our understanding of these systems. The formation of unexpected structure types exemplifies the large region of parameter space that remains to be surveyed before the prediction of structural outcomes is possible, though certain structural themes continue to emerge under the appropriate reaction conditions. Through the accumulation of motifs generated in these

systems, a structural data base can be created to aid in the exploitation of structures and properties in the design of multifunctional materials.

6.6 References

[1] D. I. Arnold, X. Ouyang, A. Clearfield, *Chem. Mater.* **2002**, *14*, 2020.

[2] S. Jones, H. Liu, K. Schmidtke, C. J. O'Connor, J. Zubieta, *Inorg. Chem. Comm.* **2010**, *13*, 298.

[3] N. G. Armatas, W. Ouellette, K. Whitenack, J. Pelcher, H. Liu, E. Romaine, C. J. O'Connor, J. Zubieta, *Inorg. Chem.* **2009**, *48*, 8897.

[4] E. Burkholder, V. Golub, C. J. O'Connor, J. Zubieta, *Inorg. Chem.* **2003**, *42*, 6729.

[5] W. Ouellette, S. Jones, J. Zubieta, *Cryst. Eng. Comm.* **2011**, *13*, 4457.

[6] J. Gooch, A. Anan, S. Jones, M. M. Maye, A. Müller, J. Zubieta, *in progress*.

Vita

STEPHANIE F. JONES

105 Remington Ave., Apt. 6
Syracuse, NY 13210
(315) 443-3731 (work)
(215) 266-7525 (cell)
sfjone02@syr.edu

Education:

Ph.D., Chemistry, Syracuse University, Syracuse, NY, expected May 2012
Dissertation topic: Synthesis and characterization of multi-component hybrid organic-inorganic materials
Advisor: Professor Jon A. Zubieta

M.Phil., Chemistry, Syracuse University, Syracuse, NY, 2008
Advisor: Jon A. Zubieta

B.A., Biological and Chemical Sciences – Chemistry, with distinction
Minor in Mathematical and Physical Sciences – Mathematics
Magna cum laude, Wells College, Aurora, NY, 2006
Thesis title: *New Building Blocks for Colloid-Based Materials by Imprinting Peanut Shape*
Advisor: Professor Christopher T. Bailey

Awards:

2009 Syracuse University Department of Chemistry Outstanding Graduate Teaching Assistant, William D. Johnson Award
2006 Distinction in Biological and Chemical Sciences
2006 Ruth M. Dunlap Prize in Chemistry
2006 Wells Women in Science Prize
2006 Phi Beta Kappa
2006 Koch Prize for Best Senior Research Paper – Honorable Mention
2002-2006 Dean's List
2004, 2005, 2006 Who's Who Among American Colleges And Universities
2003 CRC Press Freshman Chemistry Award

Teaching Experience:

2011: Teaching Assistant, Syracuse University, Syracuse, NY
General Chemistry Honors & Majors Recitation (1 semester)

Responsibilities included teaching 2 recitation sections per week, holding weekly office hours, running exam review sessions.

2006-2008: Teaching Assistant, Syracuse University, Syracuse, NY
General Chemistry Recitation (5 semesters)

Responsibilities included teaching 2-3 recitation sections per week, holding weekly office hours, running exam review sessions.

2003-2006: Teaching Assistant, Wells College, Aurora, NY
General Chemistry Laboratory (6 semesters)

Responsibilities included lab preparation, set-up, clean-up, supervision of students during lab, running exam review sessions.

Research Experience and Internships:

2006 – present: Graduate Research Assistant, Syracuse University, Syracuse, NY
Advisor: Professor Jon. A. Zubieta

Summer 2005: National Science Foundation Research Experience for Undergraduates, Cornell University, Ithaca NY

Project entitled "New Building Blocks for Colloid-Based Materials by Imprinting Peanut Shape", under the direction of Professor Chekesha M. Liddell.

Summer 2004: National Science Foundation Research Experience for Undergraduates, Harvard University, Cambridge MA

Project entitled "Creaming in Emulsions with a Depletion-Induced Attraction", under the direction of Professor David Weitz.

January 2002: Intern, Epsilon Associates, Maynard MA

Aided in the preparation of Environmental Impact Reports and research of future testing sites.

Presentations:

(1) American Chemical Society National Meeting - poster presentation "Solid state coordination chemistry: Organic-inorganic hybrid materials constructed from copper 5-(4'-pyridyl)tetrazole networks with embedded molybdate clusters" August 2010, Boston, Massachusetts.

(2) Wells College Science Colloquium – invited talk "Solid State Coordination Chemistry: Structural Diversity of the Bimetallic Copper-Molybdodiphosphonate System of Organic-Inorganic Hybrid Materials" October 2009, Aurora, NY.

(3) American Chemical Society National Meeting - poster presentation "Structural influence of diphosphonate tether length and fluoride incorporation on bimetallic copper-molybdophosphonates" March 2009, Salt Lake City, Utah.

(4) National Conference for Undergraduate Research - oral presentation "New Building Blocks for Colloid-Based Materials by Imprinting Peanut Shape" April 2006, University of North Carolina-Asheville.

Publications:

(1) **Stephanie Jones** and Jon Zubieta, Structural chemistry of bimetallic oxides constructed from molybdodiphosphonate building blocks, *Metal Phosphonate Chemistry* **2012**, 192-234.

(2) Luke A. Burke, Grazia Gonella, Fenton Heirtzler, Hai-Lung Dai, **Stephanie Jones** and Jon Zubieta, A self-assembled, metallo-organic supramolecular frequency doubler, *Chem. Comm.* **2012**, *48*, 1000-1002.

(3) Wayne Ouellette, **Stephanie Jones** and Jon Zubieta, Solid state coordination chemistry of metal-1,2,4-triazolates and the related metal-5-(pyrid-4-yl)tetrazolates, *Cryst. Eng. Comm.* **2011**, *13*, 4457-4485.

(4) Mark Bartholomae, **Stephanie Jones** and Jon Zubieta, Construction of bimetallic oxide materials from molybdate building blocks and copper-ligand tethers with flexible spacers: Structures of the two-dimensional $[\{Cu_2(L4)(H_2O)_2\}Mo_8O_{26}(H_2O)_2]$ and of the three-dimensional $[\{Cu_2(L4)\}_2(Mo_8O_{26})(MoO_4)_2]$ (L4 = N1,N1,N4,N4-tetrakis(pyridine-2-ylmethyl)butane-1,4-diamine), *Inorg. Chem. Comm.* **2011**, *14*, 107-110.

(5) Paul DeBurgomaster, Kari Darling, **Stephanie Jones** and Jon Zubieta, Metal-organodiphosphonates: Structural consequences of introducing aromatic tethering groups. The structures of $[Cu(phen)\{HO_3P(C_{12}H_8)PO_3H\}]$, $[\{Cu(phen)\}_2\{HO_3P(C_{12}H_8)PO_3H\}]$ and $[Cu(terpy)\{HO_3P(C_{12}H_8)PO_3H\}]$ and of

the bimetallic materials [{Cu(LL)}$_2$MoO$_2${HO$_3$P(C$_{12}$H$_8$)PO$_3$H}$_3$] (LL = 2,2-bipyridine, o-phenanthroline), *Inorg. Chim. Acta* **2010**, *364*, 150-156.

(6) **Stephanie Jones**, Hongxue Liu, Wayne Ouellette, Katherine Schmidtke, Charles C. O'Connor and Jon Zubieta, Hydrothermal synthesis and structure of a two-dimensional bimetallic copper-molybdophosphonate, [{Cu$_4$(H$_2$O)$_2$(phenbisterpy)$_2$(HO$_3$P(CH$_2$)$_4$PO$_3$H)}(Mo$_4$FO$_{12}$)$_2${O$_3$P(CH$_2$)$_4$PO$_3$}]·4 H$_2$O, constructed from {MO$_4$FO$_{12}$}$^{1-}$ clusters and copper-ligand chains (phenbisterpy = 1,4-bis(2,2':6',2"-terpyridin-4'-yl-benzene), *Inorg. Chem. Comm.* **2010**, *13*, 491-494.

(7) **Stephanie Jones**, Hongxue Liu, Charles C. O'Connor and Jon Zubieta, Solid state coordination chemistry of polyoxomolybdate clusters: Hydrothermal synthesis and structures of {[Cu$_3^{II}$(4-pt)$_2$(4-Hpt)$_2$(H$_2$O)$_2$}{MO$_8$O$_{26}$}]·2H$_2$O and [{Cu$_{10}^{I}$(4-pt)$_6$(4-Hpt)$_2$}{Mo$_8$O$_{26}$}]·2H$_2$O (Hpt = 5(4'-pyridyl)tetrazole), *Inorg. Chem. Comm.* **2010**, *13*, 412-416.

(8) **Stephanie Jones**, Hong-Xue Liu, Katherine Schmidtke, Charles C. O'Connor and Jon Zubieta, A bimetallic oxide framework, [{Cu(bpy)}$_2$Mo$_4$O$_{10}$(O$_3$PCH$_2$C$_6$H$_4$CH$_2$PO$_3$)$_2$], constructed from novel {Mo$_4$O$_{10}$(O$_3$PR)$_4$}$_n^{4n-}$ chains, *Inorg. Chem. Comm.* **2010**, *13*, 298-301.